CRANFIELD UNIVERSITY

Frank G Noppel

COMPARISON OF UNCONVENTIONAL AERO ENGINE ARCHITECTURES

School of Mechanical Engineering

PhD Thesis

Cranfield University

School of Engineering

Department of Power and Propulsion

PhD Thesis

Frank G Noppel

COMPARISON OF UNCONVENTIONAL AERO ENGINE ARCHITECTURES

30 April 2011

Supervisor: Professor Riti Singh

Abstract

In the light of global warming, the associated socio economical consequences, and the projected shortage of natural energy resources and ever rising oil prices, this thesis examines the potential for unconventional aero engine architectures to reduce fuel consumption of passenger aircraft. Current aircraft engines are based on the Brayton cycle, where the working fluid successively experiences isentropic compression, isobaric combustion, and isentropic expansion. Deviations from the ideal cycle in real engines occur through component inefficiencies. The maximum achievable thermodynamic efficiency of the Brayton cycle increases hand in hand with its peak cycle temperature. Since the peak cycle temperature is limited by material properties of the turbine, the maximum cycle efficiency of current jet engines is limited by the laws of thermodynamics. Hence, efficiency improvements of jet engines beyond what is possible with conventional turbofan designs are only feasible through unconventional engine architecture.

Several technologies enabling unconventional engine architectures for aircraft propulsion have been identified. They include wave rotor, pulse detonation and internal combustion. These technologies are merged with conventional jet engine technology to form hybrid designs. A one dimensional engine performance model was developed to calculate the performance and allow a comparison of the hybrid cycles with a conventional turbofan cycle. Gradient optimisation techniques were applied to the allow comparison of the best possible designs. Results suggest that of the examined cycles, the hybrid internal combustion cycle has the best potential for fuel savings compared to conventional turbofan cycles.

Acknowledgements

My sincere gratitude belongs to Professor Riti Singh and Professor Pericles Pilidis from the Department of Power and Propulsion at Cranfield University. Their continued and enduring support of any kind and emotional backing is exceptional and greatly acknowledged. Many, many thanks!

All the help and assistance from Sam Broe and all the staff at the Department of Power and Propulsion is very much appreciated.

I would also like to thank Mattia, Guido, Luismi, Pavlos, Costas, Jacinto, Javi and all my friends whom I met at Cranfield University for the wonderful time I had. Please, stay all in touch.

My family have always backed me during the time when I worked on my PhD, for which I am very thankful.

This thesis is devoted to Lama, the love of my life and woman on my side.

Table of Contents

List of Figures

List of Tables

Nomenclature

Symbol	Description	Unit
a	Area	m^2
AFR	Air to fuel ratio	-
C	Technology parameter	-
CFD	Computational fluid dynamics	-
c_p	Specific heat	-
c_v	Specific heat	J/(kg K)
Δ	Difference operator	-
η_0	Overall efficiency	-
F_s	Specific thrust	N/(kg/s)
γ	Ratio of specific heats	-
IC	Internal combustion	-
HR	Enthalpy ratio	-
L/D	Lift to drag ratio	-
M	Mach number	-
$\dot{m}$	Mass flow	kg/s
n	Cycle speed	1/sec

NO_x	Nitrogen oxides	-
OPR	Overall pressure ratio	-
P	Total pressure	N/m^2
p	Static pressure	N/m^2
pf	Purge fraction	-
PR	Pressure ratio	-
q	Heat, fuel net calorific value	J/kg
RF	Radiative forcing	W/m^2
SFC	Specific fuel consumption	(kg/s)/N
t	Static temperature	K
T	Total temperature	K
TET	Turbine entry temperature	K
TRL	Technology readiness level	-
U	Internal energy	J
v	Velocity	m/s
V	Volume	m^3
VR	Compression ratio	-
ε	Polytropic/isentropic efficiency	-

1 Introduction

For a long time throughout human history, the dream of flight, the desire to disobey the law of gravity and develop the ability to disconnect from earth, had remained a vision. Although flight could be observed in other animals, such as birds or insects, humans were not equipped with the necessary physical features to overcome the laws of gravity on their own and were hence bound to the ground.

Therefore, flight was regarded to be an ability beyond human nature. The desire to overcome the limits imposed on men has led to the stylisation of flight as means to deal with human inability. This inability can lead to lethal outcomes, which our earliest possible ancestors were already aware of. It is believed that humans' worst reoccurring night dream, which is a falling person, roots from the prehistoric world of our genetic ancestors where falling from a tree would most certainly imply a fatal outcome[1].

Stylisations of flight can be found in almost every culture in its various forms, where they can play a central part in myths, legends or religions. The capability to penetrate into to humans inaccessible space, towards the sky, was given to winged creatures only existent in the fantasies of men. Angels, fairies or dragons were invented to provide projection grounds for human desires and inspired men throughout history with remarkable results. Take scientist and inventor Robert Goddard as example, who climbed a cherry tree on October 19th, 1899, age 17, and became transfixed by the sky. He later developed essentially all aspects of the modern rocket. His memoirs read:

"On this day I climbed a tall cherry tree at the back of the barn . . . and as I looked toward the fields at the east, I imagined how wonderful it would be to make some device which had even the possibility of ascending to Mars, and how it would look on a small scale, if sent up from the meadow at my feet. I have several photographs of the tree, taken since, with the little ladder I made to climb it, leaning against it. […] I was a different boy when I descended the tree from when I ascended. Existence at last seemed very purposive[2]."

With symbolic uniformity across the various cultures, the ability to fly implies freedom and supernatural power. Therefore, flying creatures often have metaphysical or supernatural attributes and were given the position of heroes and gods. Relicts of developed ancient cultures dating back as long as 5,000 years ago, such as shown in Figure 1, demonstrate the importance of flight in a religious context; and this has not changed: "And look into space; you shall see Him walking in the cloud, outstretching His arms in the lightning and descending in rain."[3]

Figure 1: Horus, a flying god of the Ancient Egyptian religion, was an important deity symbol of power.

As the idea of flight developed in the peoples' minds over centuries, the desire for flight went beyond stylisation only. Attempts to achieve human flight can be found throughout history. By at least 549 AD paper kites were flown in ancient China[4], paving the way for human flight. However, it took almost another one and half millennia until the Wright brothers accomplished the first sustained and controlled heavier-than-air powered flight capable of carrying a human being.

Today, when this sentence is written, we are writing the year 2011; the centenary of British Powered Flight has passed. Aviation became one of the modern economy's prime movers; it connects cultures and continents and sits at the heart of globalisation. We see millions of airline passengers carried by aircraft every day, a highly developed infrastructure, and military aircraft operating in conflict zones. Aircraft have evolved to the most sophisticated man made machinery ever built, combining various scientific and technological disciplines in a single unit.

Humans are equipped with a brain of disproportionally large capacity that makes it possible to absorb their natural environment in a different way compared to other living species on this planet. While predominantly instinctive behaviour can be found in animals, humans are conscious observers of the reality, constantly trying to comprehend it and attaching meaning to it. During that process, humans discover that they live in a world where beauty and terror, birth and death, creation and destruction coexist. Facing the terrors of nature, they enter an existence dilemma, causing perplexity and helplessness[5].

As a result, reality becomes overwhelmingly incredible and incomprehensible and imposes an experiential burden on individuals: they do not know why they were born, what they are doing on this planet or what they are supposed to do. Their own existence is incomprehensible to them, miraculous like the rest of their natu-

ral environment[6], which, following the anthropic principle[7], is a result of many coincidences that happen to have favoured the emergence of reality as we know it and with it the human race.

Humans do not want to admit to themselves that, ultimately, living species, including human beings, are nothing else than, to put it in Richard Dawkins' words, survival machines for DNA embedded in complex proteins structures that form a living organism[8]. The human being is struck by the ambivalent nature which has been imposed onto him. On the one hand, he is conscious, apparently equipped with the luxury of a free will. On the other hand he shares his destiny of death with all other terrestrial creatures. It is the godlike that people is ambivalent about, fascinate by and fearful of, motivated to and defensive against[9].

Humans develop coping mechanisms and defence techniques to protect themselves from becoming conscious of the unpleasant and dangerous truths[10]. These defence techniques support an illusion of equanimity that becomes the basic driving force of individuals. They have the purpose of spurring the illusion of superiority and control over their natural environment. Humans are driven by things that help them to generate a second reality with a human meaning. Creating challenges which they are able of controlling by defying them[6], humans fashion an ideology of self-justification, a heroic dimension that is life itself to the symbolic animal[6].

As means to transform the threatening reality, the human being invents cultural contrivances that serve as self-hypnotic devices to fascinate himself with the powers of transcendence over natural reality[11]. The artist creates a second reality by swallowing his natural environment, digesting it and throwing it up again in the various forms that we call art. The joy and pain he witnesses in life are expressed through his art, and his peers take advantage and use it in defiance of their animal

condition. Religion provides another pillar of self delusion. It gives life a purpose by putting a god above it and, as common in most religions, promise eternal life, taking away the fear of death. The left-brained scientist tries to master reality by developing descriptive abstractions that represent reality in human language. Although not in control of reality, the scientist is at least rewarded with the illusion of being able to understand it. Technology provides the illusion of overcoming nature, freeing humans of their complete dependence. The designer benefits from the experience of building a device that defeats nature and the one applying technology obtains the skills of directly defying it.

If challenges keep the individual alive, what is more of a challenge than overcoming the fundamental laws of gravity that kept him on Earth since his origin about half a million years ago - in other words: flight? Equipped with their natural features, humans are limited to traversing the planet in two dimensions only. Although a third dimension can temporarily be added by going under water, rising towards the sky has somewhat more heroic than trying do conquer the deep sea, which, as humans being a child of the ocean, would be step backwards in evolutionary terms.

The ability to fly is the gateway to heaven, inspires the artist, challenges the scientist and keeps the technologist occupied. The aeronaut catapults himself in a ruling position, giving him the illusion of being in control, facilitating transcendence over nature in a dimension that has never been achieved prior to the advent of human flight. While the philistine abuses flight to distract him from reality, the strong introvert can find satisfaction while exploiting flight for military purposes. Having discovered that aircraft serve well as troop carriers, surveillance vehicles or bombers, the one in charge over such machinery can gain immense power. Al-

though still far from being able to act like a god, he can at least destroy like a god, as has been demonstrated by military powers and dictators of this planet. However, despite its destructive potential, flight can have a more romantic touch when it provides the bridge to overcome large distances, connecting the traveller with unknown and heavenly territory.

Flying machines have become the synonym for ultimate transcendence over nature. They stand for hope and destruction in conflict zones, serve the egos of their military and civil operators in its own ways, go hand in hand with wealth creation and satisfy melancholic desires further adding to their mystic. Being amongst the most complex manmade machines, they are beyond the technological understanding of the majority of the population, causing respectful admiration and miraculous amazement.

Today, it is generally acknowledged that commercial aviation is amongst the principal enablers for a global economy and the ongoing globalisation and brings intrinsic value and quality of life improvements to the society. It is suggested that aviation may account for as much as 8% of the global gross domestic product when tourism, probably the world's largest industry, and air cargo is taken into consideration[12].

Although the aeroplane holds the pole position in terms of specific energy demand of all modes of transport[13], since the emergence of jet engine powered commercial aeroplanes, advances were of incremental nature in both airframe and engine technology and have contributed to the improvements in the fuel efficiency and reductions in emissions of aircraft. The aerospace community recognises that the current growth rates in air traffic will increase the contribution of aircraft emissions to global warming and that the rate at which aircraft fuel efficiency is im-

proving is not offsetting emissions associated with growth in air traffic. Furthermore, increasing fuel prices and declining natural energy reserves add to the pressure to reduce fuel consumption and hence more radical technological approaches are sought to facilitate long term sustainability in the aviation industry. It is acknowledged that due to maturing technology levels, more radical approaches of disruptive nature are required in both airframe and engine technology to achieve more drastic long term fuel efficiency improvements.

The objective of this study is to examine unconventional engine architectures that enable fuel efficiency improvements in jet engines. Current jet engines are based on the Brayton cycle, where the working fluid successively experiences isentropic compression, isobaric increase in temperature, and isentropic expansion. Deviations from the ideal cycle in real engines occur through component inefficiencies. The maximum achievable thermodynamic efficiency of the Brayton cycle increases hand in hand with its peak cycle temperature. Since the peak cycle temperature is limited by material properties of the turbine, the maximum cycle efficiency of current jet engines is limited by the laws of thermodynamics. Hence, efficiency improvements of jet engines beyond what is possible with conventional designs are only feasible through unconventional cycles that incorporate features such as constant volume combustion.

Several technologies enabling novel cycles for aircraft propulsion have been identified. They include wave rotor, pulse detonation and internal combustion. This study focuses on hybrid turbofan cycles designs incorporating these technologies.

1.1 The Jet Engine

The enabling technology for modern flight is the jet engine, derived from gas turbine technology. The jet engine is a prime example of a disruptive technology. Disruptive technologies are innovations that change the rules of the game, introducing a new value proposition. They do not have to outperform the technologies they seek to replace, but they must offer some new, valuable feature that will justify their implementation. If enough momentum can be gathered, the new disruptive technology will evolve to replace its predecessor[14]. In the late 1920s, Frank Whittle, an RAF officer, became interested in high altitude, high speed flight. He saw it as the key that would enable aviation to grow further, providing safer, faster and more comfortable travel above the weather. Whittle concluded that incremental improvements in existing piston propeller configurations were unlikely to enable flight at higher altitudes and speeds, and this conclusion led him to begin the development of what would eventually become the first jet engine[15].

Early jet engines performed poorly compared to the well established piston engines of the time. However, they opened the door to faster air travel at higher altitudes, allowing passengers to fly above the weather and resulting in shorter, more comfortable trips. These advantages allowed the jet engine to replace the piston engine as the prime mover of choice for civil aircraft. The jet engine made air travel accessible to ever growing numbers of passengers and the initial fuel consumption, reliability and cost issues were overcome. The form of air travel that we enjoy today has come about through a combination of technological leaps and bounds and relentless research and development to improve performance, enhance safety and comfort, and reduce the cost of air travel (see Figure 2).

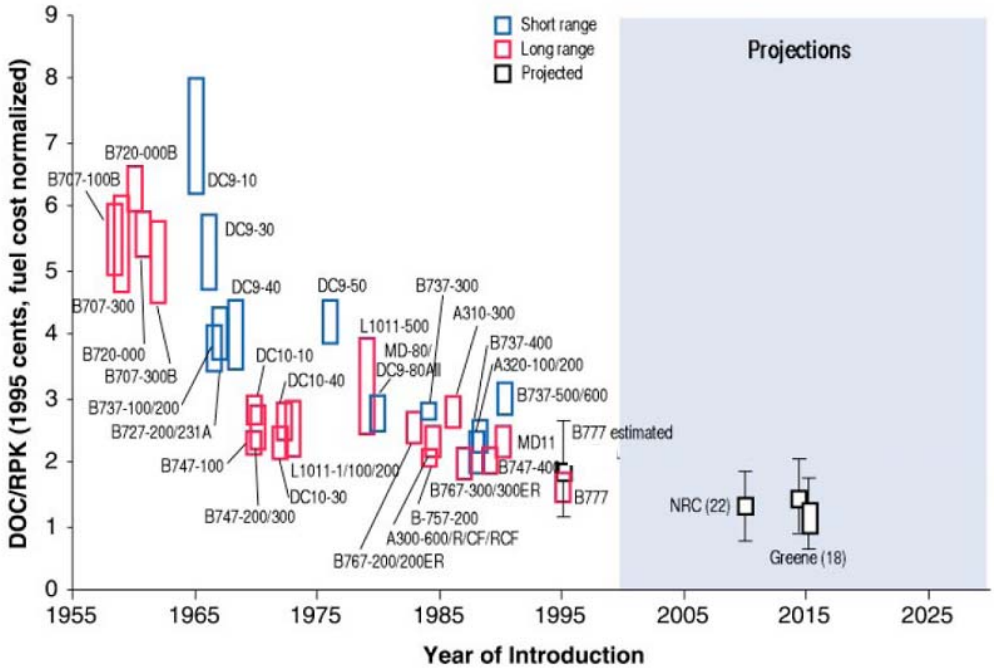

Figure 2: Historical trends in direct operating cost per revenue passenger-kilometre for short and long-range aircraft.[16]

Fuel consumption of aero gas turbines depends on two main parameters: thermal efficiency and propulsive efficiency. The former is a measure of how well the engine converts heat energy, and the latter describes how well the engine uses the kinetic energy of the jet to generate thrust. High thermal efficiency requires a high overall pressure ratio between air entering the jet engine and air in the combustion chamber, high component efficiencies, for example how efficiently a compressor stage compresses air, and a high turbine entry temperature. The propulsive efficiency depends on jet velocity. The higher the jet velocity the lower the propulsive efficiency as kinetic energy is dissipated in the engine exhaust.

The different design parameters have evolved over the years to meet different challenges in a quest for lower fuel consumption, weight, costs and environmental

issues[17]. Increasingly high turbine entry temperatures, the advent of the high by-pass ratio turbofan and improvements in component efficiencies were the main enabling technologies to meet these challenges. Investments have resulted in high temperature resistant materials and improved turbine cooling techniques. Whereas the turbine entry temperature of early engines only reached about 1,200K, today's turbofans operate with turbine entry temperature approaching 2,000K (see Figure 3).

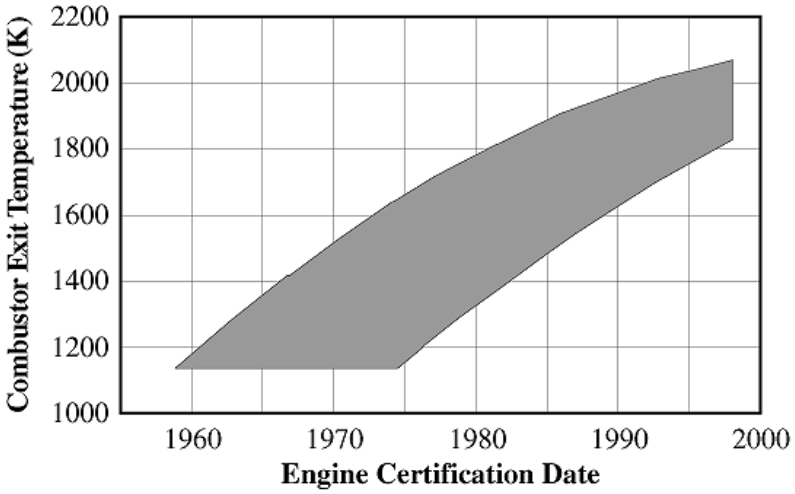

Figure 3: Combustor exit temperature trend with time.[18]

Considerable research has been undertaken to improve major components in the engine 'gas path'. Initially, the efficiency and weight of components were improved by means of experimentation, but high performance computing marked the advent of computational fluid dynamics, which allowed detailed simulation and optimisation of components for example to design fan blade geometries capable of higher pressure ratios. The cumulative effect of these efficiency improvements has

been very significant and resulted in an increase in thermal efficiency of jet engines.

The propulsive efficiency can be improved by increasing the gas turbine's bypass ratio. However, this would result in an increase of the overall diameter of the engine, resulting in fan cowl drag and weight increase that eventually offsets the advantages offered by a higher propulsive efficiency. It is expected that installed fuel efficiency improvements peak for a bypass ratio of 20. Increasing the bypass ratio further is likely to show adverse effects[19,20]. More innovative nacelle design and approaches to minimise installation penalties could provide the solution to allow further improvements. For a bypass ratio above 20, however, other propulsor technologies are required such as open rotors or distributed propulsion.

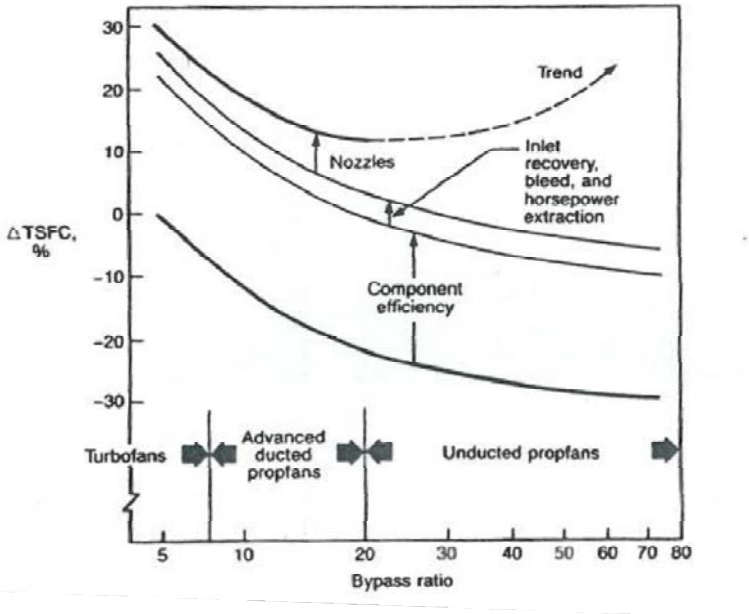

Figure 4: Specific fuel efficiency versus bypass ratio taking into account friction losses of cowlings and nacelles[19,20].

As shown in Figure 5, open rotors and high temperature technologies could bring about a 30% improvement in fuel consumption compared to current technology level but improvements in engine efficiency are ultimately constrained by physical laws, the stoichiometric turbine entry temperature and open rotor propulsive efficiency. The theoretically achievable maximum overall engine efficiency of conventional cycles is about 55%.

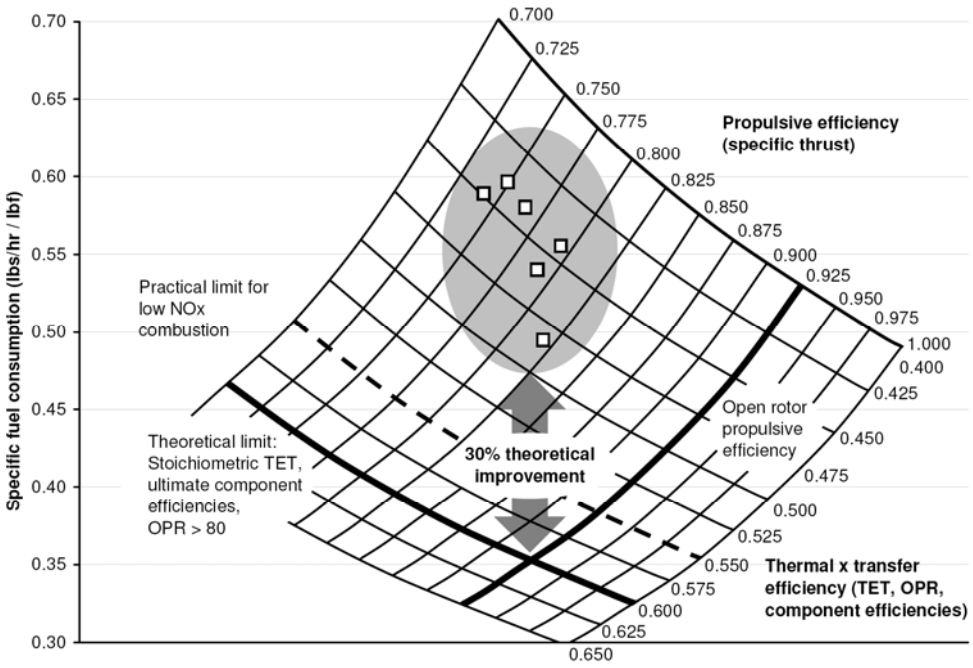

Figure 5: Specific fuel consumption of current engines as it relates to thermal and propulsive efficiency[21].

This fact represents the dilemma of the aerospace industry today: every improvement in engine efficiency is a step toward the maximum achievable overall engine efficiency. As this value is approached, the law of diminishing returns sets in: im-

provements become more and more difficult to achieve, and take place at subsystem level with larger time spans between equivalent amounts of efficiency gains. Larger research and development spending is required for ever smaller improvements, reducing profit margins in an effort to remain competitive.

Figure 6 offers a view of the evolution in gas turbine fuel consumption from 1960 to present day. Large improvement in the early years, partly due to the adoption of the turbofan can be seen, and a constant reduction in fuel consumption ever since. Research and development programmes today are looking at concepts that could lead to step fuel efficiency improvements. In the short to medium term, we might see open rotor configurations emerge. Medium to long term solutions may exhibit a more disruptive character than short term solutions, as more time for development is available. However, long term solutions could require more radical innovations, such as the application of wave rotor, pulse detonation or internal combustion cycles.

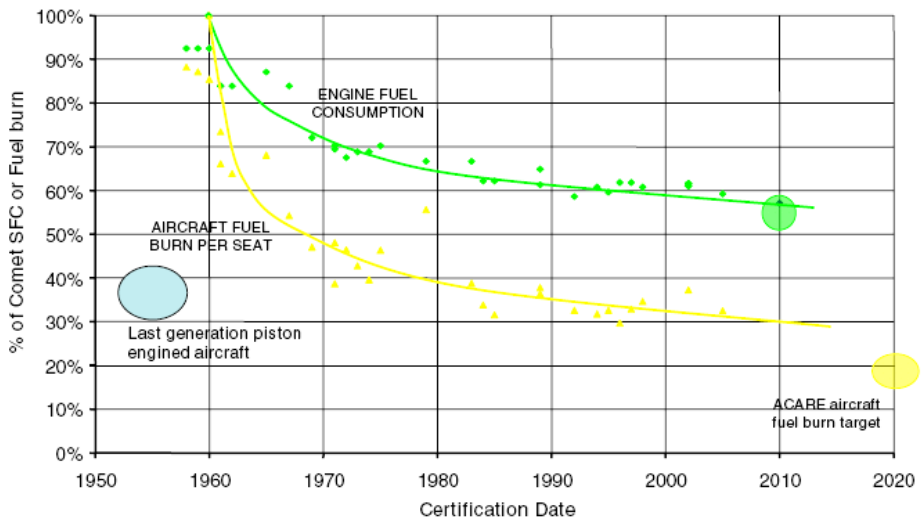

Figure 6: Fuel efficiency development of gas turbines[22].

2 External Factors

2.1 Climate Change

Whilst speed, range and comfort were the primary drivers in civil aviation in the early 20th century, the picture has changed with the dawn of the new millennium[23]. Two concerns are now drastically increasing the need for fuel efficient technology over the past decade: depletion of natural fuel reserves and climate change, also known as global warming. Scientists fear that with ongoing levels of current greenhouse gas emissions, global temperatures could increase by several degrees by the end of the 21st century.

Global warming is caused by solar radiation being absorbed by the planet's atmosphere and surface and converted into heat energy. The natural occurrence of greenhouse gases results in equilibrium conditions where terrestrial infrared radiation is offset by incoming solar radiation, and the energy fluxes of the ingoing and outgoing radiation are approximately equal on average, keeping the planet at a habitable temperature. So called pollutants, which can be of human origin or natural, for example resulting from volcanic eruptions, such as carbon dioxide, impose a perturbation on the equilibrium state by absorbing additional solar radiation which converts into heat energy. The amount of energy absorbed is generally denoted by radiative forcing[24], which is the amount of radiation forced to remain within the 'Earth system', i.e. the atmosphere, oceans and soil. As more and more heat is absorbed, the Earth's temperature increases. A temperature rise will then occur, continuing until the outgoing and the ingoing radiation are in equilibrium again.

The expected temperature change due to a certain pollutant depends on the strength of its radiative forcing. A positive radiative forcing will cause a temperature rise, whereas a negative radiative forcing will cause a temperature drop by shielding the Earth from incoming radiation. Furthermore, the temperature change is also determined by a pollutant-specific climate feedback parameter. It can be understood as a gain factor, accounting for three-dimensional atmosphere-ocean feedback mechanisms such as cloud or sea ice formation. The feedback parameter determines how effective the radiative forcing of the pollutant is and over what time period the temperature rise will take place.

Carbon dioxide is the dominant mode through which carbon is constantly transferred in the natural environment between a variety of carbon reservoirs (see Figure 7). Burning fossil fuels, representing one reservoir, implies taking carbon from beneath the Earth's surface, converting it to carbon dioxide and emitting it into the atmosphere - a process which can take up to 100 years. Atmospheric carbon dioxide is absorbed by natural carbon dioxide sinks such as oceans or plants, which take up carbon and facilitate the formation of carbonates and forests. The process of carbon transfer between carbon reservoirs is referred to as the 'carbon cycle'.

The consequences of additional carbon dioxide in the atmosphere, causing a global temperature rise, are projected to be devastating: sea level rise, frequency and intensity of extreme weather events, changes in agricultural yields, or an increases in the ranges of disease vectors just to name a few. These consequences might have a catastrophic impact on our society, and current public consensus calls for an urgent reduction to counter act current trends. Although aviation only represents approximately 5% of manmade carbon emissions, projected passenger

and cargo growth rates make it a potential major stakeholder in the drive towards lower emissions, and more environmentally friendly aircraft technology will be required [25].

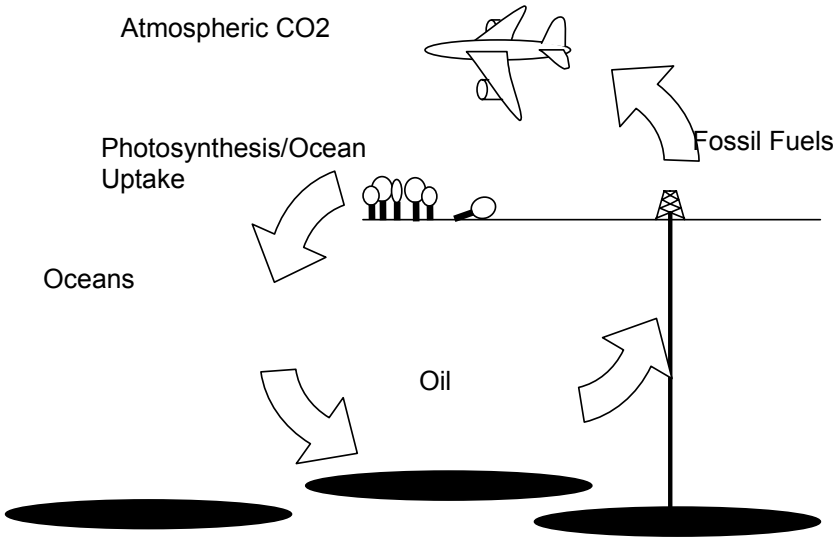

Figure 7: Simplified schematic of the carbon cycle.

However, carbon dioxide is not the only pollutant resulting from air traffic, and the fact that pollutants are released in areas of the atmosphere where their impact is potentially worse than at sea level results in technology trade-offs due to the different pollutants and their impacts. For example, higher turbine entry temperatures in aircraft engines result in higher thermal efficiencies and less carbon dioxide emissions, but also cause an increase in the emission of nitrogen oxides. These contribute to the formation of ozone in the upper troposphere and decrease the concentration of methane, another greenhouse gas, implying a cooling of the atmosphere. Both effects, tropospheric ozone formation and methane depletion, ap-

proximately cancel each other out. Nevertheless, stratospheric nitrogen oxide emissions facilitate a reduction of ozone where it is needed to shield earth from highly energetic cosmic radiation. When emitted at low altitudes, e.g. in the vicinity of airports, nitrogen oxides exhibit additional environmental and health hazards. Nitrogen oxides can react to form nitric acid that can penetrate into sensitive lung tissue and causes severe health damage and premature death in extreme cases. Inhalation of such particles may cause or worsen respiratory and heart diseases.

Water, which in its vapour phase is a relatively strong greenhouse gas, is also a combustion product. Water emitted by aircraft precipitates relatively shortly after emission, whereas stratospheric water can have longer residence times and hence cause radiative forcing, even though it is marginal compared to other aviation pollutants.

Alleviated atmospheric aerosol concentrations caused by air-traffic are relatively small compared to the contribution from surface sources. Soot emissions tend to warm the atmosphere, whereas sulphates have an opposite effect. Compared to other aircraft emissions, the direct radiative forcing of soot and aerosols is relatively small. Aerosols also play an important role in the formation of cirrus clouds that would not form in the absence of aviation, resulting in enhanced cloud formation and the modification of the radiative properties of natural cirrus clouds.

Contrails are artificial clouds composed of ice crystals. They form in the aircraft wake if water saturation occurs during the mixing process of the engine's exhaust gases with ambient air. An analogy can be found by comparing the formation of contrails to human breath in a cold winter day, which can become visible in the form of steam. Contrails can persist in the atmosphere if it is ice-supersaturated.

Due to the shape and size of contrail ice crystals, contrails reflect incoming solar radiation to a lesser extent than terrestrial infrared radiation. As a result, heat energy is trapped in the atmosphere below the contrail. Although radiative properties of contrails vary depending on the ambient conditions, occasionally even leading to local cooling of the atmosphere below the contrail, the average effect of global contrail occurrences is a net contribution to global warming.

Moreover, dependent on ambient conditions, line-shaped persistent contrails can spread to form large-scale cirrus clouds, so called contrail cirrus. Since they cover much larger areas than line-shaped contrails, and thus trap more heat in the atmosphere, it is estimated that their environmental impact is larger than that of line-shaped contrails. Furthermore, locally alleviated atmospheric soot and aerosol concentrations due to air-traffic can initiate water nucleation, leading to the formation of so called secondary cirrus clouds. These clouds, with radiative properties similar to those of contrails, also contribute to global warming. It is important to note that they would not form in the absence of air traffic[26,27].

Climate assessments have emphasized the environmental impact from persistent contrails and contrail cirrus. Their radiative forcing might already exceed the radiative forcing from all other air-traffic pollutants combined.

The consequences of climate change are far reaching and are predicted to affect the world's population in its various forms. The predictions are based on numerical models, which are accurate within the boundaries provided by large scale computational climate simulations and results depend on the various simplifying assumptions made and emission scenarios used.

Climate models suggest that the increase in global temperatures will result in decreasing arctic summer sea ice, which will allow more shipping and mining on the one hand, but the landscape of which indigenous peoples were once an integral part will diminish. Some mountain glaciers reduce in size and some are predicted to disappear.

Various factors affect the volume and mass of the world's oceans which can lead to long term changes in the sea level. The two primary factors causing a rise in sea level are global temperature change due to the temperature dependent volumetric density of water, and the amount of water stored on land and also sea in solid form that would become liquid and flow in the oceans.

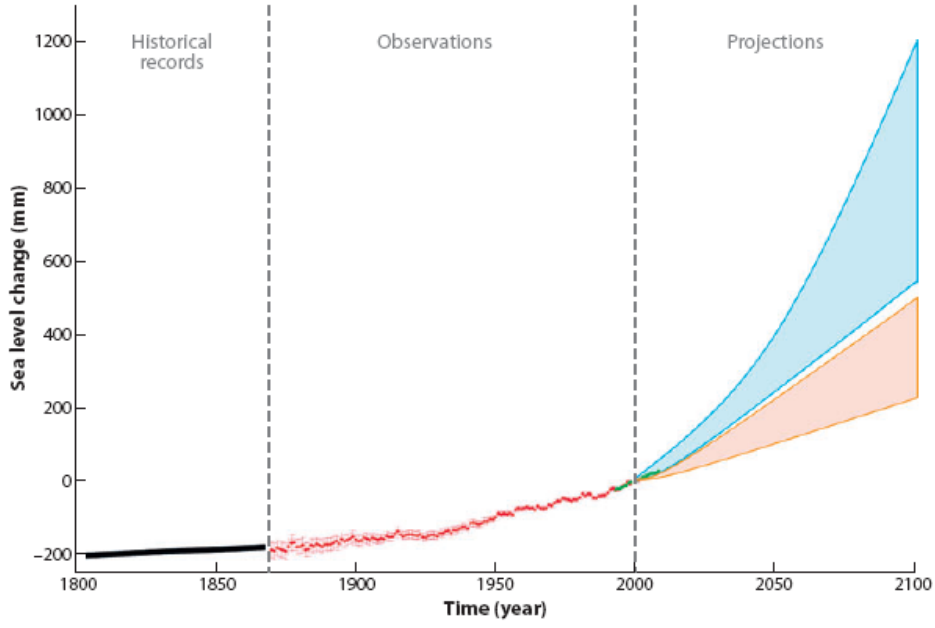

Figure 8: Evolution of the global mean sea level between 1800 and 2100 from observations and model projections[28]. Pink and blue shaded regions include projections from coupled climate models.

Sea level rise predictions by the year 2100 are uncertain and range from 0.2 m to 1.2 m (see Figure 9). While underlying volumetric expansion associated with increasing atmospheric temperatures is less difficult to predict, the behaviour of the Greenland and West Antarctic ice caps and associated increase in water masses of the oceans cannot be predicted with great accuracy. As a result of rising water levels, coast lines will travel in land and river deltas will be flooded, whereas the societal impact is predicted to be more severe in case of river deltas as replenishing sediments become increasingly held up by irrigation, hydropower production and flood-control projects.

Tropical cyclones, which can cause damage in costal areas by pushing water inland, may become less frequent. However, the occurrence of more destructive hurricanes is likely to increase. Warmer oceans may suffer from coral bleaching caused by increasing water temperatures whereas reefs currently immersed in colder water will experience an increase in water temperature and may thus be colonised by new corals. Both will have an impact on fishing and tourism, which will be to the disadvantage of the nearby population that is now benefiting from coral reefs, populations nearby emerging coral reefs will benefit. The increasing concentration of atmospheric carbon dioxide will lead to ocean acidification but impacts are uncertain.

It is predicted that shifting precipitation patters will result in the drying of already dry places such as southern Africa and the south-western United States. Places that are already wet, such as much of South-East Asia, are likely to get wetter. In colder areas especially in the northern hemisphere, some land will become more suitable for farming whereas in the tropics and subtropics some marginal land will become barely inhabitable. In general, the increase in average temperature will be

less noticeable than extreme cases. Figure 9 showing the probability of a summer warmer than the warmest on record suggest more extreme temperatures across the globe.

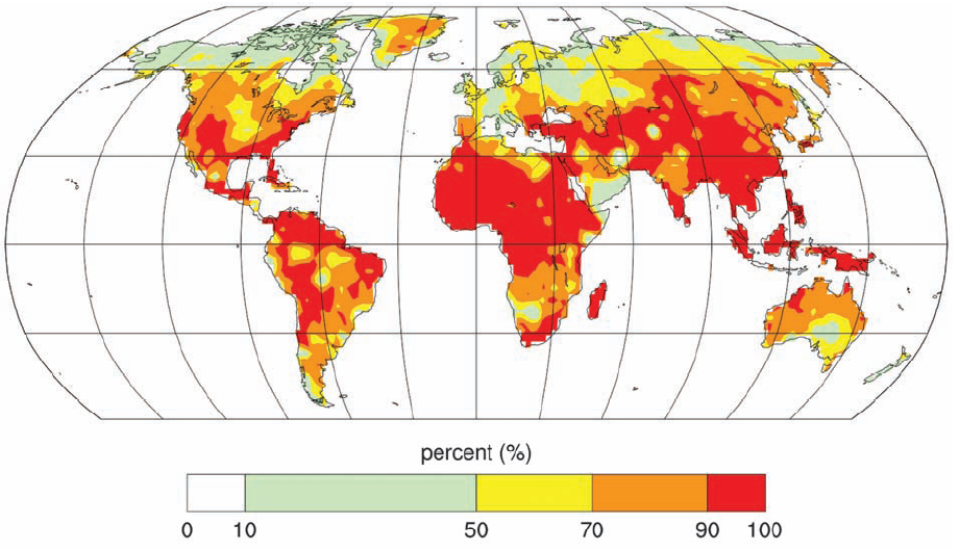

Figure 9: Probability in percent that future summer average temperatures will exceed the highest summer temperature observed on record in 2090[29].

The list of possible impacts climate change will have and the resulting socio economic consequences could be continued. Undisputable is that temperature records show a global warming by approximately 1K between the 19th and the 20th century. Figure 10 shows the global near surface air temperature record 1880 until 2010. Every year since the year 2000 has been warmer than any but one, 1998, of the years during the 20th century (see Figure 10). The emission of more carbon dioxide will further increase atmospheric carbon dioxide concentration and increase the global temperature.

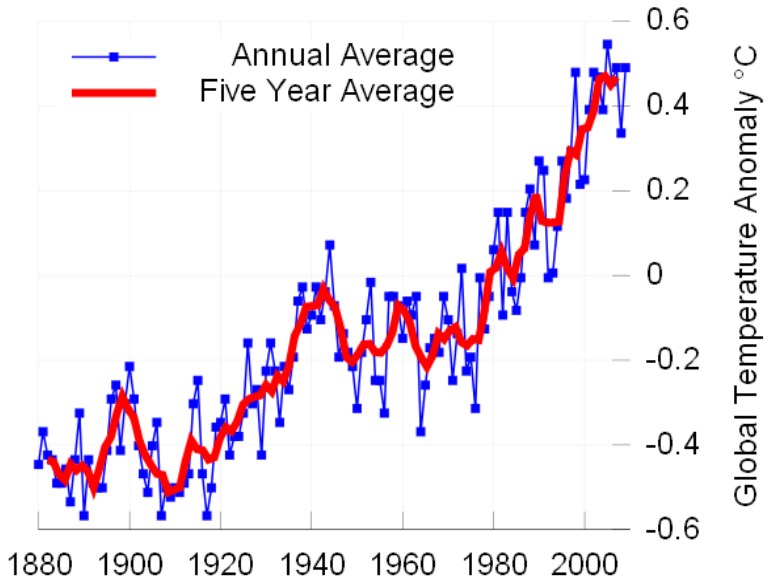

Figure 10: Global near surface air temperature record 1880 until 2010 [30]. Following the common practice of the IPCC, the zero on this figure indicates the mean temperature from 1961-1990.

International efforts to curb carbon emissions did not have the desired effects and continued to increase rather than decrease. It is predicted that even if carbon dioxide levels in the air could be maintained at current levels (currently almost 390 parts per million, 40% more than before the industrial revolution) the world's atmosphere would probably warm by a further half a degree due to oceanic feedback mechanisms over the next decades. However, carbon dioxide emissions continue to rise despite 20 years of climate negotiation (see Figure 11).

In an attempt to reduce carbon dioxide emissions, delegates from 194 countries came together to find a solution at Cancún climate conference in December 2010. The introduction of Copenhagen accord was debated in a sequence of summits over several years and eventually adopted by all participating parties. In essence,

the Copenhagen accord is a non-binding document which aims to keep the temperature increase by 2100 not more than 2°C above pre-industrial averages.

This is, however, a matter of debate. The World Energy Outlook calculated a 3.5°C increase by 2100 if emissions were curbed according to the 'new policies scenario' incorporated in the accord[31]. The new policies scenario requires a 2.8% reduction in carbon dioxide emissions in the coming decade and a 5.5% rate thereafter until 2035. It is the opinion of many scientists, campaigners and policymakers, that two degrees is a wishful dream and unlikely to become reality.

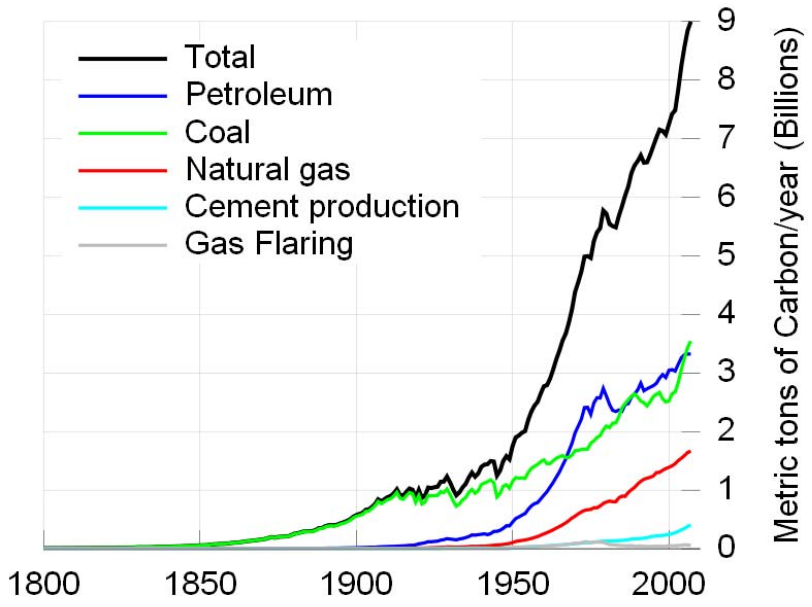

Figure 11: Global, anthropogenic Carbon emissions[32].

As it seems that a more significant increase of global mean temperatures becomes inevitable, it will be required to develop means to adapt to e.g. scarcer water, higher peak temperatures and higher sea levels. Even though these measures will

help reducing the socio economic impacts, they will not protect everyone from all harm that climate change may bring. Besides intensified research into improved crop yields and higher tolerance of temperature and water scarcity, programs for disease control, improving and conserving soil, cropping patterns and crop-management techniques may be required. This will ensure that enough food for the projected 9 billion planet's inhabitants can be produced under the new circumstances without much of the planet's remaining uncultivated areas being turned into farmland.

While the developed countries are more likely to be able to afford and provide resources to adapt to climate change, poor countries will often lack the financial means, technical expertise or political institutions necessary for such endeavours. In addition, they may often be at increased risk due to their dependency on farming and agriculture, principally because they are usually more dependent on farming than rich countries, and no other human activity is so intimately bound up with the weather. Crop yields are sensitive to changes in patterns of rainfall and peak temperature, as well as to average temperature and precipitation; so are the pests and diseases that attack them.

2.2 World Energy Reserves

Climate change and its consequences are not the only reason why the consumption of fossil fuels should be reduced or even abandoned. The world's reserves of fossil fuels are diminishing due to their continuous exploitation. With an estimated $1.33\ 10^{12}$ barrels of global oil reserves[33] and assuming a daily oil consumption of $85.1\ 10^{6}$ barrels[34], the world's oil reserves are estimated to last until 2054, or for another 43 years (if you read this in 2011). This assumes no increase in oil

demand by then; but the reality will probably be that oil consumption will peak at some point in the future before gradually declining as oil reserves diminish and their exploitation becomes increasingly expensive.

With diminishing natural oil reservoirs, aircraft fuel could be synthesised from charcoal via synthesis, which is a range of chemical processes: in the first step syngas, which is a mixture of carbon monoxide and hydrogen as, is obtained from coal through high temperature gasification with oxygen and steam. Subsequent Fischer-Tropsch synthesis converts the mixture of carbon monoxide and hydrogen into liquid hydrocarbons, which could be turned into aircraft fuel.

With an estimated 826 10^9 tonnes global coal reserves, and an annual consumption of 5.7 10^9 tonnes[33], the world will run out of coal in 144 years from 2011. Again, this assumes global coal consumption remaining at 2009 levels, which is unlikely to occur in the real world.

On the other hand, above estimates may be too high by several factors as a decrease of global energy demand and substituting fossil fuels with renewable energy sources or nuclear reactors will reduce the demand for fossil fuel. However, considering the range of scenarios and possibilities, there are many reasons to believe that mankind can expect a serious shortfall of fossil fuels within the next 2-4 generations and precautionary actions should be taken to avoid worst case scenarios. This time period is approximately similar to the time that has passed between the Wright Brothers have undertaken their first heavier-than-air flight with Kitty-Hawk and this sentence was written.

Aircraft engine design engineers are faced with the challenge to reduce the fuel consumption of jet engines over time. This is achieved initially through step

changes and incremental improvements of existing designs. These changes are associated with low risk as they are based on proven practice. However, these incremental improvements will increasingly require disproportionally larger investment and are eventually restricted by the laws of physics. The law of diminishing returns will cause a shift of attention towards technologies with larger long term potential. The risk of introducing a new technology, which is a measure of the amount of investment required and probability of success, is outweigh by the diminishing advantage the existing technology exhibits. For example, investment in existing engine technology to achieve a limited improvement in performance of existing technology could be used instead to develop far superior technology. If the investments become equal then there will be a time that the change to more disruptive technologies is considered.

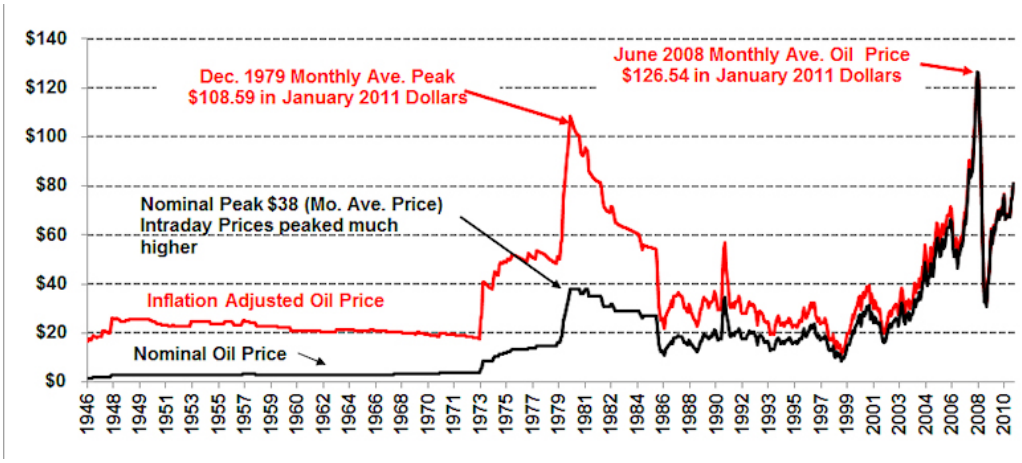

Figure 12: Inflation adjusted monthly crude oil prices (1946 – 2011) in June 2010 US Dollars[35].

The trigger for the change may well be external circumstances, such as economical advantages, war or natural threads. As long as people have the feeling that natural resources are abundant and that climate change is not a direct thread, investing in new technology may be seen as unnecessary. In the meanwhile, possible disruptive technologies are being invented and developed.

"Most people are unwilling to spend a lot of money to a future problem, especially when the outcome is uncertain. One good reason for waiting is that there will be less costly options available in the future"[36].

As fossil fuels become less abundant and more expensive (compare with Figure 12) and effects of climate change are posing a more direct thread to humans, more disruptive solutions are becoming introduced, which will lead to new engine configurations where eventually alternative energy sources are used once a revolution in fuel infrastructure has taken place[37].

3 Computational Model

A computational model was created to calculate the theoretical performance of various thermodynamic cycles in order to facilitate a comparison. The performance of jet engines can be measured by indicators such as specific fuel consumption (SFC), specific thrust (F_S) and the overall efficiency (η_0).

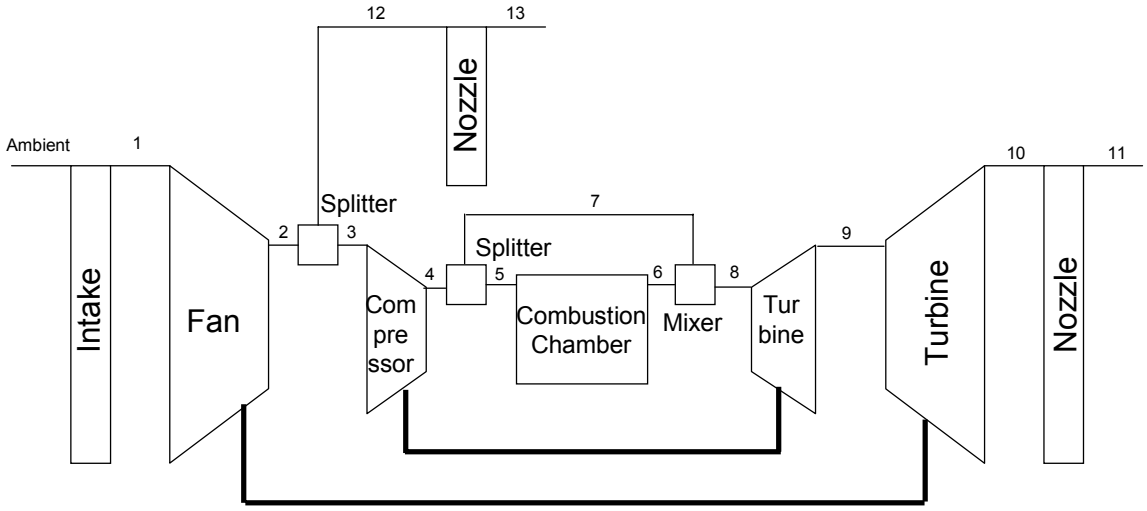

Figure 13: Representation of the mathematical model.

The performance parameters are indicators of the fuel efficiency and size of the engine. The specific fuel consumption denotes the mass unit of fuel consumed per mass unit of propulsive force generated. The overall efficiency is a measure of how efficiently the chemical energy stored in the fuel is converted into useful energy utilised for propulsion. The higher the specific fuel consumption, the lower the overall efficiency. The specific thrust denotes the mass unit of thrust generated by the engine per mass unit of air passing through the engine. For a given thrust

requirement, lower specific thrust indicates more air to pass through the engine resulting in larger engine dimensions.

Underlying to the computational model is a mathematical model which was derived from thermodynamic relations. The mathematical computer model used in this study represents the design of a two spool jet engine with a bypass and separated nozzles between the bypass and the engine core. A representation of the cycle can be found in Figure 13 and Figure 14 shows the cycle on a temperature-entropy diagram.

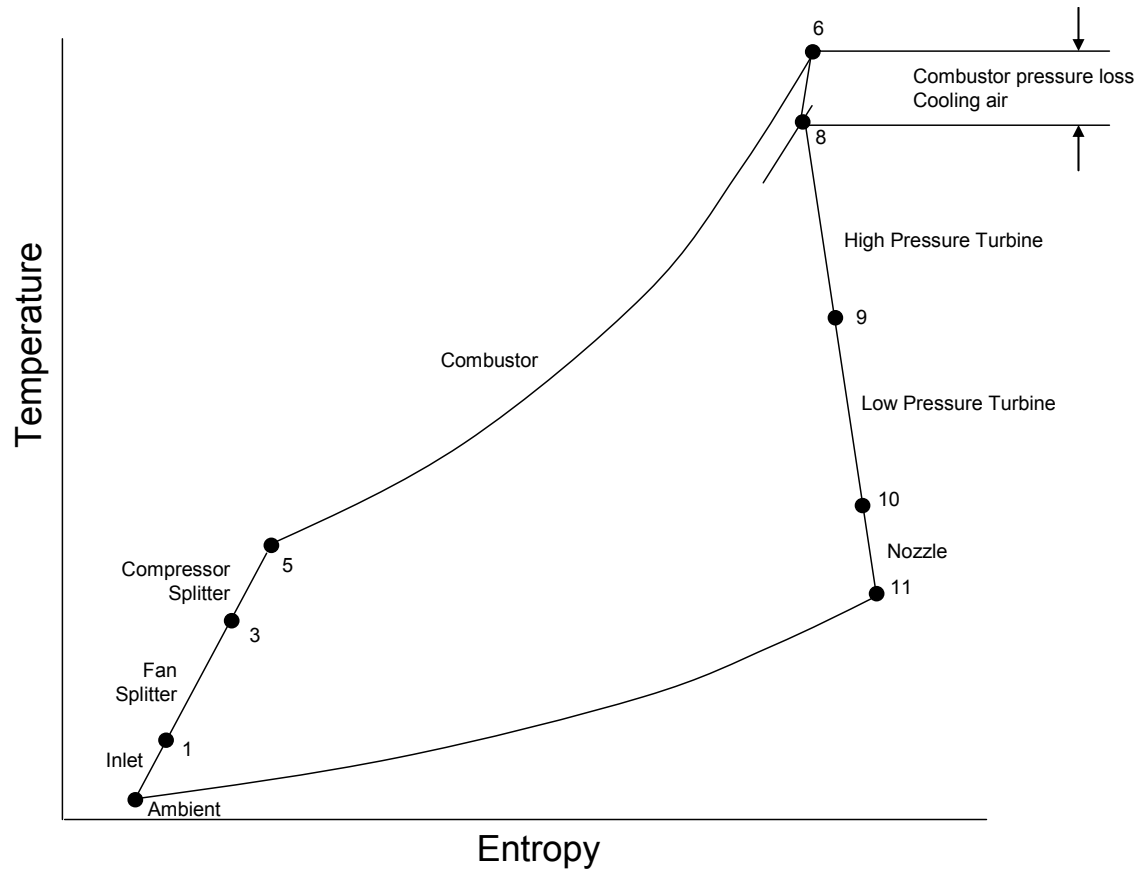

Figure 14: Temperature – Entropy diagram (not to scale) of the mathematical model.

The mathematical model was translated into a computer code to perform the calculations to predict the theoretical performance of the various engine designs investigated in this thesis. MATLAB was chosen as computer language, which is a programming environment intended for numerical computing and which allows the optimisation to obtain a set of engine parameters that result in the best possible fuel efficiency. The computational model was coded with enough flexibility to allow the replacement of the combustor unit of a conventional cycle with different core cycles: wave rotor, pulse detonation and internal combustion.

The computational model incorporates a one dimensional, thermodynamic description of the engines' gas paths. As the main purpose of the model was to compare the performance of conventional jet engine designs to the performance of unconventional, hybrid designs, constant gas parameters were used throughout all calculations for simplification. The compression and expansion processes in the model are assumed to take place adiabatically and the International System of Units (SI) was used.

Defining cruise altitude, the ambient conditions are calculated from the ISA standard atmospheric model. The cruise Mach number defines the velocity of the air at the diffusor, which decelerates the air relative to the engine before it enters the first compression stage, the fan. This is to avoid supersonic speeds at the tips of the fan blades. The total pressure rise across the inlet occurs due to the ram effect and is calculated from the thermodynamic relations

$$\frac{P_1}{P_a} = \left(1+\varepsilon_{\text{Inlet}} \ \frac{\gamma\text{-}1}{2} \ M^2 \right)^{\frac{\gamma}{\gamma\text{-}1}} \qquad \textbf{Equation 1}$$

where ε_{Inlet} is the isentropic compression efficiency of the diffusor to account for component losses. The total temperature rise across the diffusor is calculated from the following thermodynamic relation

$$\frac{T_1}{T_a} = \left(1+\frac{\gamma\text{-}1}{2}M^2\right) \qquad \textbf{Equation 2}$$

Once passed through diffusor, the incoming air is compressed in two stages before a fraction of it is heated in the combustion chamber.

The first stage is the fan stage, where all of the incoming, decelerated air is compressed. The compression ratio is defined by the fan geometry and rotational speed, which determines the total temperature rise across the compression stage. The increase in pressure across the fan in modern turbofan engines is typically between 1.2 and 1.6 and varies during the flight as thrust requirements change along the mission profile with decreasing aircraft weight, which causes a change in the throttle setting. A change in throttle setting generally causes a change in all processes as including bypass ratio, compressor pressure ratio and mass flow. The temperature rise across the fan and the other compression stage is calculated from the polytropic relation

$$\frac{T_2}{T_1} = \left(\frac{P_2}{P_1}\right)^{\frac{1}{\varepsilon_{Compressor}}\frac{\gamma\text{-}1}{\gamma}} \qquad \textbf{Equation 3}$$

As the compression of the air in turbomachinery is never ideal and occurs with an increase in entropy, for example due to small scale turbulences, the polytropic efficiency ε is used to account fur such losses. The air leaving the fan stage is now partially directed into the bypass duct and the mass flow ratio of the air entering the bypass to the air entering the engine core is defined as the bypass ratio. Further compression of the air in the engine core takes place. As the overall pressure ratio of the engine is defined externally, which is the increase of the total pressure between the diffusor inlet and the combustor, the pressure rise across the core compression stage is defined as

$$PR_{Core} = \frac{PR_{Overall}}{PR_{Fan}} \qquad \textbf{Equation 4}$$

The compressed air leaving the core compressor enters the combustor where the air is injected with fuel, which is burned, and as a result increases the temperature of the air. Although the high temperature combustion of petro chemicals changes the composition of the air in a way that the water and carbon dioxide content is increased and other, secondary components such as for example soot and nitrous oxides, are added, the properties of the hot gases leaving the combustor are assumed to be the same than that of air in this study. Simplified models for gas properties are used as the calculations' primary aim is identifying and comparing trends rather than making accurate predictions. The properties of air used throughout all calculations are given in Table 1.

Constant	Value
Specific heat capacity of air (c_p)	1,000 J/(kg K)
Gas constant (R)	287 J/(kg K)
Ratio of specific heats (γ)	$c_p/(c_p\text{-}R)$
Fuel net calorific value (q_{Fuel})	43E6 [J/kg]

Table 1: Definition of constants in the computational model.

A fraction of the air entering the combustion stage is directed around the flame section and used to keep the temperature of the combustor walls and the turbine blades below the melting point of the material they are made of. The fraction of air used for cooling is typically 5% of the air in the engine core. In the computational model, a total pressure loss is taken into account over the combustion stage, which occurs due to aerodynamic friction within the combustion device and also the momentum changes produced by the combustion process itself. The turbine entry temperature is defined by the throttle setting and knowing the total temperature entering the combustion chamber, the fuel mass flow required can be calculated from

$$\dot{m}_{Fuel} / \dot{m}_{Air} = \frac{c_p \ \Delta T_{Combustor}}{q_{Fuel}} \qquad \textbf{Equation 5}$$

whereas $\Delta T_{combustor}$ is the temperature difference between T_6 and T_5, the temperature at the inlet and the outlet of the combustor.

In the computational model, the mixing of the cooling air and the hot gases exiting the combustion stage is assumed to take place stoichiometrically and adiabatically before the hot gases enter the turbine stages. In reality, the cooling flow would be injected through drillings in the turbine blades to provide a cooling film between the hot combustion gases and the blade itself.

The total pressure and total temperature loss in the turbines is defined by the work required to compress the air in the compression stages. The mechanical power that is generated in the high pressure turbine equals the mechanical power required to drive the high pressure compression stage. From this relationship, the temperature exiting the turbine is calculated and taking into account efficiency losses, the total pressure change over the turbine stage is calculated from

$$\frac{P_9}{P_8} = \left(\frac{T_9}{T_8} \right)^{\frac{\gamma}{\gamma\text{-}1} \frac{1}{\varepsilon_{Turbine}}} \qquad \textbf{Equation 6}$$

The work extracted from the hot gases in the low pressure turbine equal the work to drive the fan stage. The above mentioned calculation is repeated in the low pressure turbine stage.

In order to calculate the thrust generated by the engine, it is required to calculate the velocity of the air exiting the turbine stages and the bypass duct. This com-

puter model assumes two nozzles, one for the bypass duct and one for the core. For each nozzle separately, it is calculated if the speed of the air in the equals the speed of sound. If this is the case, a static pressure difference between the static pressure in the nozzle and the ambient air is calculated, which contributes to the overll thrust generated by the engine. In that case the engine is operating under choked conditions and the mass flow of air through the engine cannot be further increased. The critical total pressure ratio across the nozzle is calculated from

$$PR_{Critical} = \left(1\text{-}1/\varepsilon_{Nozzle}\,\frac{\gamma\text{-}1}{\gamma+1}\right)^{\frac{-\gamma}{\gamma\text{-}1}} \qquad \textbf{Equation 7}$$

In case the nozzle is not choked, the jet velocity can be found calculating the static temperature of the hot gases exiting the nozzle. This assumes the static pressure being equivalent to the ambient pressure. Taking into account component losses associated with the nozzle, the jet velocity is calculated in the computational model from

$$t_{Nozzle} = T_{Nozzle}\left(1\text{-}\varepsilon_{Nozzle}\left(1\text{-}\left(p_{Ambient}/P_{Nozzle}\right)^{\frac{\gamma\text{-}1}{\gamma}}\right)\right) \qquad \textbf{Equation 8}$$

$$v = \sqrt{\left(T_{Nozzle}/t_{Nozzle}\text{-}1\right)2\,c_p\,t_{Nozzle}} \qquad \textbf{Equation 9}$$

In the case the nozzle is choked, them jet velocity becomes equivalent to the speed of sound. The static temperature and the jet velocity, respectively, is then calculated from

$$t_{Nozzle} = \frac{2}{\gamma+1} T_{Nozzle} \qquad \textbf{Equation 10}$$

$$v = \sqrt{\gamma R t_{Nozzle}} \qquad \textbf{Equation 11}$$

The difference of static pressure between the hot gases in the nozzle and the ambient air can be calculated from Equation 7. With the nozzle operating under choked conditions, it is required to calculate the specific area of the nozzle as the mass flow is not defined. The specific area is obtained from

$$a_{Nozzle} = \sqrt{t_{Nozzle} \frac{R}{\gamma}} \left(1+\frac{(\gamma\text{-}1)}{2}\right)^{\frac{1}{2}} \frac{1}{p_{nozzle}} \qquad \textbf{Equation 12}$$

Applying Equations 1 to 12, all states in the gas path of the engine shown in Figure 13 can be calculated. This enables the calculation to performance specific parameters of the engine: specific thrust, overall efficiency and specific fuel consumption.

Specific thrust is the thrust produced by the engine for each unit of mass of air passing through the engine. It is calculated from a momentum balance of the hot air exiting the nozzles and the pressure difference of the air within and outside the nozzles. The thrust for the bypass and core is calculated separately and combined in one figure.

$$F_S = \left(v_{Jet} - v_{Ambient} \right) + a_{Nozzle} \left(p_{Nozzle} - p_{Ambient} \right) \qquad \textbf{Equation 13}$$

The overall efficiency is an indicator of how much of the chemical energy stored in the fuel is converted into useful energy. Useful energy is the product of thrust and velocity of the engine through the air it passes whereas the chemical energy consumed is a product of fuel consumption and the energy stored for each mass unit of fuel.

$$\eta_0 = \frac{v_{Ambient} F_S}{c_p \Delta T_{Combustor} \frac{\dot{m}_{Combustor}}{\dot{m}_{Total}}} \qquad \textbf{Equation 14}$$

The specific fuel consumption indicates how much fuel is used for each unit of thrust generated by the engine.

$$SFC = \frac{c_p \, \Delta T_{Combustor}}{q_{Fuel}} \frac{\dot{m}_{Combustor}}{\dot{m}_{Total}} \frac{1}{F_S} \qquad \textbf{Equation 15}$$

In addition, entropy changes between the different stages were calculated to allow a graphical representation of the cycle in form of a Temperature – Entropy diagram. Entropy changes are calculated from

$$\Delta s = c_p \log\left(\frac{T}{T'}\right) - R \log\left(\frac{P}{P'}\right) \qquad \textbf{Equation 16}$$

4 Conventional Turbofan

The theoretical performance of a conventional turbofan was used as baseline engine and comprises a design as outlined in the previous section. It consists of an inlet, fan, compressor, bypass, combustor, turbines and nozzles. Certain technology parameters and operating conditions were assumed as summarised below.

The altitude for which ambient conditions are calculated remained the same for all calculations performed in this study. For longer range, turbofan-powered aircraft, average cruise altitudes have remained fairly constant over the past 35 years at approximately 10.5 – 11.5 km although some commercial aircraft have ceilings of up to 13 km (Figure 15)[38]. Aircraft sometimes cruise below optimum design cruise altitudes for reasons associated with air traffic control or severe weather conditions, for example storms and clear air turbulence. Flying at lower cruise altitudes can significantly increase fuel burn depending on range and passenger load. As for civil aircraft the cruise altitude is not expected to increase above 13 km over the next 50 years as a result of physical and cost limitations and aircraft often fly lower than the design altitude, this study assumes 10 km throughout all calculations.

At 10 km, the standard atmosphere model yields 223 K for ambient temperature and 261 hPa[39] for ambient pressure.

In terms of cruise speed, this study assumes Mach 0.85 for all calculations. This is in alignment with cruise speeds observed for most commercial airliners powered by turbofan engines, which is about 500 knots and equates to approximately Mach 0.85 (see Figure 16). A summary of the flight conditions is given in Table 2.

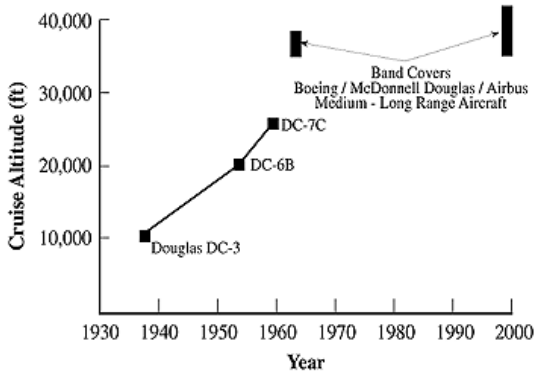

Figure 15: Cruise altitudes of commercial transport aircraft. Modern airliners' cruise altitude averages at approximately 10 km[38].

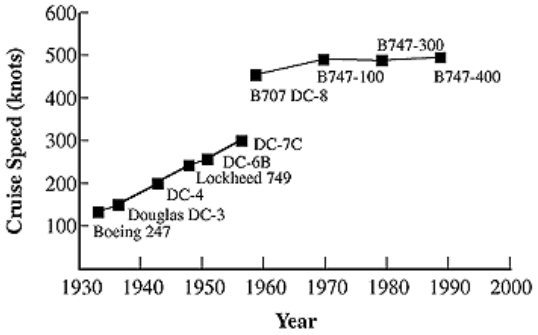

Figure 16: Cruise speed for long range airliners, equating to approximately Mach 0.85[38].

Flight condition parameters	Value
Altitude	10,000 m
Mach Number (M)	0.85
Ambient Temperature	223 K
Ambient Pressure	261 hPa

Table 2: Flight conditions used in the computational model.

The isentropic and also polytropic component efficiencies used throughout this study are summarised in Table 3. They represent state of the art technology levels and were obtained from data available in the public domain and various discussions with industry experts. Although different in a mathematical context, isentropic efficiency and polytropic efficiency both denote the absorption of useful work and define the ratio of actual and ideal work transfers. Assuming processes to take place adiabatic, the ideal process would be isentropic – without increasing the entropy of the system during the process. The ideal process compared to the actual process defines the efficiency of the system. The useful work gained during a process defined by a specific isentropic efficiency does not necessarily relate to the same value if translated into polytropic efficiency although the difference in value may not be vast.

In case of a compressor, the power required to compress air can be directly related into the pressure difference of the air before and after the compression process, or the pressure ratio. There is a theoretical maximum of the pressure ratio that can be achieved in a compressor but in practice, the achievable pressure ratio will always be below the theoretical maximum. The polytropic efficiency for compressors varies with the pressure rise across the compression stage. In general, the higher the desired pressure rise across the compression stage, the higher the associated efficiency losses that occurs. In addition, axial flow compressors used in gas turbines operate with varying efficiencies depending on the mass flow that passes through the engine. For turbines, the effect is reversed. Turbines convert energy more efficiently with increasing pressure ratios across the turbine stage.

In case of inlets or nozzles, the isentropic efficiency implies that kinetic energy is inefficiently used. The kinetic energy could otherwise be used to increase the total

pressure in case of the engine inlet, or enhance the thrust of the engine in case of a nozzle.

Component Efficiency (Polytropic)	Value
Intake	0.99
Fan pressure compressor	0.88
Low pressure compressor	0.88
Low pressure turbine	0.92
High pressure turbine	0.92
Nozzles	0.99

Table 3: Component efficiencies, combustor pressure loss and cooling flow used in the computational model.

The pressure loss that occurs during the combustor as a result of friction and due to the momentum exchange during the combustion process is taken into account during this study and is assumed to be 5% of the inlet pressure to the combustor. The cooling flow extracted form the flow after the compression stage and is assumed to be redirected to the flow after the combustor. The mixing of the hot and cold gases is assumed to take place isentropically.

Cycle Parameters	
Combustor compressor loss	5%
Fraction of combustor cooling flow	5%

Table 4: Combustor pressure loss and cooling flow.

In the first instance, the computational model was used with typical values under cruise conditions for fan pressure ratio, the bypass ratio, turbine entry temperature and compressor ratio to calculate the performance of a conventional turbofan without the optimisation of the cycle. Table 5 summarises typical values for the above mentioned parameters. They represent modern technology levels of jet engines used for commercial air transport and were obtained from the public domain and discussions with experts in the field.

Parameter	Value
Fan Pressure Ratio	1.5
Bypass Ratio	15
Turbine Entry Temperature	2,000 K
Compressor Pressure Ratio	40
Overall Pressure Ratio	56

Table 5: Values of engine parameters.

The initial calculation yields a specific fuel consumption of 1.31 10^{-5} (kg/s)/N, a specific thrust of 110.4 N/(kg/s) and overall efficiency of 0.45, which is in line with the performance figures of modern, conventional turbofan engines[40].

Figure 1 shows the calculated cycle on a temperature – entropy diagram. The compression of the air results in an entropy increase and an increase of temperature. The temperature difference between ambient air and air entering the combustor is 694K; the combustor delivery temperature is 950K compared to 256K ambient temperature. The temperature of the air leaving the turbine stages is 808K, which is higher than the air entering the combustor. In the bypass, the temperature increase due to fan compression is 29.7K. Both nozzles are choked and the exit temperature of the air in the bypass nozzle is 309 m/s compared to 520 m/s for the much hotter core air.

Performance Parameter	Value
Specific Fuel Consumption	1.31 10^{-5} kg/s/N
Specific Thrust	110.4 N/(kg/s)
Overall Efficiency	0.45

Table 6: Performance results.

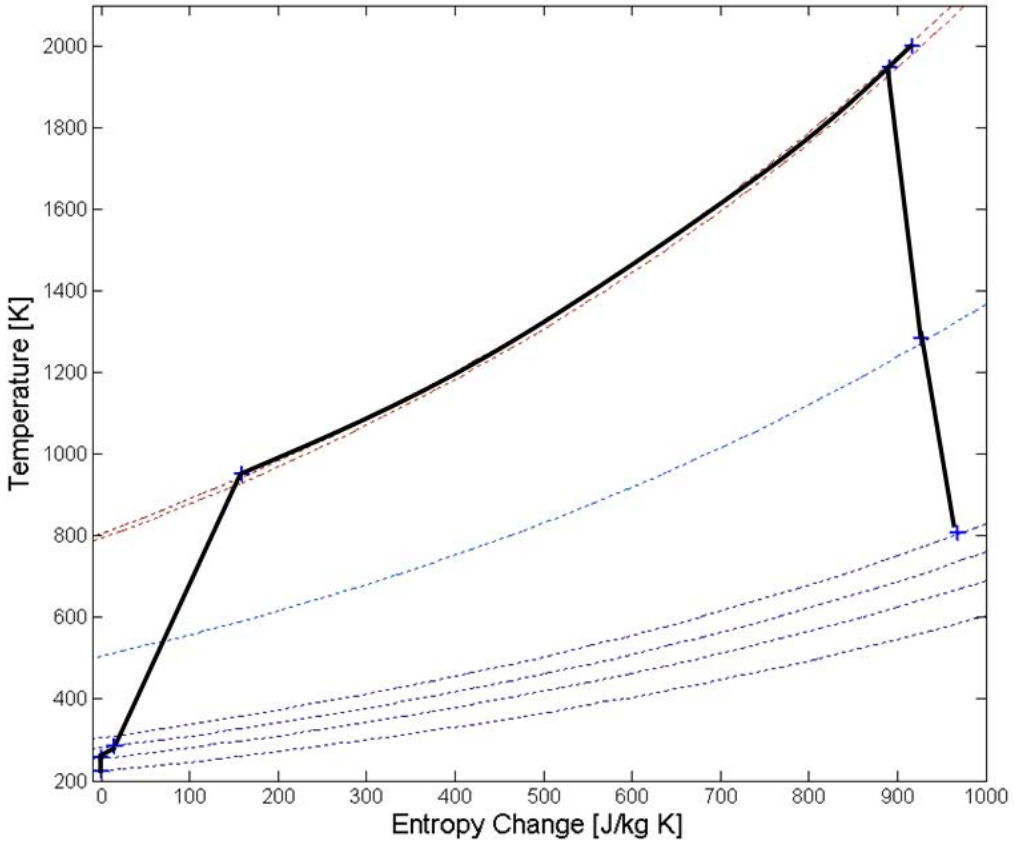

Figure 1: T-S diagram of a conventional turbo fan (bypass not shown). Dashed lines are isobars.

4.1 Sensitivity Analysis

A sensitivity analysis was performed to calculate the relative change in performance for relative changes in the engine parameters based on results of the initial calculation. The engine parameters, fan pressure ratio, the bypass ratio, turbine entry temperature and compressor ratio, were varied by ±10% at a time while the other parameters were held constant and the resulting performance was recorded.

Relative changes in engine performance due to the variations are shown in Table 7.

A 10% change in fan pressure ratio has the biggest effect on the performance of the engine. The overall efficiency increases by 5.4% for a 10% increase in fan pressure ratio and decreases by 15.2% for a 10% reduction in fan pressure ratio. The specific fuel consumption is affected adversely and increases by 18.0% for a 10% decrease in fan pressure ratio and decreases by 5.1% for a 10% increase in fan pressure ratio. The specific thrust comes down by 12.6% if the fan pressure ratio is reduced by 10% as the bypass mass flow is contributing less propulsive force and increases by 2.4% for a 10% increase in fan pressure ratio.

The cycle performance is least sensitive for changes in the compressor pressure ratio where changes of less than 2% were recorded for a 10% change in compressor pressure ratio in both directions. The specific thrust is marginally affected and increases by 1.3% in both directions.

A 10% increase in bypass ratio had a beneficial effect on engine performance as it resulted in a 3.2% increase in overall efficiency and 5.6% decrease in specific fuel consumption. The opposite would occur for a 10% decrease in bypass ratio. The specific thrust increases by 6.1% for a 10% decrease in bypass ratio but comes down by 5.6% for a 10% increase in bypass ratio.

An increase of 10% in turbine entry temperature resulted in a 7.6% decrease of the overall efficiency of the cycle. For the Brayton cycle and its derivatives, analysis predicts an increase in overall efficiency for increasing cycle temperature. However, results of the sensitivity analysis suggest the opposite. This means that the combination of the engine parameters used in this calculation does not result in

the theoretically maximum achievable overall efficiency for the given turbine entry temperature. The specific thrust increases by 10.0% for a 10% increase in turbine entry temperature and falls by 15.5% for a 10% decrease.

	Fan Pressure Ratio		Bypass Ratio		Turbine Entry Temperature		Compressor Pressure Ratio	
Change rel. to initial calculation	-10%	10%	-10%	10%	-10%	10%	-10%	10%
Specific Fuel Consumption	18.0%	-5.1%	4.0%	-3.1%	-4.3%	8.2%	1.8%	-1.6%
Specific Thrust	-12.6%	2.4%	6.1%	-5.6%	-15.5%	10.0%	1.3%	-1.3%
Overall Efficiency	-15.2%	5.4%	-3.9%	3.2%	4.4%	-7.6%	-1.7%	1.6%

Table 7: Change in performance for changes in engine parameters relative to initial calculation.

The sensitivity analysis suggests that an increase in fan pressure ratio, increase in bypass ratio and increase in compressor pressure ratio would result in a cycle with higher overall efficiency and lower specific fuel consumption. Therefore, the optimisation of the cycle is performed, which means finding the combination of engine parameters that yield maximum overall efficiency for a given turbine entry temperature.

4.2 Optimisation

MATLAB was used to find the combination of cycle parameters resulting in the theoretically lowest possible specific fuel consumption. A medium scale algorithm was chosen, which is as part of the MATLAB command 'fmincon' and which attempts to find a constrained minimum of a scalar function of several variables starting at an initial estimate. This is generally referred to as constrained, nonlinear optimisation, or also nonlinear programming. The medium-scale algorithm used in this study incorporates a sequential quadratic programming method. In this method, the function solves a quadratic programming sub-problem at each iteration and an estimate of the Hessian of the Lagrangian is updated at each iteration[41,42]. A line search is performed using a merit function similar to that described in references [43], [44] and [45]. The quadratic programming sub-problem is solved using an active set strategy[46].

A set of optimisation parameters was defined used by both the medium-scale and large-scale algorithms. They limit function evaluations, define termination tolerance and set the minimum and maximum change of the function variables (the engine parameters). The objective of the optimisation was to find a set of engine parameters for a given turbine entry temperature that yield the lowest possible specific fuel consumption. By definition, the specific fuel consumption should have a value greater than 0 and the magnitude of its sensitivity to changes in engine parameters is comparable to the magnitude of changes in the engine parameters as seen in the sensitivity analysis. A 10% change in the engine parameters, for example in bypass ratio, yielded in a comparable, relative change of the specific fuel consumption. Hence, the specific fuel consumption of an optimised cycle should be in the range of $0 - 10^{-5}$ and the difference in terms of specific fuel con-

sumption between two optimised cycles should be within that range. A termination tolerance of 1E-10 was set which gives sufficient margin as differences in terms of specific fuel consumption between two optimised cycles are expected to be in the range of several per cent. The table below summarises all optimisation parameters used in this study. In case that the optimisation terminated due to maximum iterations or function evaluations or meaningless results were generated, necessary adjustments were made and the other parameters and constraints were reviewed.

Optimisation constraints for the engine parameters were defined as outlined in Table 8. In case the optimisation terminated due to constrain violations, the constraints were reviewed and the optimisation repeated. The fan pressure ratio was constraint to values between 1 and 2. Values lower than one have no meaning as the fan has the purpose to accelerate the air in the bypass. The pressure ratio across a fan is typically in the range of 1.2 - 1.6 as higher values become difficult to achieve without fan performances losses unless several fan stages are utilised. The constraints for compressor pressure ratio were 2 - 200 and bypass ratio were 5 - 100. Compressor ratios of about 50 can be found in modern turbofan engines whereas bypass ratios are about 15. Larger bypass ratios would indicate alternative propulsor technology such as open rotors or distributed propulsion[47]. If the optimisation termination was due to constraint violation, results were reviewed and the optimisation repeated if necessary.

Parameter	Value
Max. iterations	500
Max. function evaluations	1E5
Termination tolerance of function value	1E-10
Termination tolerance on constraint violation	1E-10
Termination tolerance on x	1E-10
Max. change in variables	0.1
Min. change in variables	1E-10

Table 8: Optimiser parameters.

Variables	Constraints (lower, upper)
Fan Pressure Ratio	1 – 2
Compressor Pressure Ratio	2 – 200
Bypass Ratio	5 – 100

Table 9: Optimisation constraints

The turbine entry temperature was held fixed during optimisation since the maximum achievable overall efficiency increases with increasing temperature. In the first instance, the turbofan cycle was optimised and results compared to initial results as described in Section 4. The optimisation took 38 iterations until the magnitude of the directional derivative in the search direction was less than 2 times the termination tolerance of the function value as specified in Table 8. All subsequent optimisations in this thesis took comparable iterations to terminate because the termination tolerance on the function value was exceeded. Figure 17 shows the development of the function value (specific fuel consumption) for each iteration step.

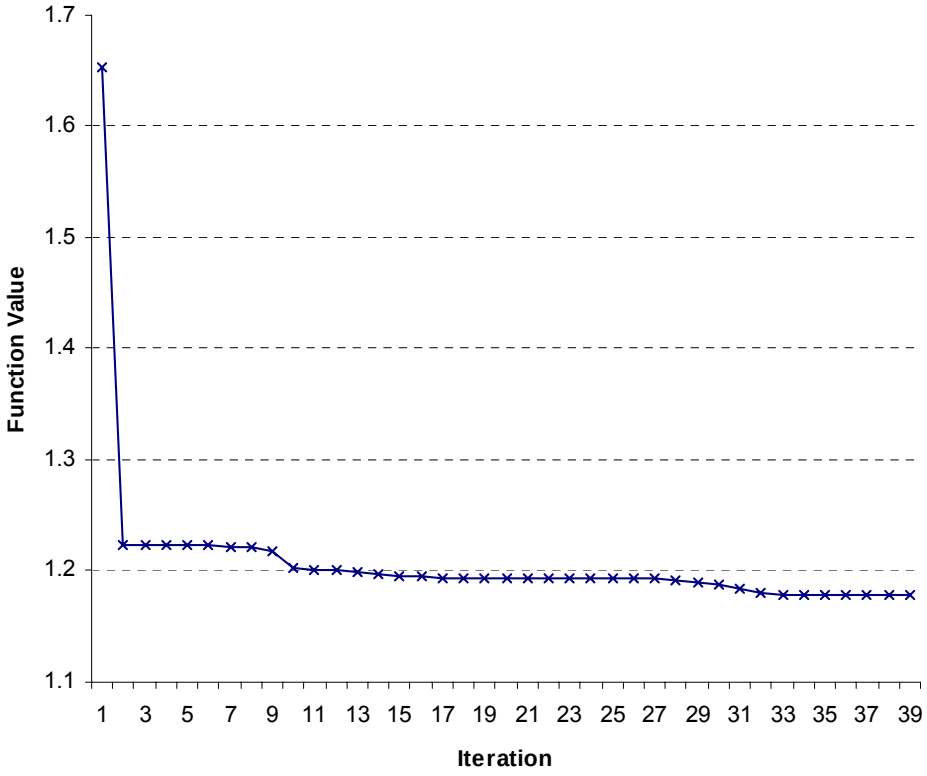

Figure 17: Function value for each optimisation iteration.

The cycle optimised for minimum specific fuel consumption with a turbine entry temperature of 2,000K has a fan pressure ratio of 1.26, a bypass ratio of 23.7 and a compressor ratio of 84. The calculated fan pressure ratio is well within what is achievable with current fan technology and even below what is current practice. The bypass ratio of 23.7 is, however, exceeding what is achievable with conventional turbofan technology and indicates the requirement for alternative propulsor technology. The calculated compressor pressure ratio of 84 is very high for current standards. Higher pressures result in smaller turbomachinery and the efficiency losses associated with blade tip clearances. Compared to the performance of the non optimised cycle, the fan pressure ratio is 10% lower, the bypass ratio is 58% higher and the compressor pressure ratio is 110% higher as shown in Table 10.

Parameter	Initial Value	Optimised Cycle
Fan Pressure Ratio	1.4	1.26 (-10%)
Bypass Ratio	15	23.7 (+58%)
Turbine Entry Temperature	2,000 K	2,000 K
Compressor Pressure Ratio	40	84 (+110%)
Overall Pressure Ratio	56	106.3 (+90%)

Table 10: Values of engine parameters for initial cycle and optimised cycle.

Performance Parameter	Initial Value	Optimised Cycle
Specific Fuel Consumption [10^{-5} (kg/s)/N]	1.31 10^{-5}	1.18 10^{-5} (-10%)
Specific Thrust [N/(kg/s)]	110.4	62.9 (-43%)
Overall Efficiency [-]	0.45	0.50 (+11%)

Table 11: Performance results for initial cycle and optimised cycle.

In terms of performance, the theoretical performance of the optimised cycle is indicates a 10% reduction in terms of specific fuel consumption, a 43% decrease in terms of specific thrust and a 11% increase in terms of overall efficiency. Table 11 summarises the results of the optimised cycle compared to initial results.

The optimisation of the cycle was repeated for a range of turbine entry temperatures. The turbine entry temperature was varied from 1,700K to 2,200K in 100K steps and results recorded as summarised in Table 12. The calculated bypass ratios range from 18.2 to 27.5 and increases for higher values of turbine entry temperature. A similar trend is visible for the compressor pressure ratio which ranges from 53.5 to 110.2, whereas the fan pressure ratio resulting in minimum specific fuel consumption is independent of turbine entry temperature with a value of 1.26.

In terms of performance, higher turbine entry temperatures result in more fuel efficient cycles ranging from 47% to 52% whereas the impact on specific thrust is relatively low (from 63.3 down to 62.8 N/(kg/s)).

It should be noted that although the different cycles represent a 2 spool turbofan configuration, the actual engines that would operate with the particular cycles would be very different. A higher bypass ratio is resulting in a larger engine di-

ameter and larger, heavier compressors with more stages are required to deliver higher compressor ratios.

Turbine Entry Temperature [K]	1,700	1,800	1,900	2,000	2,100	2,200
Fan Pressure Ratio [-]	1.26	1.26	1.26	1.26	1.26	1.26
Bypass Ratio [-]	18.2	20.0	21.8	23.7	25.6	27.5
Compressor Pressure Ratio [-]	53.5	62.8	73.0	84.3	96.7	110.2
Specific Fuel Consumption [10^{-5} (kg/s)/N]	1.26	1.23	1.20	1.18	1.16	1.14
Specific Thrust [N/(kg/s)]	63.3	63.1	63.0	62.9	62.8	62.8
Overall Efficiency [-]	0.47	0.48	0.49	0.50	0.51	0.52

Table 12: Summary of engine parameters and performance of optimised cycles for different TETs.

The increase in bypass ratio also leads to complications with respect to the installation of the engine on the wing and induced drag offsetting performance gains achieved through larger bypass ratios.

The optimisation of the turbofan cycle was repeated for a range of turbine entry temperatures whereas the bypass ratio was fixed to 15. Hence, the only optimisa-

tion variables were fan pressure ratio and compressor ratio. Results shown in Table 13 indicate higher fan pressure ratios ranging from 1.33 to 1.42. The higher the turbine entry temperatures, the higher the fan pressure ratio. Compressor ratios were slightly higher than in the previous case and the overall efficiency of the cycles ranges from 41% to 51%, which is slightly lower than for cycles where the bypass ratio was not constrained.

Turbine Entry Temperature [K]	1,700	1,800	1,900	2,000	2,100	2,200
Fan Pressure Ratio [-]	1.30	1.33	1.35	1.37	1.40	1.42
Bypass Ratio [-]	15.0	15.0	15.0	15.0	15.0	15.0
Compressor Pressure Ratio [-]	55.5	66.5	79.3	93.8	110.5	129.4
Specific Fuel Consumption [10^{-5} (kg/s)/N]	1.26	1.23	1.21	1.19	1.18	1.17
Specific Thrust [N/(kg/s)]	73.1	78.0	82.7	87.0	91.1	94.9
Overall Efficiency [-]	0.47	0.48	0.49	0.50	0.50	0.51

Table 13: Summary of engine parameters and performance of optimised cycles for different TETs and fixed BPR.

A direct comparison between optimised cycles operating with a turbine entry temperature of 2,000K but different bypass ratio is given in Table 14. Notable is the relatively marginal difference in terms of overall engine efficiency of 0.7%. This indicated that in the absence of very high bypass ratio propulsor technology, it would be more beneficial to in crease the fan pressure ratio and compressor pressure ratio. This would result in an increase in overall efficiency not much below what is theoretically be achievable with very high bypass ratio propulsors.

Also notable are the relatively high compressor pressure ratios, which are beyond what is current practice but could for example be achieved with combustion processes where the pressure is further increased, such as pulse detonation or internal volume combustion.

With a fair understanding of the theoretically achievable fuel consumption of a conventional, 2 spool turbofan engine, next sections cover the optimisation and performance calculation of engine designs that incorporate unconventional architectures.

	Unconstrained BPR	Constrained BPR
Turbine Entry Temperature [K]	2,000	2,000
Fan Pressure Ratio [-]	1.26	1.37
Bypass Ratio [-]	23.7	15
Compressor Pressure Ratio [-]	72.9	93.8
Specific Fuel Consumption [10^{-5} (kg/s)/N]	1.178	1.194
Specific Thrust [N/(kg/s)]	62.9	87.8
Overall Efficiency [-]	50.3%	49.6%

Table 14: Cycle optimisation results of a 2 spool turbofan engine.

5 Wave Rotor Technology

5.1 Introduction

The turbine blades of the high pressure turbine stage experience high temperatures from the hot air delivered directly from the combustor. The blades are cooled with bleed air and there are practical limits to the temperatures that can be endured by turbine blades. This limit is the main driver of the cycle temperatures found in modern turbo fan engines. Peak cycle temperatures, and hence the overall efficiency of engines, can only be increased if more temperature resistant materials or better cooling techniques are developed for the turbine blades.

However, the wave rotor could comprise a viable solution to increase the overall pressure ratio and combustor temperature without exposing the turbine blades to higher temperatures. Note that the combustor is susceptible of enduring higher temperatures than turbine blades due to the application of more effective cooling techniques and materials that can be used because of its geometry and dimensions. Wave rotors are non-steady flow pressure exchange devices based on wave processes. A wave rotor acts as a compressor and turbine without blades; between the wave rotor's 'compressor' and 'turbine' is a steady flow combustor.

In its most common form, the wave rotor is an array of cylindrically arranged tubes in the form of a drum as depicted in Figure 18.

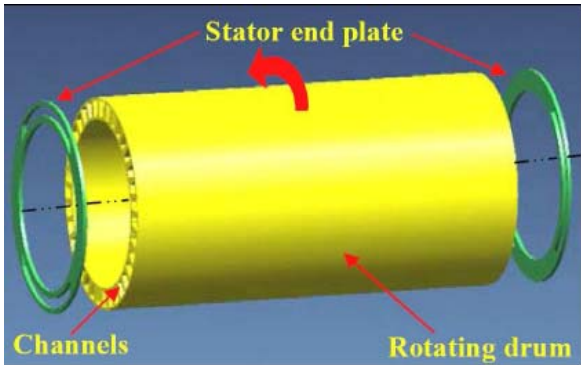

Figure 18: A wave rotor drum consisting of cylindrically arranged tubes[48].

In the four port configuration, the wave rotor is located between the compressor exit, the inlet as well as the outlet of a combustion unit, and the turbine inlet (see Figure 19). The rotation of the drum causes a periodical opening and closing of both sides of the tubes in a way that the working fluid can either enter or exit the tubes.

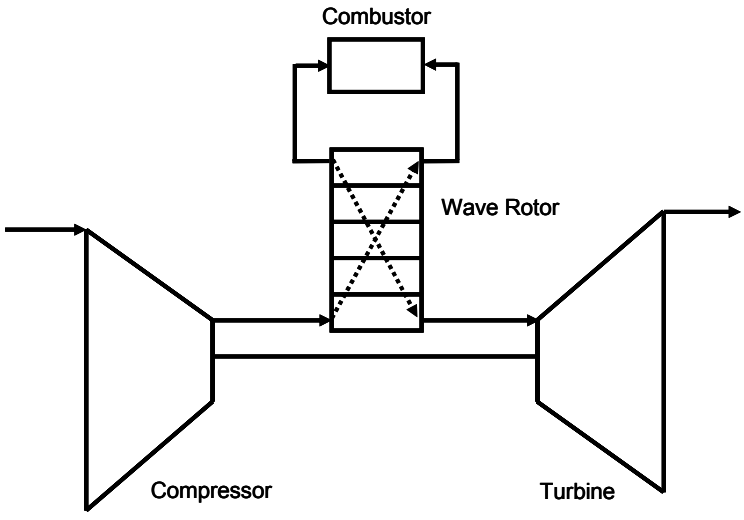

Figure 19: Gas turbine with a wave rotor and continuous flow combustor.

5.2 Process

A fundamental description of a wave rotor is given in Figure 20. In the first step, air from the compressor stages enters the tubes of the wave rotor. Through the rotation of the drum, the ports of the tubes become connected with the outlet of the combustor containing high pressure gas. This causes compression of the low pressure air via shock waves. The rotation of the drum causes the opening of the end of the tube with the cold, compressed air with the combustor inlet and, in effect, the cold, compressed air enters the combustor. That leaves the tube with the gas that was delivered by the combustor at elevated temperature and pressure. Through further rotation of the drum, the tube is now connected with the exit leading to the turbine and the hot and compressed gas leaves the tube to drive the turbine. Further rotation of the drum causes the opening of one end of the drum to allow air from the compression stages entering the tube and the cycle begins again. Through the arrangement of several tubes in a drum as shown in Figure 18, the mass flow through the wave rotor is determined through the rotational speed, the number of tuber and their diameter and length. All three are designed to match the shock wave patterns within the tubes.

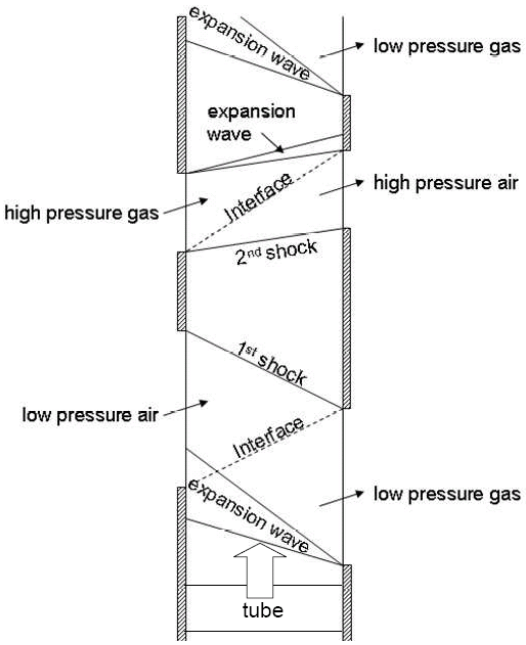

Figure 20: Cyclic operation of a four port wave rotor (simplified wave diagram)[49]. Note that the tube is travelling upwards in the diagram and the velocity of the tube is in accordance with the shock wave patterns that occur through the opening and closing of the tube ends.

The general advantage of wave rotor topping becomes apparent in a temperature-entropy diagram given in Figure 21, showing both a conventional and topped cycle. It is apparent that both cycles operate with the same turbine entry temperature and overall pressure ratio achieved in the turbomachinery (excluding the wave rotor). In both cycles, the temperature of the gas delivered to the high pressure turbine stage is the same. However, the output work of the wave rotor topped cycle can be expected to be higher due to the pressure gain in the wave rotor and higher peak cycle temperatures.

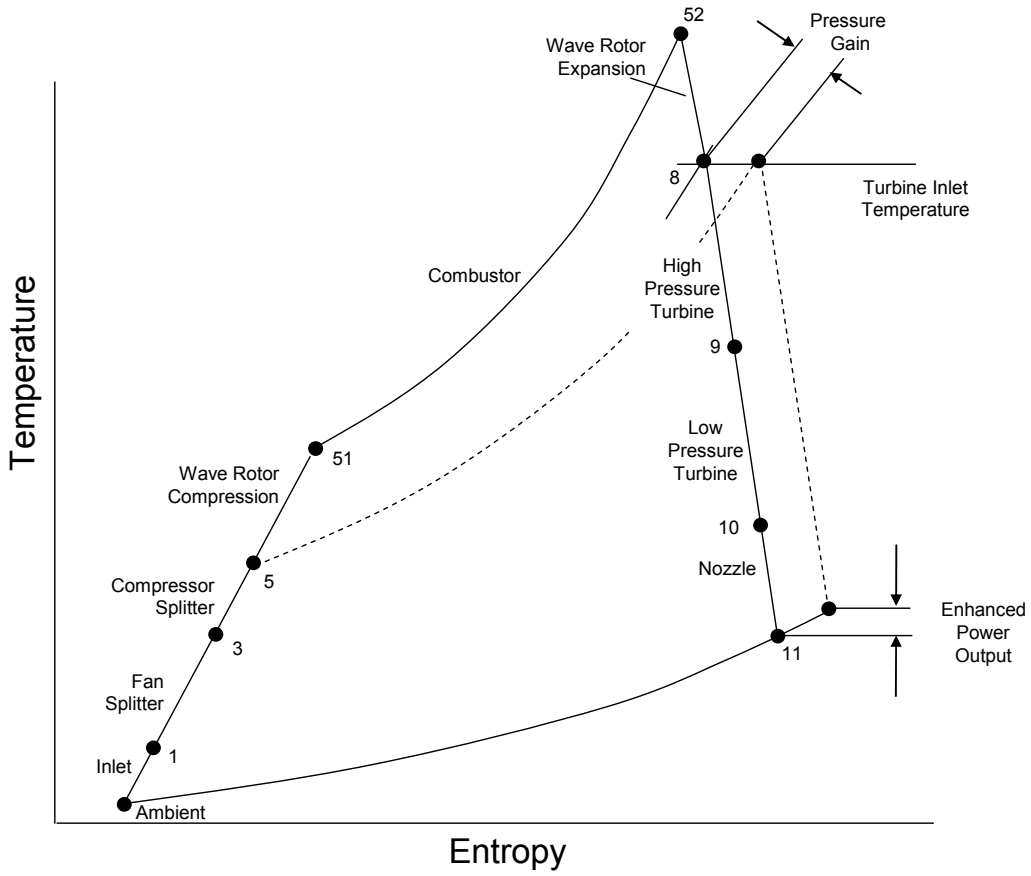

Figure 21: Schematic T-S diagrams for a gas turbine baseline engine (dashed) and the additional wave rotor stages[50]. Cooling air not shown.

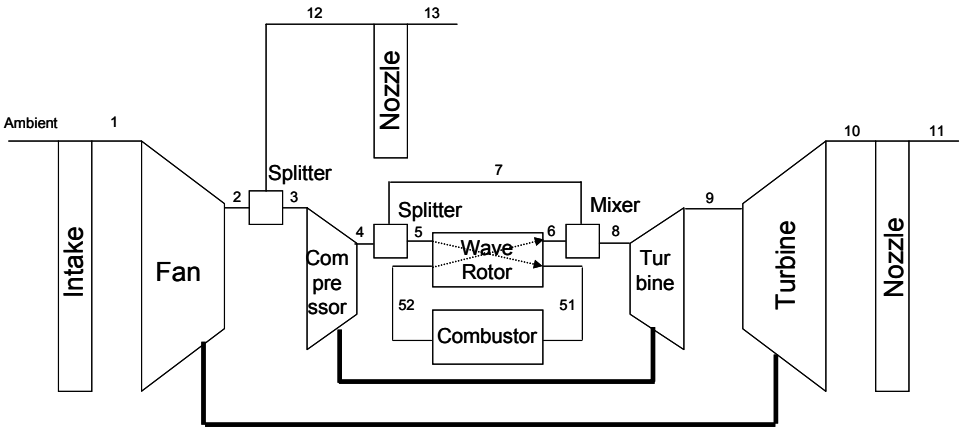

Figure 22: Graphical representation of a gas turbine cycle with wave rotor technology.

Assuming compression of the cold air entering the wave rotor to take place adiabatically, the temperature rise during the compression process is given by

$$T_{51} = T_5 \left(\frac{\left(\frac{P_{51}}{P_5} \right)^{\frac{\gamma-1}{\gamma}} - 1}{\eta_{compression}} + 1 \right) \qquad \textbf{Equation 17}$$

where T_{51} in the temperature of the compressed air leaving the wave rotor and enter the combustor. The practically achievable internal pressure ratio of wave rotors can be found in the literature, which also gives values for the isentropic efficiency of the compression process. The values are based on experimental data and computational fluid dynamics calculations.

As for the compression process, the expansion process in the wave rotor can be assumed to take place adiabatically. With the isentropic efficiency for the expansion process known, the temperature change across the expansion process can be calculated from

$$\frac{T_{52}}{T_6} = \frac{\eta_{expansion} \left(\frac{P_{52}}{P_6} \right)^{\frac{\gamma-1}{\gamma}}}{1 - \left(\frac{P_{52}}{P_6} \right)^{\frac{\gamma-1}{\gamma}} \left(1 - \eta_{expansion} \right)} \qquad \textbf{Equation 18}$$

where $\eta_{expansion}$ is the isentropic expansion efficiency and P_{52} is the pressure of the gases delivered by the combustor. The work required in the compression process equals the work released during the expansion process and the temperatures in the cycle relate to as

$$T_{51} - T_5 = T_{52} - T_6 \qquad \textbf{Equation 19}$$

Rearranging Equation 19 yields

$$T_6\left(\frac{T_{52}}{T_6} - 1\right) = T_5\left(\frac{T_{51}}{T_5} - 1\right) \qquad \textbf{Equation 20}$$

The objective is to calculate the overall pressure gain across the wave rotor P_6/P_5 as a function of the internal pressure ratio P_{51}/P_5, the temperature at the wave rotor inlet and the temperature at the exit port (the turbine entry temperature). Assuming $P_{51} = P_{52}$, rearranging Equation 18 and substituting the temperature ratios with Equations 18 and 19 yields

$$\frac{P_6}{P_5}=\frac{P_{51}}{P_5}\left(\frac{1-\frac{1-\eta_{expansion}}{\eta_{expansion}\,\eta_{compression}}\frac{T_5}{T_6}\left(\left(\frac{P_{51}}{P_5}\right)^{\frac{\gamma-1}{\gamma}}-1\right)}{1+\frac{1}{\eta_{compression}}\frac{T_5}{T_6}\left(\left(\frac{P_{51}}{P_5}\right)^{\frac{\gamma-1}{\gamma}}-1\right)}\right)^{\frac{\gamma}{\gamma-1}} \qquad \textbf{Equation 21}$$

where T_5 is the inlet temperature to the wave rotor, and T_6 is the outlet temperature of the wave rotor. The pressure loss in the combustor is assumed to be covered by the compression and expansion efficiencies calculated from experimental data.

Knowing the peak cycle temperature T_{52} and the temperature to the combustor T_{51}, which can be calculated from Equations 18 and 19, the heat added to the air in the combustor and hence the fuel flow can be calculated from Equation 5, whereas $\Delta T_{combustor}$ is the temperature difference between T_{52} and T_{51}.

5.3 Technology Parameters

The technology parameters of the wave rotor, which are particularly the efficiencies of the compression and expansion processes as well as the internal pressure ratio, can be obtained from experiments and computational fluid dynamics calculations. These parameters were obtained in laboratories and are available in the literature. Figure 23 shows the theoretical pressure rise versus the temperature ratio across the wave rotor calculated form Equation 21. It has been accepted that experiments confirm the underlying theoretical description of wave rotor performance which is used in this study.

Figures for achievable wave rotor internal pressure ratio and isentropic efficiencies can be found in the literature with $PR_{51/5} = 1.8$ and $\eta_{compression} = \eta_{expansion} = 0.83$[51]. These are performance characteristics derived from current experimental wave rotors. It is assumed that with adequate efforts in research and development, these characteristics might be found in commercially applicable wave rotors in the 10 years time frame.

Further development of the wave rotor has the potential to further increase the achievable internal pressure ratio. It is presumed that advanced wave rotors can achieve internal pressure ratios of up to $PR_{51/5} = 3.6$ due to the presence of stronger shock waves.

As compression and expansion efficiencies generally decrease as the shock waves become stronger, $\eta_{compression} = \eta_{expansion}$ are assumed to remain at 0.83 for the characteristics of an advanced wave rotor. It is assumed that commercially applicable wave rotors could have these characteristics in the 25 years time frame.

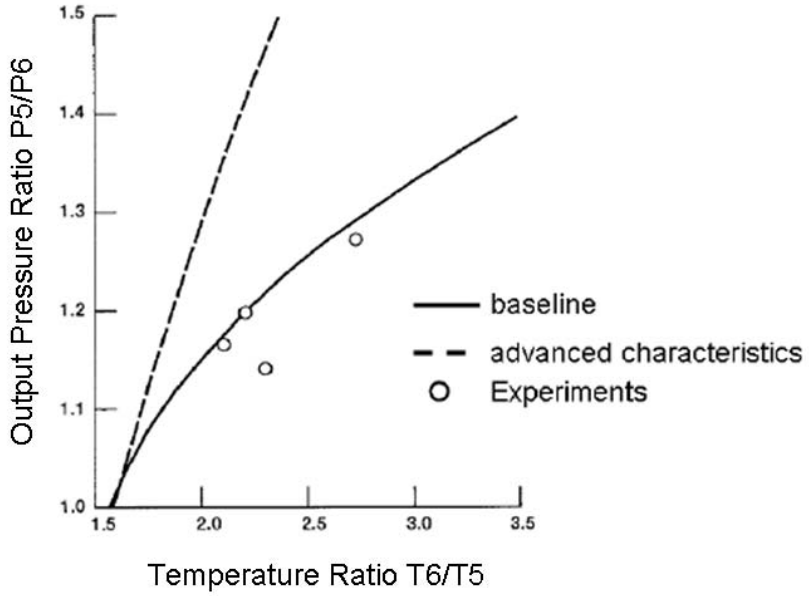

Figure 23: Pressure ratio across the wave rotor as function of temperature ratio calculated from Equation 18[52] and experimental data.

5.4 Optimisation

The computational model described in Chapter 2 was amended to calculate the performance of a hybrid wave-rotor turbofan engine. Therefore, the conventional combustor in the computational model was replaced by a code representing the wave-rotor. The underlying mathematics in the code are based on Equations 17 to 21.

Four sets of optimisations were carried out whereas the only fixed cycle parameter within a given set was the turbine entry temperature, ranging from 1700K to 2,200K. In two sets the bypass ratio was unconstrained with the only difference between the sets in the internal pressure ratio of the wave rotor; and in the other

two sets the bypass ratio was constrained to 15 with the only difference in the internal pressure ratio of the wave rotor.

As described in the previous section, the internal pressure ratio of the wave rotor was 1.8 and 3.6, whereas expansion efficiency and compression efficiency was held constant in all calculations. Table 15 summarises the wave rotor parameters used in the optimisations.

	Short term	Advanced
Internal Pressure Ratio	1.8	3.6
Expansion Efficiency	0.83	0.83
Compression Efficiency	0.83	0.83

Table 15: Wave rotor parameters for the computational model.

The first set of optimisations was performed without constraining the bypass ratio. Results show that the fan pressure ratio remains at 1.26 for the entire turbine entry temperature range, which is consistent with results of previous calculations where the bypass ratio was not constrained. The bypass ratio increases from 25.2 to 38.0 with higher turbine entry temperature. The compressor pressure ratio ranges from 24.8 to 46.0 whereas optimising the cycle for higher turbine entry temperatures results in higher compressor ratios. Values for compressor ratio are significantly below that of the conventional turbofan cycles studied in the previous chapter as the wave rotor substitutes the high pressure compressor stages to some extend. The overall efficiency of the cycles ranges from 44% to 48%, which is lower than

for the conventional turbofan cycles. Changes in specific thrust are marginal and range from 62.9 to 62.5 (kg/s)/N, which is comparable to the conventional turbofan cycles where the bypass ratio was unconstrained during optimisation. Table 16 summarises the results of this set of optimisations.

Turbine Entry Temperature [K]	1,700	1,800	1,900	2,000	2,100	2,200
Fan Pressure Ratio [-]	1.26	1.26	1.26	1.26	1.26	1.26
Bypass Ratio [-]	25.2	27.7	30.2	32.8	35.4	38.0
Compressor Pressure Ratio [-]	24.8	28.4	32.4	36.6	41.1	46.0
Specific Fuel Consumption [10^{-5} (kg/s)/N]	1.35	1.32	1.29	1.26	1.24	1.22
Specific Thrust [N/(kg/s)]	62.9	62.8	62.7	62.6	62.5	62.5
Overall Efficiency [-]	0.44	0.45	0.46	0.47	0.48	0.48

Table 16: Summary of engine parameters and performance of optimised, hybrid wave rotor cycles for different TETs with an internal wave rotor pressure ratio of 1.8.

A second set of optimisations was carried out with a higher internal wave rotor pressure ratio of 3.8 and results are given in Table 17. The fan pressure ratio remains at 1.26 whereas higher values are calculated for the bypass ratio, ranging

from 30.6 to 45.5. Since the internal pressure ratio of the wave rotor is increased, the compressor pressure ratio is now lower, ranging from 10.7 to 18.6. Values for overall efficiency range from 41% to 46% which is less than values for overall efficiency found in the hybrid wave rotor cycle. The specific thrust changes marginally with turbine entry temperature and ranges from 62.7 to 62.4 N/(kg/s) with differences compared to the hybrid wave rotor found only in the first decimal place.

Turbine Entry Temperature [K]	1,700	1,800	1,900	2,000	2,100	2,200
Fan Pressure Ratio [-]	1.26	1.26	1.26	1.26	1.26	1.26
Bypass Ratio [-]	30.6	33.5	36.4	39.4	42.4	45.5
Compressor Pressure Ratio [-]	10.7	12.1	13.5	15.1	16.8	18.6
Specific Fuel Consumption [10^{-5} (kg/s)/N]	1.44	1.40	1.37	1.35	1.32	1.30
Specific Thrust [N/(kg/s)]	62.7	62.6	62.5	62.5	62.4	62.4
Overall Efficiency [-]	0.41	0.42	0.43	0.44	0.45	0.46

Table 17: Summary of engine parameters and performance of optimised, hybrid wave rotor cycles for different TETs with an internal wave rotor pressure ratio of 3.6.

A subsequent set of optimisations was performed where the bypass ratio was constrained to 15. Table 18 summarises results where the internal wave rotor pressure ratio is set to 1.8. The resulting range of fan pressure ratios have much higher values than in any of the previous calculations, ranging from 1.43 to 1.64. The compressor pressure ratio ranges from 25.1 to 49.3, which is lower than for compressor ratios found in conventional turbofan cycles calculated in previous sections. The overall efficiency of the cycles ranges from 43% to 45%. The specific thrust is higher by a factor of 1.5 to 2 compared the hybrid wave rotor cycles where the bypass ratio was not constrained during optimisation.

Turbine Entry Temperature [K]	1,700	1,800	1,900	2,000	2,100	2,200
Fan Pressure Ratio [-]	1.43	1.47	1.51	1.56	1.60	1.64
Bypass Ratio [-]	15.0	15.0	15.0	15.0	15.0	15.0
Compressor Pressure Ratio [-]	25.1	29.1	33.4	38.2	43.5	49.3
Specific Fuel Consumption [10^{-5} (kg/s)/N]	1.38	1.35	1.34	1.32	1.31	1.30
Specific Thrust [N/(kg/s)]	97.7	105.1	112.3	119.3	126.1	132.7
Overall Efficiency [-]	0.43	0.44	0.44	0.45	0.45	0.45

Table 18: Summary of engine parameters and performance of optimised, hybrid wave rotor cycles for different TETs with an internal wave rotor pressure ratio of 1.8 and constrained bypass ratio of 15.

In the last set of cycle optimisations, the bypass ratio was constrained to 15 and the internal wave rotor pressure ratio was set to 3.6, indicating advanced wave rotor technology. Table 18 summarises the results of this set of optimisations. The fan pressure ratio exceeds those of the previous set where the internal wave rotor compressor ratio was set to 1.8. The values for fan pressure ratio in this set range from 1.55 to 1.84, which again indicates that conventional fan technology may not be applicable for this set of cycles and other solutions would be required to build the engine around this set of cycles. Since the internal wave rotor pressure ratio is higher than in the previous set, the compressor pressure ratio has lower values ranging from 9.6 to 15.5. The overall efficiency of the optimised cycles in this set ranges from 40% to 41%, which is lower than for the hybrid wave rotor cycles where the bypass ratio was unconstrained during optimisation. The specific thrust is highest amongst all hybrid wave rotor cycles and ranges from 117.8 to 161.2 N/(kg/s). With relatively low values for the compressor pressure ratio and high fan pressure ratios, engines based on this cycle would be very compact and could be used where axial flow compressors are not feasible due to constraints given be small dimensions.

Turbine Entry Temperature [K]	1,700	1,800	1,900	2,000	2,100	2,200
Fan Pressure Ratio [-]	1.55	1.60	1.66	1.72	1.78	1.84
Bypass Ratio [-]	15.0	15.0	15.0	15.0	15.0	15.0
Compressor Pressure Ratio [-]	9.6	10.7	11.8	13.0	14.2	15.5
Specific Fuel Consumption $[10^{-5}$ (kg/s)/N]	1.50	1.48	1.46	1.45	1.44	1.43
Specific Thrust [N/(kg/s)]	117.8	126.8	135.7	144.4	152.9	161.2
Overall Efficiency [-]	0.40	0.40	0.40	0.41	0.41	0.41

Table 19: Summary of engine parameters and performance of optimised, hybrid wave rotor cycles for different TETs with an internal wave rotor pressure ratio of 3.6 and constrained bypass ratio of 15.

A summary of all four sets of the cycles with a turbine entry temperature of 2,000K is given in Table 20. In general, results of optimisations where the bypass ratio is unconstrained yield in lower fan pressure ratio, higher compressor pressure ratio, lower specific fuel consumption and specific thrust, and higher overall efficiencies. Differences between the hybrid wave rotor cycles in terms of overall efficiency are in the 2-3% range. The bypass ratios in the set of unconstrained optimisations are in excess of 30, indicating installed performance losses due to

large fan diameters and the associated weight and drag penalties. However, if the bypass ratio is constrained to 15, fan pressure ratios are in excess of 1.5, indicating the requirement of more developed fan technology. The compressor pressure ratio is reduced in all cases compared to conventional turbofan cycles as the wave rotor substitutes some of the high pressure compressor stages. This would be especially beneficial if small, compact engines were to be designed where the pressure ratio delivered by axial flow compressors was to be enhanced[53].

	Unconstrained BPR		Constrained BPR	
Wave Rotor Internal Pressure Ratio	1.8	3.6	1.8	3.6
Turbine Entry Temperature [K]	2,000	2,000	2,000	2,000
Fan Pressure Ratio [-]	1.26	1.26	1.56	1.72
Bypass Ratio [-]	32.8	39.4	15.0	15.0
Compressor Pressure Ratio [-]	36.6	15.1	38.2	13.0
Specific Fuel Consumption [10^{-5} (kg/s)/N]	1.26	1.35	1.32	1.45
Specific Thrust [N/(kg/s)]	62.6	62.5	119.3	144.4
Overall Efficiency [-]	0.47	0.44	0.45	0.41

Table 20: Summary of hybrid wave rotor cycles for a turbine entry temperature of 2,000K.

However, the specific fuel consumption of the conventional turbofan cycles examined earlier on is not matched by the hybrid wave rotor. This is due to the less efficient compression and expansion processes that take place inside the wave rotor and cannot be offset by the benefits associated with higher peak cycle temperatures.

6 Pulse Detonation

6.1 Introduction

Constant volume combustion offers a pressure increase during combustion and lower fuel consumption as no volumetric work is carried out during the combustion process. It can be modelled as isochoric, reversible process. With the ideal gas model, the heat energy added to a closed system at constant volume can be calculated from

$$q_{in} = u_2 - u_1 + \int_1^2 p\,dV = c_v\left(T_2 - T_1\right) \qquad \text{Equation 22}$$

where the integral denotes volumetric work, which is zero if the combustion process occurs under isochoric conditions. Technologies that have been identified to enable constant volume combustion within turbofan engines include pulse detonation or internal combustion cycles.

Pulse detonation is a non-steady flow quasi constant volume combustion process. As opposed to deflagrations, detonations are supersonic combustion waves. Across a detonation front, the pressure increases while the specific volume decreases. A detonation taking place in a tube that is closed at one end will leave hot, pressurised gas behind. In its simplest form, a pulse detonation engine is a tube where one end is repeatedly opened and closed while a combustible gas is

ignited. Hot, pressurised gas exits the tube at its open end shortly after ignition takes place. A wide variety of applications have been proposed for pulse detonation engines. Due to the high specific impulse of the exhaust gas, thrust-generating pulse detonation engines exhibit much higher fuel consumption than turbojets in the low Mach number regime. However, pulse detonation engines would outperform turbojets above Mach numbers of about 3.5. An application of pulse detonation engines for subsonic, commercial airliners is hence less attractive from an economical point of view.

However, pulse detonation engines could be used in hybrid mode to increase the performance of conventional aero engines[54 55], which is investigated in this study. In the ultimate embodiment of this concept, the pulse detonation engine takes the place of the combustor and, depending on the overall design, a set of high pressure compressor stages (see Figure 24). The air leaving the high pressure compressor stage enters a pulse detonation tube, which delivers hot gases at increased pressure to the turbine. Combining pulse detonation with conventional aero engine technology would hence enable higher turbine delivery pressure without the need to increase the turbine entry temperature.

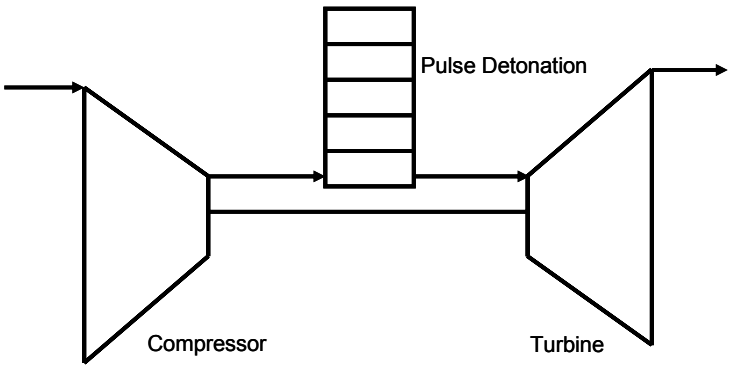

Figure 24: Hybrid Aero Engine with Pulse Detonation Technology.

The detonation is understood to be an exothermic reaction of components within a medium whereas the reaction front expands at a speed that causes the formation of a shock wave in front of it. A detonation that occurs within a tube causes a pressure increase across the detonation front while the specific volume decreases. The detonation process within a tube is depicted in Figure 25.

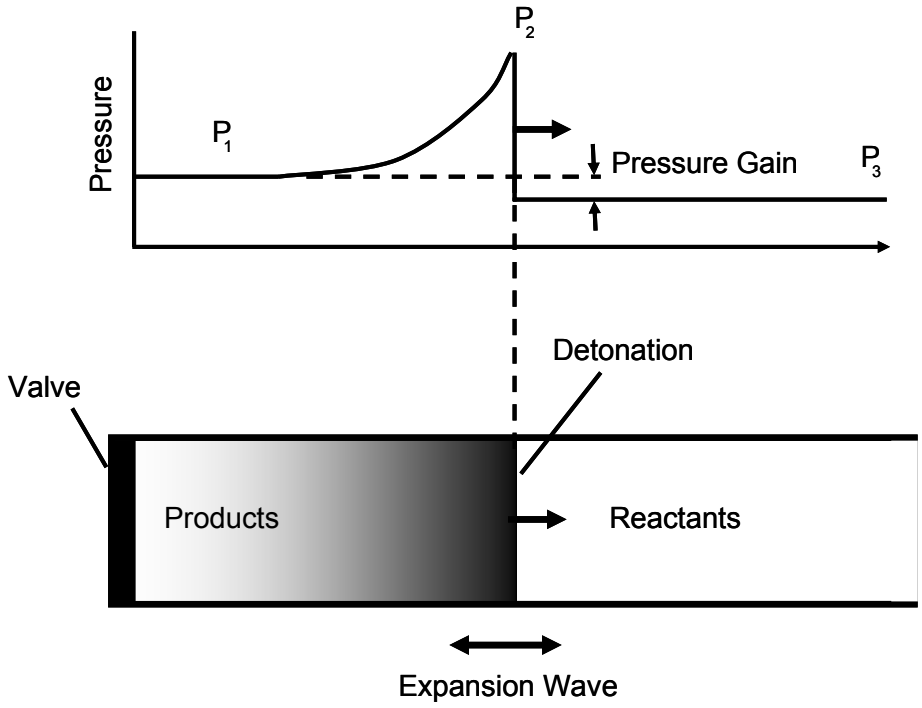

Figure 25: Detonation propagating from the closed end of a tube[56].

The cycle of a pulse detonation engine is shown in Figure 26: a closed tube is filled with an air/fuel mixture, which is ignited at the closed end of the tube (detonation initiation). The resulting detonation wave propagates towards the exit of the tube (detonation propagation). When the detonation wave reaches the open end of the tube, the products expand outside the tube (blow-down). A diffracted

shock and a reflected wave are created. The tube is left with reactants and the valve opens allowing air to enter the tube (purge) supported by the reverberating wave pattern. The valve closes when the tube is eventually filled with air and reactants (fuel fill) and the cycle begins again. During a cycle, thrust is generated as long as the pressure inside the tube on the thrust surface is greater than the atmospheric pressure. Experimental pulse detonation engines typically operate at frequencies of 50-100 Hz.

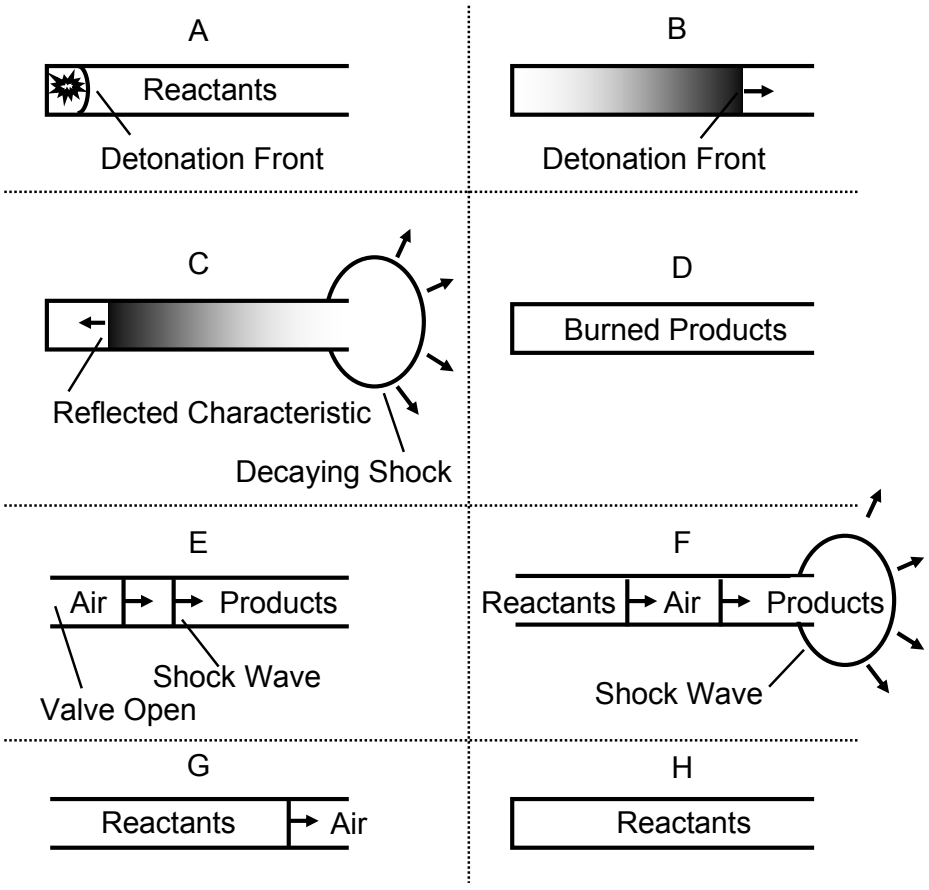

Figure 26: Schematic of a pulse detonation cycle[56].

A detonation tube can be fully purged or partially purged of the gases left behind the reaction. For a fully purged tube, the tube is left with fresh air only after the purge process, whereas a partially purged tube is left with both air and hot gases from the previous cycle.

Since relatively little work has been done on pulse detonation hybrid engines, their geometry is still a matter of debate. Most likely, the hybrid pulse detonation is an array or cylindrically arranged tubes. To open and close the tubes at their inlet, the tubes are either rotating and become obscured via a static inlet port, or alternatively, the tubes are static and a plate is rotating in front of the tubes which would have the same effect.

It should be noted that the output flow of a pulse detonation engine is unsteady and exhibits strong wave patterns. This would impact the stator and rotor blades of the turbine, whereas possible implications are not investigated sufficiently to date. The turbine would experience a wide range of inlet conditions, and turbine technology would very likely have to be adapted to these new requirements.

Since the exhaust of a pulse detonation engine is pulsating, its nozzle would have to be adjusted with the operational frequency to achieve best possible performance. Since this would require probably significant technological effort, it is questionable whether best possible performance will ever be achievable. Hence, real pulse detonation engines may always underperform when compared to predictions of theoretical models.

Figure 27 represents a developed view of a multi tube pulse detonation engine. The vertical direction represents the time dependent location of the rotating tubes. Air enters the tubes, which are closed due to the rotation, and is mixed with fuel.

Detonation initiation occurs through an igniter once the tube is closed and the expanded gases leave the tubes via the exhaust port resembling the geometry of a wave rotor engine.

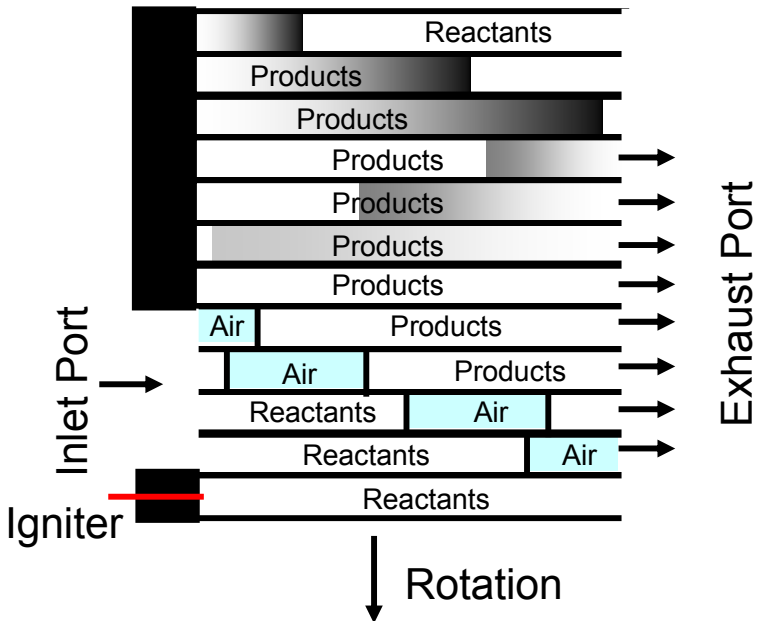

Figure 27: Schematic layout of the pulse detonation engine[57]

6.2 Process

The general advantage of the hybrid pulse detonation engine becomes apparent in a T-S diagram given in Figure 28 for both the Humphrey and Brayton cycle. The Humphrey cycle comprises constant volume combustion and approximates the hybrid pulse detonation cycle whereas the Brayton cycle is an approximation of the thermodynamic cycle of conventional turbofan engines with a continuous flow combustor.

It is apparent that both cycles operate with the same turbine entry temperature but different pressure ratios. In both cycles, the same amount of heat is added to the air prior to expansion in the turbine stages. However, the work output of a hybrid pulse detonation cycle is higher than a conventional engine with the same cycle parameters due to the pressure gain in the pulse detonator. This consequently allows the hybrid pulse detonator cycle to operate with a higher thermal efficiency.

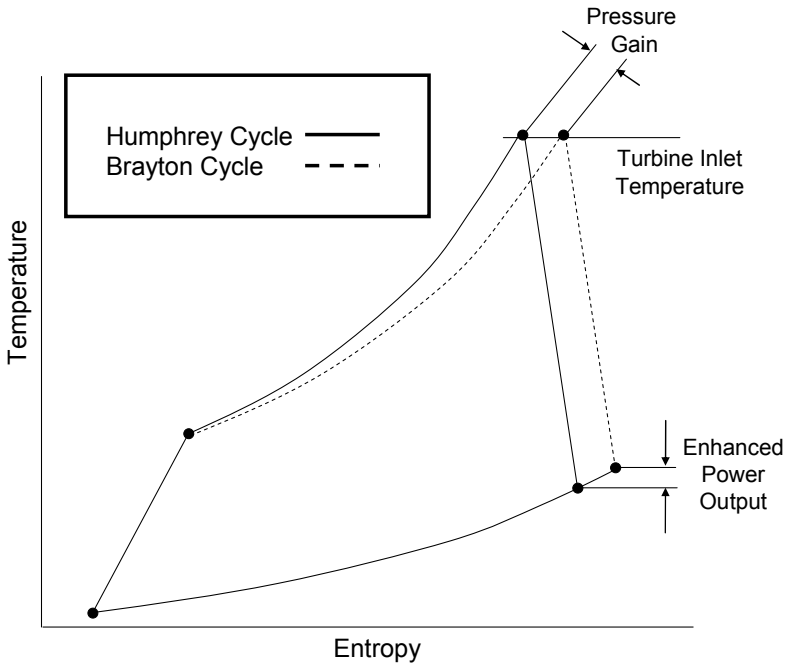

Figure 28: Comparison between the Humphrey and Brayton cycle.

The performance of a hybrid pulse detonation engine is subject to the performance of the pulse detonation process itself. The determining parameter is the pressure gain during the combustion process, which has been subject to numerous studies conducted in the laboratory or computational fluid dynamics simulations. Through

extrapolation of the experimental data, the theoretical prediction of a pulse detonation engine becomes possible.

As in the earlier sections, a quasi steady flow analysis is used to calculate the thermodynamic performance of a pulse detonation engine. A literature research has helped to derive a mathematical description and the model used herein has the underlying assumption that the effect of wave interactions can be neglected or corrected[58]. Even though such analysis provides insights into the thermodynamic aspects, it is accompanied with uncertainties.

The overall pressure ratio across a pulse detonation engine can be calculated from a semi empirical approach[59]. The pressure rise across one tube of the pulse detonation engine is calculated from the thermodynamic relation for adiabatic compression

$$PR = \left(\frac{T_5}{T_6} \right)^{C\frac{\gamma}{\gamma-1}} \qquad \textbf{Equation 23}$$

where HR denotes the ratio of the enthalpy of the working gas at the inlet and the outlet of the pulse detonation engine. The technology parameter C in Equation 21 denotes the efficiency of the process and is obtained from a curve fit through results of CFD simulations, which are based on the following assumptions:

- The process is adiabatic and non-viscid.
- The flow inside the tube contains a combination of reactant or product only.

- Both reactants and products are perfect gases with the same properties.
- The valves close instantaneously.

Other simplifying assumptions were made but are not mentioned here. Different values for C can be found in the literature, which denote how effectively the pressure gain is achieved in the pulse detonation cycle.

The purge fraction is the fraction of time when purge air is flowing through the tube inlet to the total valve open time. At the beginning of a cycle, a certain amount of air has passed through the tube of which the purge air does not remain inside the tube when the detonation takes place. The total amount of air passing through the tube is

$$m_{Air} = m_{\mathrm{Re}ac\tan ts} + m_{Purge} \qquad \textbf{Equation 24}$$

where m_{Air} denotes the total amount of air passing through the tube during one cycle, $m_{Reactants}$ denotes the amount of air left in the tube after the purge process and m_{Purge} denotes the amount of air passing through tube not being part of the detonation process. Equation 22 assumes that the density of the reactant air that includes the fuel is the same as for pure air entering the pulse detonation engine. The purge fraction pf is the ratio of purge air passing through the tube to the total amount of air passing through the tube

$$pf = \frac{m_{Purge}}{m_{Air}} \qquad \textbf{Equation 25}$$

The temperature increase across the pulse detonation engine is an average of the total amount of air passing through and includes the purge air. Hence, the heat energy added just to the air that is left in the tube after the purge process at the beginning of the cycle is defined by

$$\frac{m_{\mathrm{Re}actants}}{(1-pf)} c_p (T_6 - T_5) = m_{fuel}\, q_{net} \qquad \textbf{Equation 26}$$

In order to calculate the pressure increase across the pulse detonation engine, Equation 24 is rearranged and yields

$$\frac{T_5}{T_6} = 1 + \frac{q_0}{(1+AFR)\gamma R T_5}(\gamma - 1)(1 - pf) \qquad \textbf{Equation 27}$$

where AFR is the air-to-fuel ratio and T_5 is the temperature of the air entering the PDE at the beginning of the cycle. Together with Equation 21, the theoretical pressure gain across a pulse detonation engine can now be calculated for a given inlet and exit temperature.

The two unknown parameters for the calculation of the pulse detonation engine are the parameter C and the purge fraction pf. From the above equations it becomes apparent that higher values of C and lower values for the purge fraction are desirable to achieve a high pressure increase in the pulse detonation engine. Also, a higher value for the purge fraction implies a higher cycle time and hence a lower

frequency with which the pulse detonation engine operates. Therefore, there is another reason to operate pulse detonation engines with low purge fraction as higher frequencies are desirable to allow larger mass flows through the engine. Since this technology is still in its infancy, it is assumed that significant research into pulse detonation technology will be carried out to allow the commercial application of pulse detonation engines. In the long term, this research will eventually enable pulse detonation engines to operate with a low purge fractions. The purge fraction of experimental pulse detonation engines is quoted with different values in the literature and ranges from 0.1 to 0.7. This study assumes a purge fraction of 0.1, which is the lowest figure that that was found in the literature.

Values for the technology parameter C found in the literature range from 0.105 to 0.12. Higher values for C enable higher pressure ratios as shown in Figure 29. Therefore, this study assumes that pulse detonation engines will be available in the long term that have the performance characteristic equivalent to C = 0.12, which has already been achieved in the laboratory[15]. Table 21 summarises typical values for purge fraction and technology parameter C and shows which vales have been chosen in this study.

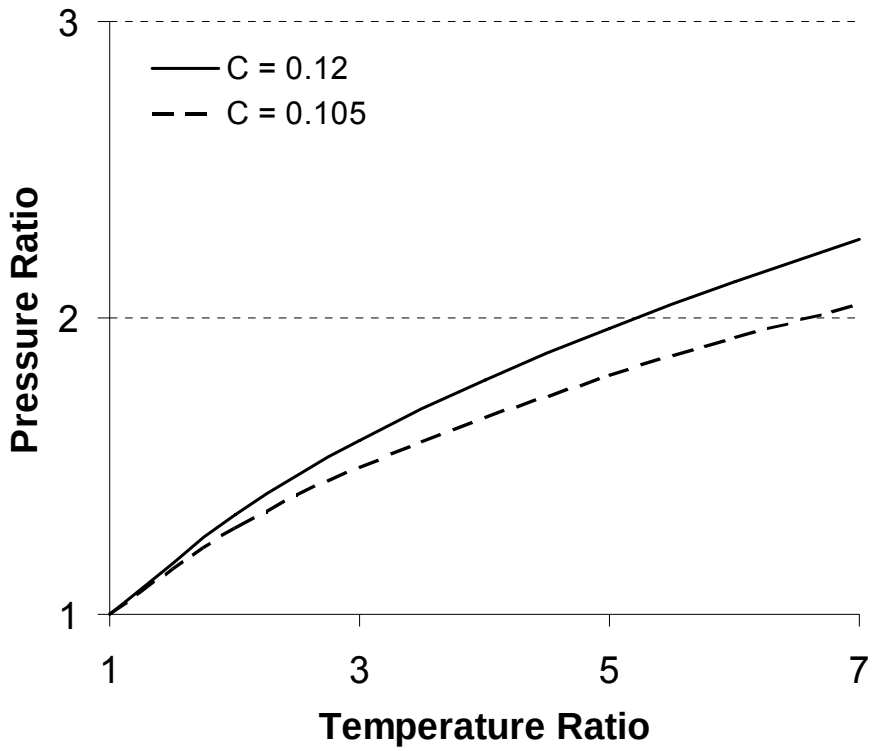

Figure 29: Pressure Ratio as a function of temperature ratio across a pulse detonator (see Equation 27).

Parameter	Purge fraction [-]	C [-]
Typical values	0.10 - 0.20[58], 0.70[59]	0.105[58], 0.12[59]
Used in this study	0.1	0.12

Table 21: Typical values for purge fraction and the technology parameter C.

For a polytropic process of a closed system, the pressure-volume relationship of the form $pV^n = const.$ applies. Since the technology parameter C is an adjustment to an ideal process which based on observations, it is required to calculate an exponent *n* that describes the pulse detonation process to allow the calculation of the heat energy into the process, which can be obtained from an energy balance. From Equation 20 it follows that for a constant volume combustion process

$$q = \Delta u = c_v \, \Delta T \qquad \textbf{Equation 28}$$

By definition, a polytropic process is described by a pressure – volume relationship in the form

$$pV^n = const. \qquad \textbf{Equation 29}$$

Substituting back into Equation 20 for $n \neq 1$ yields

$$q = c_v \Delta T + \frac{R}{1-n} \Delta T \qquad \textbf{Equation 30}$$

whereas $n = 0$ for a constant pressure process and $n = \pm\infty$ for a constant volume process. For a given temperature increase and assuming no mechanical work added to the system, the constant volume combustion process requires the lowest

amount of heat energy to achieve the temperature increase. On the other end, for a constant pressure combustion process

$$q = c_v \Delta T + R \Delta T = c_p \Delta T \qquad \textbf{Equation 31}$$

For an unknown process such as pulse detonation, *n* is to be determined in order to calculate the heat energy into the process. With Equation 21 it is possible to calculate an exponent *n* that describes the pulse detonation process and it follows that with

$$C \frac{\gamma}{\gamma - 1} = \frac{n}{n - 1} \qquad \textbf{Equation 32}$$

the polytropic exponent becomes

$$n = \frac{C\gamma}{C\gamma - \gamma + 1} \qquad \textbf{Equation 33}$$

For $\gamma = 1.4$ and the technology factor $C = 0.12$, the polytropic exponent $n \approx -1$. Hence the energy required to achieve a temperature increase ΔT becomes

$$q = c_v \Delta T + \frac{R}{2} \Delta T \qquad \textbf{Equation 34}$$

From this follows that for the pulse detonation process the energy required to achieve a certain temperature change lies somewhere half way between the constant volume and the constant pressure combustion process.

6.3 Optimisation

The computational model was modified and the combustor stage substituted to simulate the pressure gain achieved through the pulse detonation engine core. Therefore, equations in the previous section were used and incorporated in the model.

Furthermore, changes were made to calculate the fuel flow. From equations 28 and 30 it follows that

$$\frac{\dot{m}_{fuel}}{\dot{m}_{air}} = \left(c_v + \frac{R}{1 - \frac{C\gamma}{C\gamma - \gamma + 1}} \right) \frac{\Delta T}{q_{net}} \qquad \textbf{Equation 35}$$

The graphical representation of the hybrid turbofan pulse detonation engine is given in Figure 28.

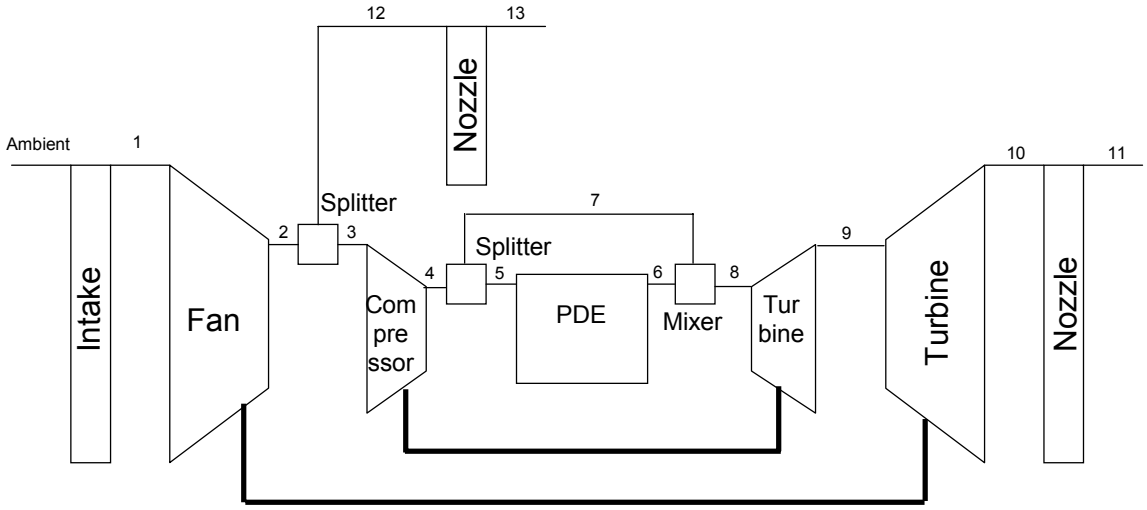

Figure 30: Hybrid pulse detonation cycle where the pulse detonation cycle is substituting the conventional combustion chamber of a turbofan cycle.

Figure 31 show the hybrid pulse detonation turbofan cycle compared to a conventional turbofan cycle. The power output is enhanced and less energy is required to achieve the temperature change of the working medium.

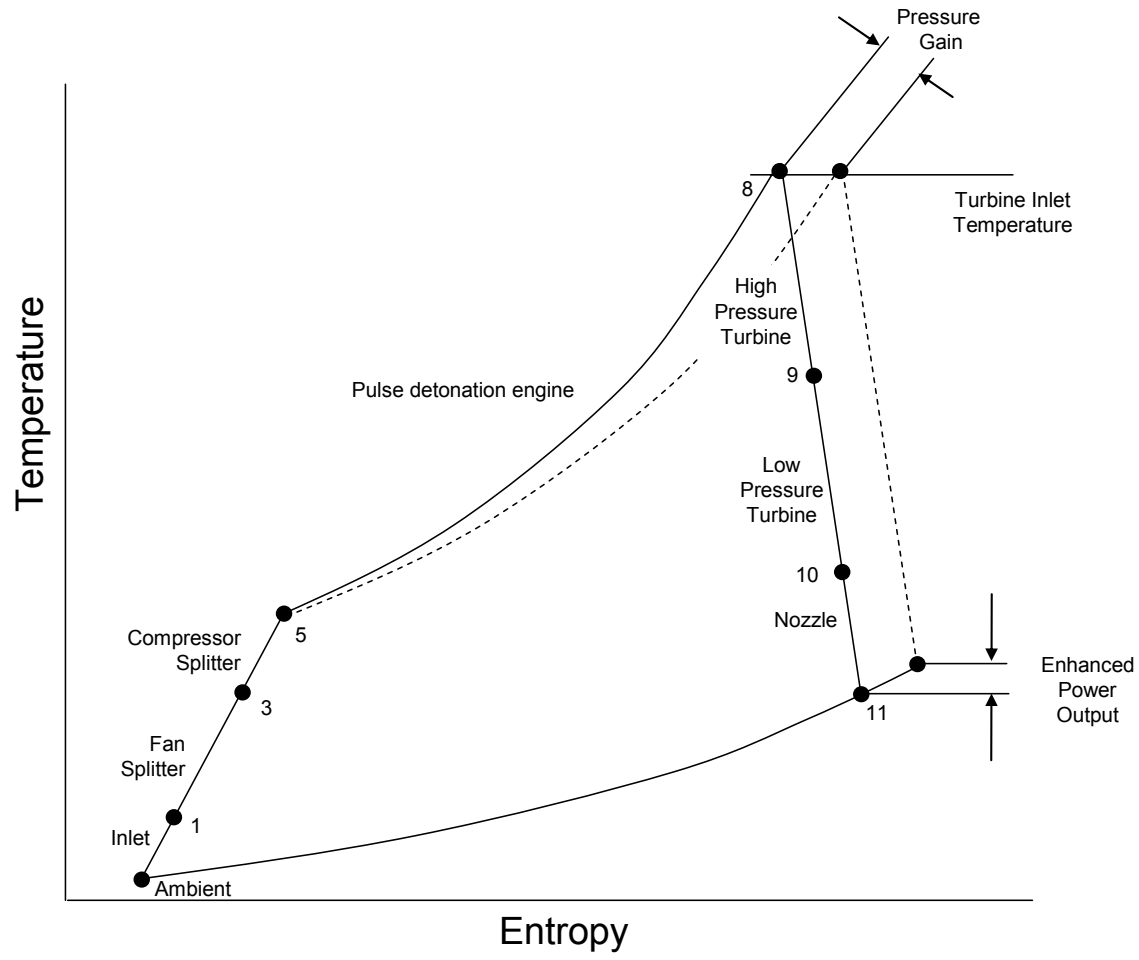

Figure 31: Hybrid pulse detonation turbofan cycle compared to a conventional turbofan cycle on a T-S diagram.

Results of the first set of optimisations with an unconstrained bypass ratio are given in Table 22. The fan pressure ratio is 1.26 across the entire turbine entry temperature range. The bypass ratio ranges from 21.1 to 31.2, which is less than for comparable wave rotor hybrids and more than for conventional turbofan cycles. The compressor ratio ranges from 46.7 to 95.4 resulting in overall efficiencies of 58% to 63%, which is higher than for the conventional turbofan and hybrid

wave rotor cycles. The specific thrust of the cycles is comparable to the specific thrust of the hybrid wave rotor cycles and only changes marginally with TET.

Turbine Entry Temperature [K]	1,700	1,800	1,900	2,000	2,100	2,200
Fan Pressure Ratio [-]	1.26	1.26	1.26	1.26	1.26	1.26
Bypass Ratio [-]	21.1	23.1	25.1	27.1	29.1	31.2
Compressor Pressure Ratio [-]	46.7	54.7	63.5	73.2	83.8	95.4
Specific Fuel Consumption [10^{-5} (kg/s)/N]	1.02	1.00	0.99	0.97	0.96	0.95
Specific Thrust [N/(kg/s)]	63.1	62.9	62.8	62.8	62.7	62.6
Overall Efficiency [-]	0.58	0.59	0.60	0.61	0.62	0.63

Table 22: Summary of engine parameters and performance of optimised, hybrid pulse detonation cycles for different TETs.

In the next set of optimisations, as in the previous sections, the bypass ratio was constrained to 15 and results are given in Table 23. The fan pressure increases with higher temperatures and ranges from 1.34 to 1.45. This results in higher compressor pressure ratios than for the unconstrained hybrid pulse detonation cycles. The overall efficiency is second highest of all cycles and only 1-2% below

the overall efficiencies of the hybrid pulse detonation cycles where the bypass ratio was unconstrained during the optimisation. The calculated compressor pressure ratio is ranging from 51.4 to 125.0, which would be a very high value for axial flow compressors based on current designs. The specific thrust varies from 80.5 to 100.5 N/(kg/s) with increasing turbine entry temperature, which is lower than for the hybrid wave rotor cycles where bypass ratios were constrained during optimisation but higher than for the conventional turbofan where bypass ratios were constrained during optimisation.

Turbine Entry Temperature [K]	1,700	1,800	1,900	2,000	2,100	2,200
Fan Pressure Ratio [-]	1.34	1.36	1.39	1.41	1.43	1.45
Bypass Ratio [-]	15.0	15.0	15.0	15.0	15.0	15.0
Compressor Pressure Ratio [-]	51.4	62.3	74.8	89.3	106.0	125.0
Specific Fuel Consumption [10^{-5} (kg/s)/N]	1.03	1.02	1.00	0.99	0.98	0.98
Specific Thrust [N/(kg/s)]	80.5	85.1	89.4	93.4	97.1	100.5
Overall Efficiency [-]	0.57	0.58	0.59	0.60	0.60	0.61

Table 23: Summary of engine parameters and performance of optimised, hybrid pulse detonation cycles for different TETs and constrained bypass ratio.

A summary of results is given in Table 24 where the main differences between the cycles where the bypass ratio was constrained and unconstrained become apparent. In case of the bypass ratio being unconstrained during optimisation and a turbine entry temperature of 2,000K, the optimisation yields a fan pressure ratio of 1.26, a bypass ratio of 27.1 and a compressor pressure ratio of 73.2. This combination of parameters results in an overall efficiency of the hybrid pulse detonation cycle of 61%. Constraining the bypass ratio to 15 during optimisation results in a slightly lower overall efficiency of 60%, which is one percent point less in absolute terms. However, a larger fan pressure ratio of 1.41 is required as well as a higher compressor pressure ratio of 89.3, indicating a larger, possibly heavier compressor. In terms of specific thrust, the cycle with the lower bypass ratio would require about two third of the mass flow through the engine of the cycle with the higher bypass ratio to deliver the same propulsive force.

	Unconstrained BPR	Constrained BPR
Turbine Entry Temperature [K]	2,000	2,000
Fan Pressure Ratio [-]	1.26	1.41
Bypass Ratio [-]	27.1	15.0
Compressor Pressure Ratio [-]	73.2	89.3
Specific Fuel Consumption [10^{-5} (kg/s)/N]	0.97	0.99
Specific Thrust [N/(kg/s)]	62.8	93.4
Overall Efficiency [-]	0.61	0.60

Table 24: Summary of hybrid pulse detonation cycles for a turbine entry temperature of 2,000K.

Internal Combustion

6.4 Introduction

The reciprocating engine consists of one or more contracting chambers where the working fluid is compressed, heated and expanded in discontinuous manner. Unlike axial flow machines, reciprocating engines perform the underlying thermodynamic cycle in finite time intervals and convert quasi linear motion into rotary motion.

The working cycle of the reciprocating engine includes the introduction of either already hot and pressurised gas into the chamber, compression of the gas through the volumetric contraction of the chamber, heating of the gas by means of ignition of fuel or through the exchange of heat, and volumetric expansion of the chamber whereby the motion that occurs through the expansion of the chamber is utilised to extract mechanical energy from the cycle.

The compression and expansion process is quasi isentropic since the compression and work extraction is not achieved through the diversion of the gas flow with the aid of blades. Due to the cyclic operation of the reciprocating engine, the high temperature and pressure of the gases, and the conversion from rotary to linear motion, more durable and robust designs typically makes the reciprocating engine heavier than the gas turbine.

In practice, the reciprocating engine in the form of an internal combustion engine typically consists of an array of cylindrical chambers where the movement of a

piston inside the chamber compresses working gas that has entered the chamber through a valve. The power to compress the working gas is either delivered from the momentum in the piston of the foregoing cycle or from the expansion of hot gases within another cylinder that is part of the array. Fuel is injected into the compressed working gas, which combines with the oxygen of the working gas exothermically while the piston movement results in the volumetric expansion of the chamber. In case the mixing of the air with fuel takes place before entering the internal combustion engine, than the temperature of the reactant during compression should not exceed its ignition temperature. This can be overcome with more sophisticated, direct injection techniques, where fuel is added and ignited when the air is compressed. While the chamber is in contracted, the working gas is heated through the rapid combustion of fuel. During the subsequent expansion of the gases, mechanical power is extracted from the process through the linear motion of the cylinder. The motion is converted into rotational motion through a crank mechanism. The extracted energy is used to compress the working gas during the following cycle. Surplus, rotational power can drive the propulsive unit such as a propeller or fan.

The gap between the piston and the chamber walls is very narrow to avoid the working gas leaking during the process, which causes frictional losses. Also, the crankshaft mechanism and the presence of a gearbox usually requires energy that is extracted from the output power of the cycle and reduces its overall efficiency. Furthermore, limited ability to control the combustion of the reactant after fuel is added to the air can result in short periods of constant pressure combustion that has an impact on the cycle efficiency.

The Otto cycle incorporated constant volume combustion while the piston is not moving and has contracted the cylinder whereas Diesel engine is usually refers to a piston engine where the combustion of the fuel occurs under quasi constant pressure when the piston is in motion. The Diesel cycle has a lower thermal efficiency than the Otto cycle at a given compression ratio. Other reciprocating engine designs include the Wankel engine, the steam engine or the Stirling engine. The Wankel design facilitates chambers contracting and expanding solely through rotating parts in the absence of pistons and engine has been developed throughout the 21st century and found its application with car manufacturers. A Wankel engine incorporating constant volume combustion may provide advantages over the piston design in a hybrid turbofan configuration Figure 35.

The Stirling engine incorporates heat exchangers and different temperature levels through which the working fluid is cyclically heated and cooled. The result is a linear motion of pistons resulting in the contraction and expansion of the working gas which is pumped between the heat exchangers. The working gas is contained within the engine and is not exchanged with its surroundings. Approximating the Carnot cycle, Stirling engines allow operation with high thermal efficiency. They found their application in various niches ranging from marine engines to computer chip cooling but would not be technically feasible in hybrid turbofan configuration as the working fluid remains inside the contracting chamber and the heat transfer is facilitated through heat exchangers.

Steam engines are the oldest form of reciprocating engines. The working fluid is steam obtained from heating water, which can be pressurised prior to entering a steam generator. The steam is used to move a piston in a cylinder but rotary designs exist as well. The steam engine came out of fashion in the early 20th century

with the advent of the internal combustion engine. Although steam engine powered aircraft were successfully flown in the 1930s [60], the heavy design and need for condensers make their application in larger aircraft unattractive.

The first ever heavier than air flight undertaken by the Wright Brothers in 1903 was powered by an internal combustion piston engine and since then piston engines find their application in civil and military aviation. The Lockheed Super Constellation shown in Figure 32 is a great example of a civil airliner powered by piston engines, which remained the main power source for aircraft until the advent of the jet engine. Today, the application of piston engines is mainly confined to smaller, general aviation aircraft.

Figure 32: Lockheed Super Constellation powered by four radial internal combustion piston engines.

Reciprocating engines that are based on the Otto cycle feature constant volume combustion as opposed to constant pressure combustion. Replacing the combustor of a jet engine with a reciprocating engine would enable constant volume combustion and more isentropic compression and expansion of the working gas. This

combined enables cycles with higher thermodynamic efficiency which, in theory, reduces fuel consumption.

The first aircraft engine combining axial flow and reciprocating components was the Napier Nomad I and Napier Nomad II, which have been developed and tested in the 1950s. The Napier Nomad I consisted of a compressor and turbine driving a propeller, and a internal combustion engine in between driving a second, counter rotating propeller. The air was compressed in two stages and intercooled. A combustion chamber is reheating the air before it enters the turbine stage. The Napier Nomad II was as much simpler design, consisting of a compressor and a turbine with an internal combustion engine in between. The internal combustion engine was driving a propeller, whereas the propeller shaft is connected to the turbine shaft through a hydraulic clutch. Even though the engines passed flight tests, they never entered into production. Figure 33 shows the layout of the Napier Nomad II engine.

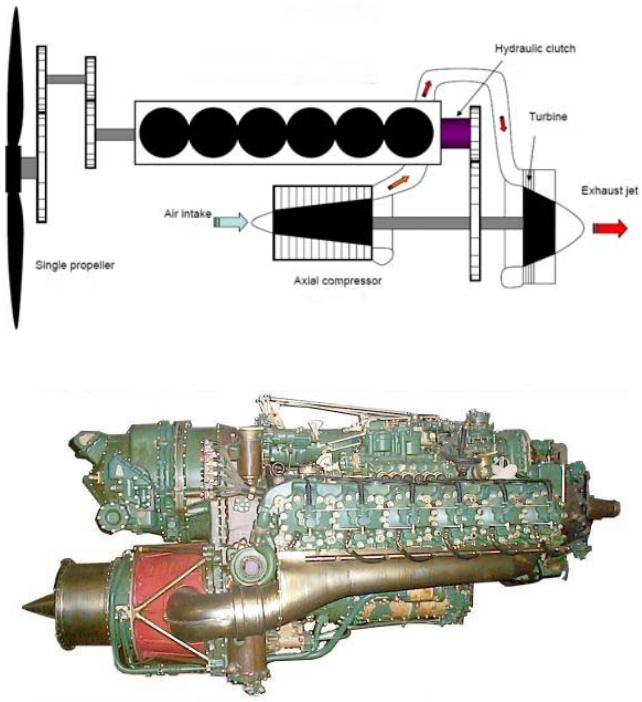

Figure 33: Napier Nomad II engine layout (top) and photography (bottom) incorporating constant volume combustion.

The most straight forward design would be a two shaft turbofan engine where the combustor is replaced with an internal combustion engine where no mechanical shaft power is extracted. The internal combustion engine would deliver hot, pressurised gas to the turbine. The schematic in Figure 34 depicts this configuration.

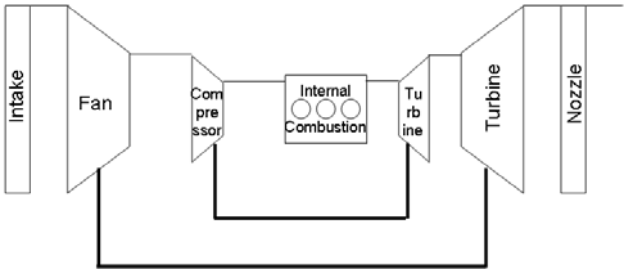

Figure 34: Two shaft turbofan configuration with an internal combustion engine in its core acting as gas generator and allowing constant volume combustion.

A more integrated design would have advantages in terms of compactness and weight as shown in Figure 35. Here, a Wankel type engine has replaced the conventional combustor in a high bypass ratio turbofan.

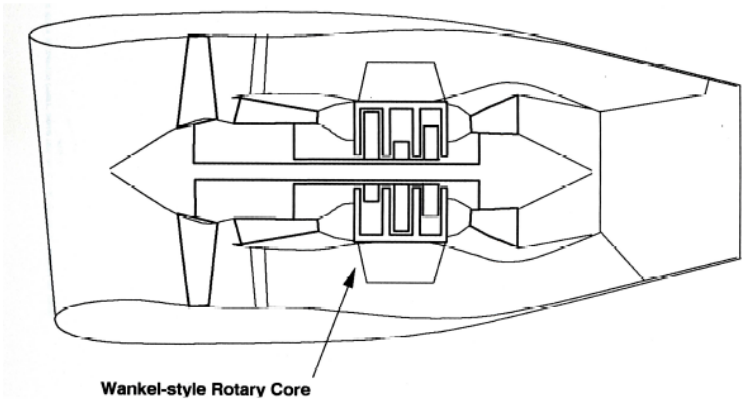

Figure 35: Rotary engine topped gas turbine[61].

A variation would be the shaft of the internal combustion engine driving the compressor unit, which would eliminate the high pressure turbine stage. Whilst this configuration would allow the extraction of mechanical energy through the internal combustion stage, there would be a mismatch between the high shaft speed of the compressor stage and the lower shaft speed of the internal combustion engine requiring a gear box with high gear ratio adding to the weight of the engine. Such configuration is depicted in Figure 36.

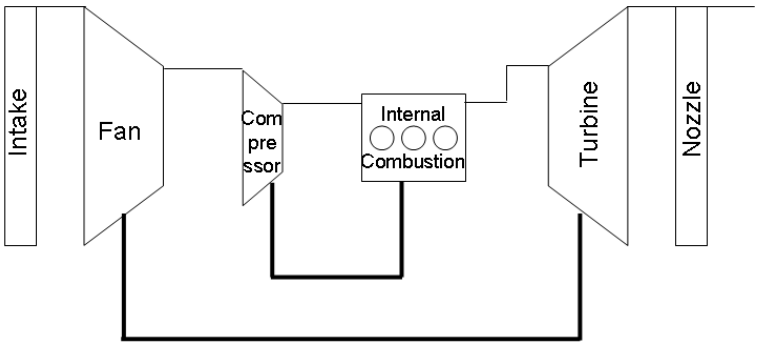

Figure 36: Two shaft turbofan configuration with internal combustion stage is driving the compressor.

A third alternative would be the configuration shown in Figure 37 where the internal combustion stage is driving the fan. The turbine shaft would be connected to the compressor. This design could avoid the need for a gearbox as the internal combustion stage shaft speed is more aligned with the rotational speed of the fan. However, this configuration would only be feasible is the two stages operated in parallel as shown in Figure 33 as the two shafts collide or other, less conventional designs were developed. The author proposes an exoskeletal design as depicted in Figure 38 where the compressor and turbine stage rotate outside the internal combustion engine. This configuration facilitates the replacement of the combustor with an internal combustion engine driving a fan.

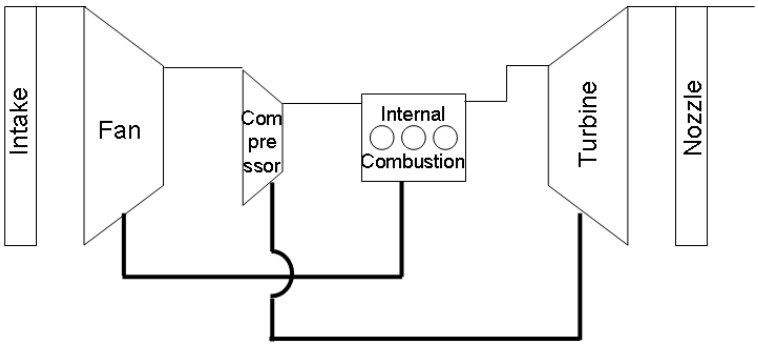

Figure 37: Two shaft turbofan configuration where the internal combustion stage is driving the fan.

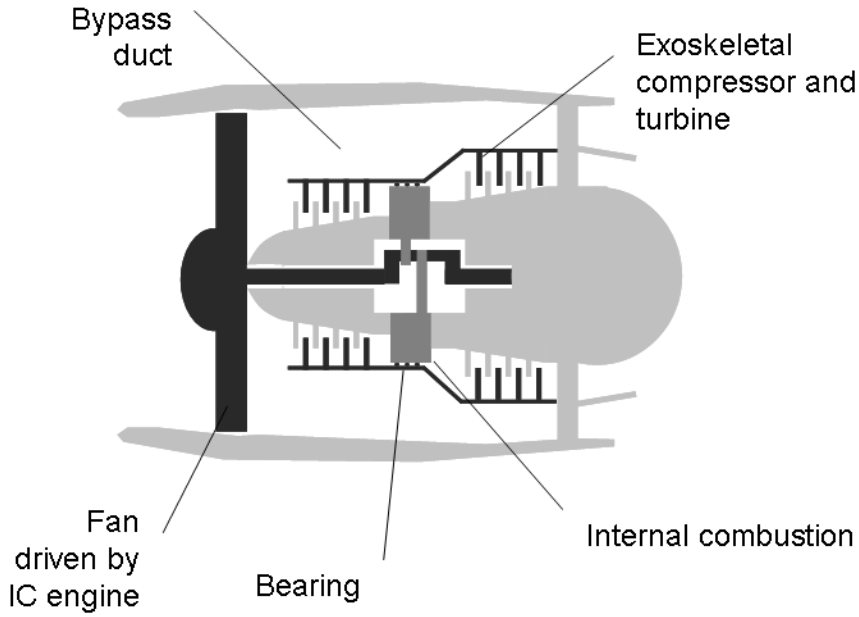

Figure 38: The author's suggestion of the exoskeletal, hybrid internal combustion turbofan configuration where the fan is driven by the internal combustion stage

6.5 Process

Figure 39 shows the internal combustion cycle featuring constant volume combustion on a temperature – entropy diagram and a pressure volume diagram where it is compared to a constant pressure combustion cycle. The volume is contracting adiabatically from 1 to 2 requiring external work. Heat energy is added from 2 to 3/3' whereas the difference in the two cycles becomes apparent on the diagrams. The expansion of the air from 3/3' to 4/4' released work which is used to compress the gases from 1 to 2. The surplus energy in the hot, compressed air is converted into mechanical energy through further expansion, which can take place inside the internal combustion engine or in the turbines in case of a hybrid internal combustion configuration.

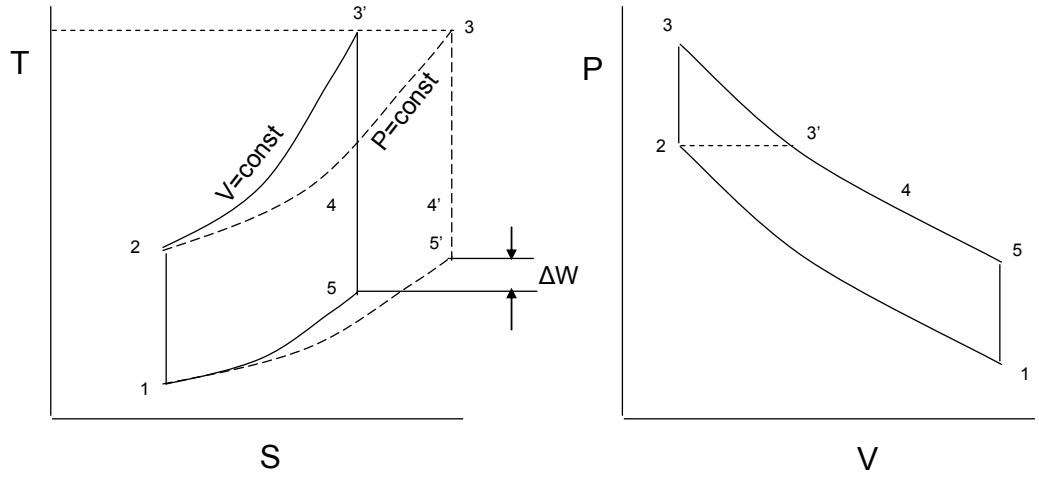

Figure 39: Temperature – entropy (left) and pressure-volume (right) diagram featuring a constant volume and constant pressure combustion cycle.

The least complex configuration is where the internal combustion engine acts purely as gas generator to deliver high temperature and pressure gas to the turbine stage of a turbofan (see Figure 40). Compressed air from the compressor stage enters the cylinders of the internal combustion engine where it is further compressed. Combustion at constant volume facilitates reduced fuel consumption and subsequent expansion delivers shaft power solely used for the compression of the air entering the internal combustion stage.

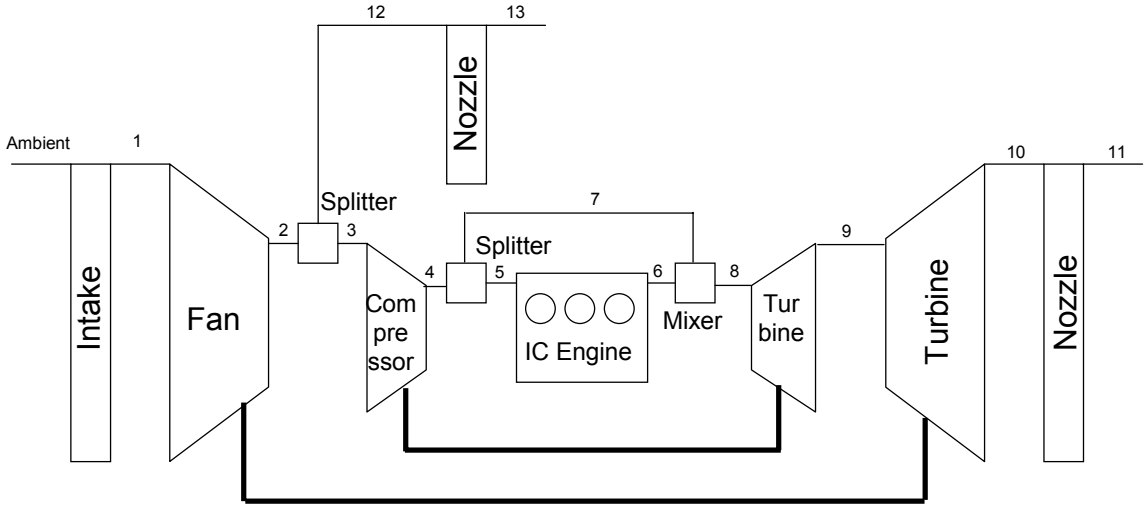

Figure 40: Turbofan engine with internal combustion engine replacing the conventional combustor. The internal combustion engine facilitates constant volume combustion and delivers high temperature and pressure gas to the turbine stage. No mechanical work is extracted from the internal combustion engine shaft.

Figure 40 depicts such layout in a flow diagram and Figure 41 shows the cycle on a temperature – entropy diagram in comparison with a conventional cycle. Although both cycles operating with the same turbine entry temperature, the cycle

featuring constant volume combustion delivers more useful power to propel the aircraft and hence increase the cycle efficiency.

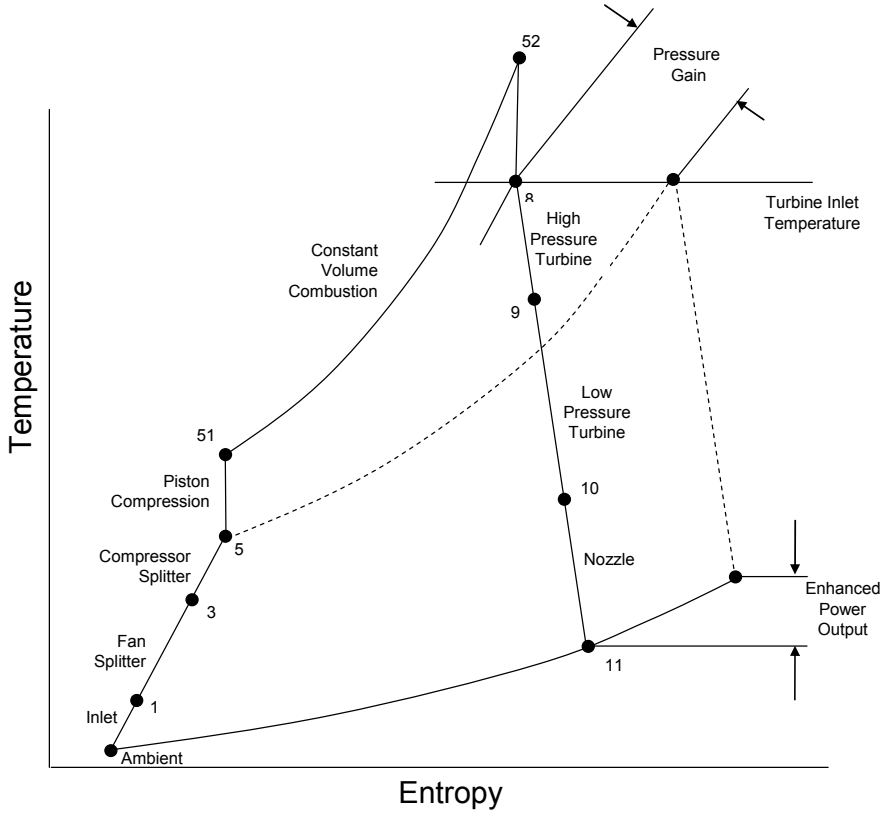

Figure 41: Temperature – Entropy diagram showing the conventional turbofan cycle (dashed) versus a conventional turbofan cycle with an internal combustion engine in its core (5-51-52-6). The turbine cooling flow is not shown in this diagram to avoid confusion and 6 is not displayed.

Knowing the delivery temperature and pressure to the internal combustion engine, the temperature and pressure rise during the compression of the air by the cylinder is determined by compression ratio VR, which is the ratio of the volume of the chamber defined by the cylinder and the piston before and after the compression

of the air. Assuming an isentropic and adiabatic process, the temperature rise of the air during the compression can be obtained from

$$T_{51} = T_5 VR^{\gamma-1} \qquad \textbf{Equation 36}$$

Hence, the pressure increase during the compression interval of the internal combustion engine is defined by

$$P_{51} = P_5 \left(\frac{T_{51}}{T_5} \right)^{\frac{\gamma-1}{\gamma}} \qquad \textbf{Equation 37}$$

The resulting temperature just after ignition of the compressed air in the cylinder is defined externally and the resulting pressure increase due to combustion at constant volume can be calculated from

$$P_{52} = P_{51} \frac{T_{52}}{T_{51}} \qquad \textbf{Equation 38}$$

The temperature at the exit of the internal combustion stage is defined by the work required to compress the air during the beginning of the cycle. Taking into account component efficiency losses for example due to the friction between the pistons and the cylinder walls or the crankshaft mechanism, it can be obtained from

$$T_6 = T_{52} - \frac{\left(T_{51} - T_5\right)}{\varepsilon_{losses}}$$ **Equation 39**

where ε accounts for internal losses associated with mechanical work in the internal combustion engine for example the crankshaft or friction between the piston and cylinder. Assuming isentropic and adiabatic expansion of the gases, the pressure of the gas at the exit of the internal combustion engine can be calculated from

$$P_6 = P_{52}\left(\frac{T_6}{T_{52}}\right)^{\frac{\gamma}{\gamma-1}}$$ **Equation 40**

With the pressures and temperatures known at each point of the theoretical cycle, the energy into the cycle required and hence the fuel flow is calculated from

$$\frac{\dot{m}_{fuel}}{\dot{m}_{air}} = \frac{c_v\left(T_6 - T_5\right)}{q_{net}}$$ **Equation 41**

With the value for c_v being lower than c_p by a factor equal to γ, the fuel required to achieve a desired temperature increase is less in case of the constant volume combustion process than in case of the constant combustion process.

6.6 Computational Model

The computational model was modified to calculate the performance of a turbofan where the combustor is substituted with an internal combustion engine as shown in Figure 40. In order to be consistent with previous calculations, the turbine entry temperature was held constant for all calculations. Therefore, Equation 37 was rearranged and the peak cycle temperature is hence dependent on compression ratio and turbine entry temperature.

This leads to the question of what the peak cycle temperature is and if it is technically feasible and meaningful. The inlet and outlet temperature to the internal combustion cycle as well as the compression ratio determine the peak cycle temperature. In hybrid configuration, the inlet temperature to the internal combustion engine varies with the compression pressure ratio, which ranges approximately between 20 and 100. The resulting compressor exit temperatures range from 775K to 1,310K. This enables plotting the peak cycle temperature of the internal combustion cycle against compression ratio as shown in Figure 42. A can be seen, the resulting peak cycle temperatures range from 2,000K to 3,315K and increase with compression ratio and higher inlet temperatures.

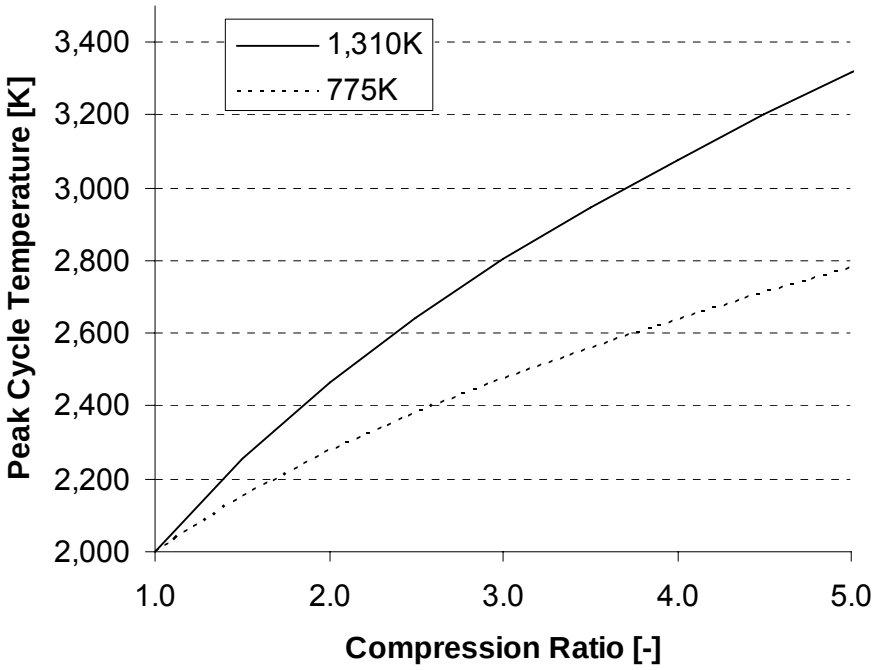

Figure 42: Peak cycle temperature for a hybrid internal combustion engine cycle for different inlet temperatures (1,310K and 775K) and compression ratios. The IC outlet temperature is 2,000K.

The pressure ratio over the internal combustion cycle, which denotes the pressure increase of the air at the inlet and the outlet to the internal combustion cycle, is also a function of the compression ratio and the inlet temperature. The dependency can be seen in Figure 43. For a given outlet temperature, the pressure ratio increases with increasing compression ratio and decreases with higher inlet temperatures. This indicates that relatively low compressor discharge temperatures resulting from relatively low compressor pressure ratios in combination with modest compression ratios in the internal combustion engine enable high overall pressure ratios. If the compression ratio is determining the weight and dimension

of the internal combustion engine in a way that higher compression ratios yield heavier and bulkier designs with larger cylinders, then a combination of relatively low compressor ratios and low compression ratio would be beneficial regarding engine weight.

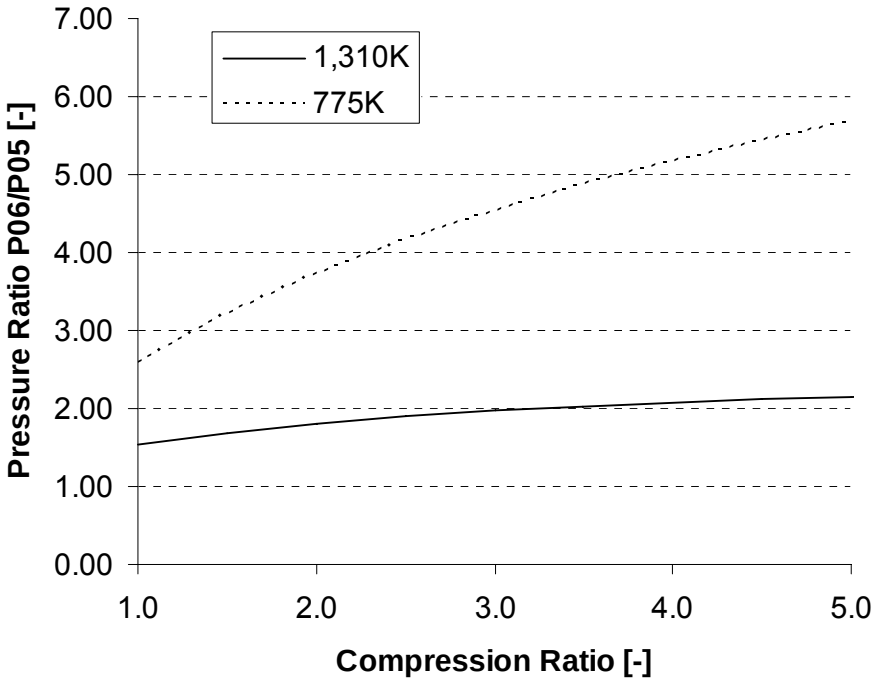

Figure 43: Pressure ratio inlet to outlet of an IC cycle in a hybrid cycle for different inlet temperatures (1,310K and 775K) to the IC cycle and compression ratios. The IC outlet temperature is 2,000K.

The optimisation of the hybrid cycle was carried out with a compression ratio of three in all sets and mechanical losses of 10%. The outlet temperature of the internal combustion engine was varied from 1,700K to 2,000K. As in previous sections, the optimisation of the cycle was carried out in two sets, whereas the bypass

ratio was set to 15 in one set. Results for the first set of optimisations are given in Table 25. The fan pressure ratio in all cases was 1.26 as in previous calculations. The bypass ratio of the cycles ranges from 37.2 to 52.4, which is higher than in any of the cycles in previous sections. The compressor pressure ratio of the cycles is between 13.4 and 24.6. The overall efficiency of the cycles ranges from 82% to 85%, which is higher than in any of the previous cycles.

Turbine Entry Temperature [K]	1,700	1,800	1,900	2,000	2,100	2,200
Fan Pressure Ratio [-]	1.26	1.26	1.26	1.26	1.26	1.26
Bypass Ratio [-]	37.2	40.2	43.2	46.3	49.3	52.4
Compressor Pressure Ratio [-]	13.4	15.3	17.4	19.6	22.0	24.6
Specific Fuel Consumption [10^{-5} (kg/s)/N]	0.72	0.72	0.71	0.70	0.70	0.69
Specific Thrust [N/(kg/s)]	62.5	62.4	62.4	62.3	62.3	62.3
Overall Efficiency [-]	0.82	0.83	0.83	0.84	0.85	0.85

Table 25: Summary of engine parameters and performance of optimised, hybrid internal combustion engine cycles for different TETs.

The optimisations were repeated with a bypass ratio constrained to 15; results are given in Table 26. Compared to the hybrid internal combustion engine cycles where the bypass ratio was unconstrained during optimisation, the fan pressure ratio is higher and ranges from 1.56 to 1.73. The compressor pressure ratio is also higher and ranges from 20.7 to 52.6. All cycles have an overall efficiency of 77% with differences only apparent in the 3rd and 4th decimal place of the efficiency values. Furthermore, the overall efficiency is decreasing with increasing turbine entry temperature.

Turbine Entry Temperature [K]	1,700	1,800	1,900	2,000	2,100	2,200
Fan Pressure Ratio [-]	1.56	1.60	1.63	1.67	1.70	1.73
Bypass Ratio [-]	15.0	15.0	15.0	15.0	15.0	15.0
Compressor Pressure Ratio [-]	20.7	25.3	30.6	36.9	44.2	52.6
Specific Fuel Consumption [10^{-5} (kg/s)/N]	0.77	0.77	0.77	0.77	0.77	0.77
Specific Thrust [N/(kg/s)]	122.7	128.5	133.9	138.9	143.6	148.0
Overall Efficiency [-]	0.774	0.774	0.774	0.774	0.773	0.771

Table 26: Summary of engine parameters and performance of optimised, hybrid internal combustion engine cycles for different TETs and a bypass ratio of 15.

A direct comparison of hybrid internal combustion cycles where the bypass ratio was unconstrained during optimisation and where it was constrained to 15 is given in Table 27. The difference in fan pressure ratio is significant, indicating that alternative propulsion technology may be required for hybrid constant volume combustion cycles with high bypass ratios. In the unconstrained case, the bypass ratio is 46.3, which is several times that of conventional turbofans. Again, alternative propulsion technologies such as open rotors would be required to achieve this bypass ratio. The compressor pressure ratio of the cycle where the bypass ratio was unconstrained during optimisation is 19.6 compared to 36.9 in the constrained case. This suggests that larger, relatively heavier compressors are required if the bypass ratio is kept low. In terms of specific fuel consumption and overall efficiency, better performance is theoretically achievable where the bypass ratio was unconstrained during optimisation but both cycles would outperform any of the other cycles previously described by far in theory. There is a 7% difference in terms of overall efficiency between both cycles. In terms of specific thrust, about half the propulsive force per mass unit of air passing through the engine can be obtained in case of the cycle with the higher bypass ratio compared to the cycle where the bypass ratio was constrained during optimisation.

	Unconstrained BPR	Constrained BPR
Turbine Entry Temperature [K]	2,000	2,000
Fan Pressure Ratio [-]	1.26	1.67
Bypass Ratio [-]	46.3	15.0
Compressor Pressure Ratio [-]	19.6	36.9
Specific Fuel Consumption [10^{-5} (kg/s)/N]	0.70	0.77
Specific Thrust [N/(kg/s)]	62.3	138.9
Overall Efficiency [-]	0.84	0.77

Table 27: Summary of hybrid internal combustion cycles for a Turbine Entry Temperature of 2,000K.

Summary

Results of the optimisations of the two spool turbofan, hybrid wave rotor, hybrid pulse detonation and hybrid internal combustion cycle are summarised in this chapter to allow a direct comparison. The below figures help to understand the performance and cycle parameters calculated in the previous chapters whereas each point indicates a cycle optimised for minimum specific fuel consumption.

Figure 44 and Figure 45 show results for the cycles where the bypass ratio was unconstrained during optimisation. Each set of cycles comprises turbine entry temperatures ranging from 1,700K to 2,200K. The overall efficiency is increasing with increasing turbine entry temperature for each set of cycles. The fan pressure ratio of cycles was calculated to be 1.26 in all cases regardless of turbine entry temperature.

Best possible fuel performance of all sets is achieved with the hybrid internal combustion engine. The overall efficiency exceeds 80%, which is achieved through constant volume combustion and more efficient compression and expansion processes facilitated by the internal combustion engine. The specific thrust is also lowest of all cycles as a result of the relatively high bypass ratios exceeding 37. These high bypass ratios would be possible if alternative fan technology was used. The compressor pressure ratio is amongst the lowest of all cycles, remaining below 25 even for a turbine entry temperature of 2,200K.

The second most fuel efficient cycle is the hybrid pulse detonation cycle with overall efficiencies around 60%. The specific thrust is higher than for the hybrid internal combustion engine and the hybrid wave rotor cycles, which is due to the

relatively low bypass ratios only undercut by the conventional turbofan cycle. The compressor pressure ratio of the hybrid pulse detonation cycles becomes relatively high for higher turbine entry temperatures and ranges from 40 and 100, which would indicate the need for relatively heavy compressors.

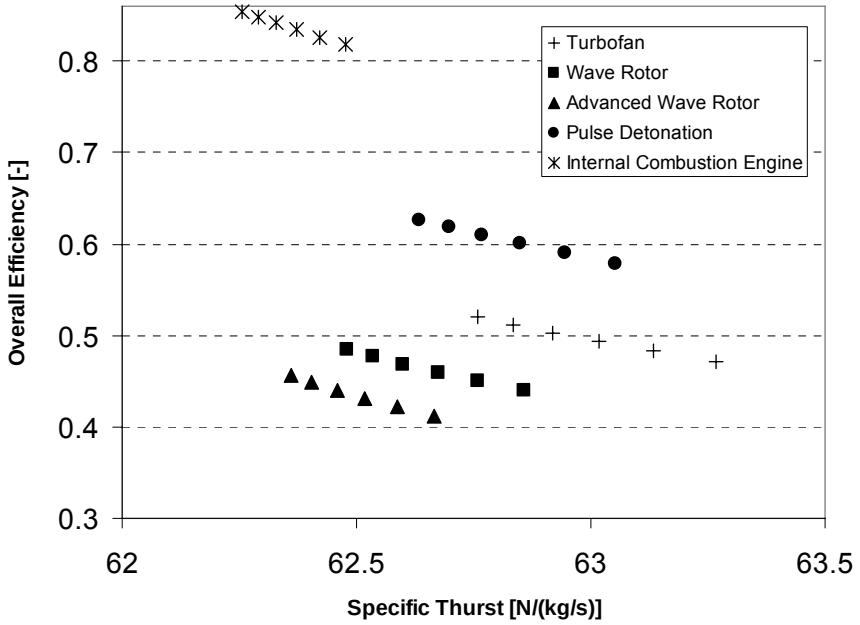

Figure 44: Overall efficiency and specific thrust of optimised cycles. TET is increasing from left to right (1,700K to 2,200K) within a given set.

Two sets of optimisations were carried out for the hybrid wave rotor cycles, whereas the hybrid advanced wave rotor cycles in based on a more advanced wave rotor design facilitating higher pressure ratios in the wave rotor. The hybrid wave rotor has a larger internal pressure ratio than the hybrid advanced wave rotor. Results suggest that hybrid wave rotor cycles are the least fuel efficient hybrid cycles studied in this thesis even with inferior performance compared to what is

theoretically achievable with conventional turbofan cycles. The calculated overall efficiency is between 40% and 50%, whereas the hybrid wave rotor cycle outperformed the hybrid advanced wave rotor cycle. The specific thrust is relatively low, only undercut by the hybrid internal combustion engine cycles, which results from the relatively high bypass ratios ranging from 25 to 45. The compressor pressure ratio is relatively low, ranging from 10 to 45, which would indicate that the resulting engine would require a relatively low number of compressor stages, possibly resulting in a lighter, more compact designs. Hybrid advanced wave rotor cycles have the lowest compressor pressure ratios of the cycles studied in this thesis.

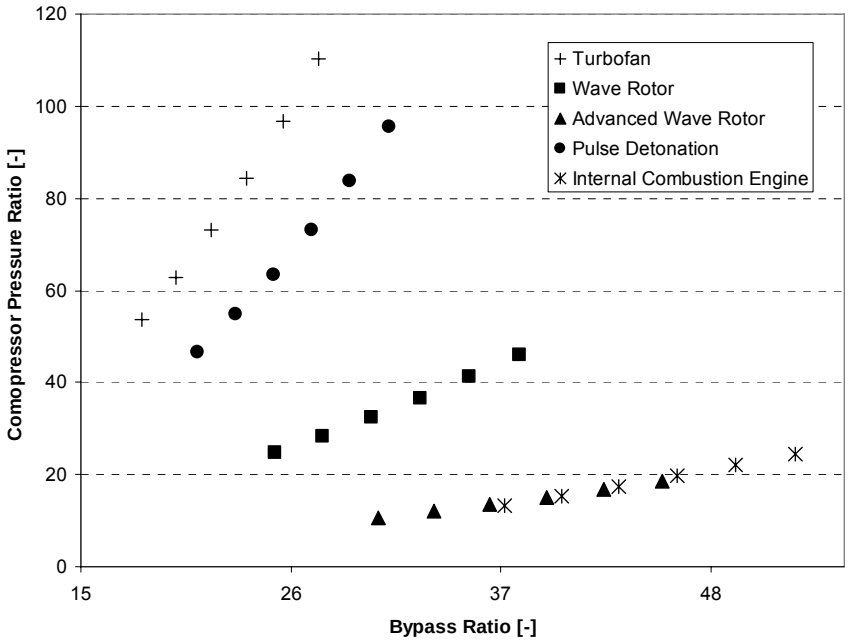

Figure 45: Compressor pressure ratio and bypass ratio of optimised cycles. The fan pressure ratio is 1.26 for all cycles. TET is increasing from left to right (1,700K to 2,200K) within a given set.

In order to avoid the challenges, weight and drag associated with high bypass ratios, the optimisations were repeated where the bypass ratio was fixed to 15. The design variables were fan pressure ratio and compressor pressure ratio only. Although the calculated values for the overall efficiencies of the optimised cycles were lower in general, a similar trend could be found with respect to which type of cycles are more fuel efficient.

The most fuel efficient cycles are the hybrid internal combustion engine cycles with overall efficiencies exceeding 75%, followed by hybrid pulse detonation (about 60%), conventional turbofans (about 50%), hybrid wave rotors and advanced wave rotors (40%-50%). Lower bypass ratios imply that less air is passing through the engine to generate the thrust. The specific thrust of the cycles with lower bypass ratios is about half the specific thrust compared to the previous cycles, which would indicate that the mass flow is reduced by half to obtain the same thrust. Since mass flow and inlet diameter are directly related, half the mass flow would imply engines diameters being smaller by a factor of $\sqrt{2}$. The hybrid advanced wave rotor cycles have the highest specific thrust, followed by the hybrid internal combustion engine and the hybrid wave rotor engine. The hybrid pulse detonation engine and conventional turbofan cycle have the lowest specific thrust of the cycles studied in this thesis.

As opposed to the optimisations where the bypass ratio was unconstrained, the fan pressure ratio varies for the different cycles as depicted in Figure 46 ranging from 1.30 to 1.85. This is higher than for all the cycles where the bypass ratio was unconstrained during optimisation where the fan pressure ratio is 1.26 in call cases. In general, it was observed that hybrid cycles have higher fan pressure ratios than conventional turbofans cycles. The fan pressure ratio is highest for the hybrid ad-

vanced wave rotor cycles ranging from 1.55 to 1.85 and probably exceeding limits of what is achievable with current fan technology. The fan pressure to the hybrid internal combustion cycles range from 1.56 to 1.73 and are more feasible considering state of the art fan technology. Hybrid wave rotor cycles are followed by hybrid pulse detonation cycles in terms of fan pressure ratio whereas turbofan cycles exhibit lowest fan pressure ratios. This order is equivalent to that observed for specific thrust as higher fan pressure ratios increase the thrust per mass unit of air passing through the engine.

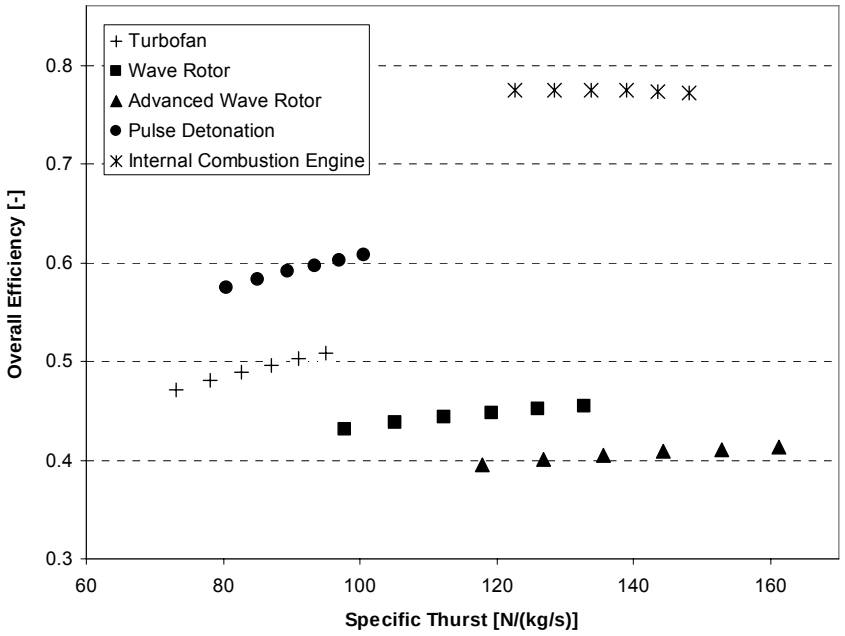

Figure 46: Overall efficiency and specific thrust of optimised cycles (bypass ratio is 15). TET is increasing from left to right (1,700K to 2,200K) within a given set.

In general, the cycles where the bypass ratio was constrained during optimisation have higher compressor ratios than the cycles where the bypass ratio was uncon-

strained during optimisation. Compressor ratios are lowest for the hybrid advanced wave rotor cycles ranging from 9.6 to 15.5, followed by the hybrid internal combustion cycles (20.7 – 52.6), hybrid wave rotor cycles (25.1 – 49.3), hybrid pulse detonation cycles (51.4 – 125) and turbofan cycles (55.5. – 129.4). Wave rotor and internal combustion engine technology exhibit strongest benefits with regards to reducing compressor size compared to conventional turbofan technology since they contribute to the overall pressure ratio and substitute compressor stages.

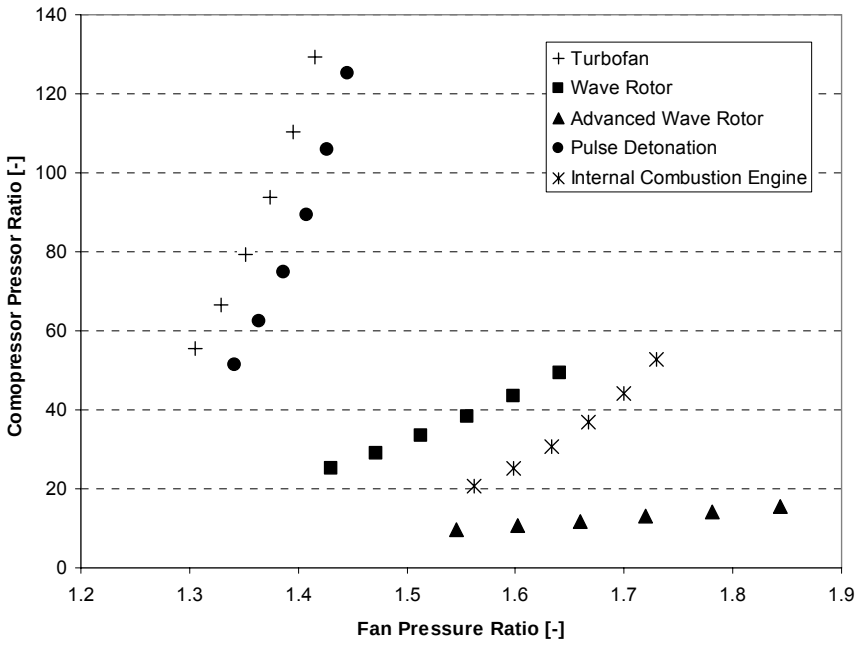

Figure 47: Compressor pressure ratio and bypass ratio of optimised cycles. The bypass ratio is 15 for all cycles. TET is increasing from left to right (1,700K to 2,200K) within a given set.

6.7 Estimating Installed Performance

The results of the previous calculations suggest that the cycle parameters in terms of fan pressure ratio, compressor pressure ratio and bypass ratio are often in excess of what is achievable with state of art engine technology. Compressor pressure ratios exceeding 60 will p4obably be difficult to achieve at current technology level. Maximum fan pressure ratios of high bypass turbofans are in the range of 1.6 beyond which alternative propulsor technology would probably be applicable. Bypass ratios exceeding 15 are not common in modern turbofan engines and efficiency advantages due to bypass ratios beyond 20 are offset due to increased weight and drag. Hence, another set of optimisations was performed with additional constraints introduced. The Turbine Entry Temperature was set to 2,000 K in all calculations. The constrains were set to values that were thought to be achievable with current engine technology and are shown in Table 28. As previously stated, the cycle of a particular engine typically varies during a flight mission with changing throttle setting and ambient conditions and parameters given here should be considered as average values.

Parameter	Upper Limit
Fan Pressure Ratio	1.5
Bypass Ratio	15
Compressor Pressure Ratio	60

Table 28: Optimisation constraints for engine parameters.

Results of the additional calculations are summarised in Table 29. In all cases, the calculated fan pressure ratio is either close or equal to the constraint set for the optimisation whereas the bypass ratio is equal to the constraint in all cases. The resulting specific thrust ranges from 102.7 – 122.5 N/(kg/s). This allows the assumption that the engines incorporating the cycles would be of approximately same inlet diameter and produce the same net thrust.

	Turbofan	Wave Rotor	Advanced Wave Rotor	Pulse Detonation	Internal Combustion
Turbine Entry Temperature [K]	2,000	2,000	2,000	2,000	2,000
Fan Pressure Ratio [-]	1.46	1.50	1.50	1.49	1.50
Bypass Ratio [-]	15.0	15.0	15.0	15.0	15.0
Compressor Pressure Ratio [-]	60.0	48.6	26.0	60.0 (26.0)	60.0
Specific Fuel Consumption [10^{-5} (kg/s)/N]	1.21	1.33	1.54	1.00 (1.11)	0.79
Specific Thrust [N/(kg/s)]	102.7	113.0	129.3	108.3 (127.2)	122.5
Overall Efficiency [-]	0.49	0.45	0.39	0.59 (0.53)	0.75

Table 29: Results for cycle optimisations with constraints.

The only significant differences can be found in terms of compressor pressure ratio. The hybrid wave rotor cycles have lower compressor pressure ratios than the other cycles, indicating the wave rotor would substitute some of the compressor stages. The number of stages substituted depends on the pressure ratio across a single stage. Assuming a pressure ratio of 1.3 across a single compressor stage, about 1-2 stages could be saved compared to the conventional turbofan case in case of the hybrid wave rotor and 3-4 stages could be saved if the advanced wave rotor was used. Depending on the weight per stage, this would result in a shorter and lighter compressor. However, considering the overall number of stages, this could only result in a small weight saving in absolute terms. For example in order to achieve an overall pressure ratio of 60 the total amount of compressor stages would be 16 if the pressure ratio per stage was 1.3 and saving 3 out of 16 stages would mean saving 20% of the overall amount of stages in the compressor unit. This would not necessarily mean that the resulting hybrid advanced wave rotor engine was 20% lighter or more compact than a comparable turbofan since the wave rotor would be added to the overall design and the conventional combustor is not replaced by the wave rotor. The overall weight difference depends on the difference in weight and dimensions of the wave rotor compared to the stages it replaces. In the literature, the weight of a particular turbofan engine is believed to increase if the wave rotor is not substituting compressor stages of the engine it is built into. The added weight to an engine due to the wave rotor is estimated to be 23%[62]. Assuming that the wave rotor does not result in a longer engine, which is theoretically possible if it is placed inside (or outside) the tubular combustor, and assuming that each compressor stage saved would result in a 6.4% weight saving of the total engine, then the hybrid advanced wave rotor would weigh 2.6% more than the comparable turbofan. This would almost be offset by the compressor

stages saved if the wave rotor was substituting compressor stages (based on the assumptions before).

In case of the hybrid pulse detonation cycle, the compressor ratio yielding maximum overall efficiency is 60, which is the same as for the conventional turbofan cycle and suggests that no weight benefits are achievable since no compressor stages are replaced. The calculated fan pressure ratio is 1.49 (compared to 1.46 for the turbofan) and the bypass ratio 15, which is the constraint that was set in the optimisation. The overall efficiency of the cycle is 59%, considerably higher than for the conventional turbofan of 49%. Since the pulse detonation cycle is not substituting compressor stages as opposed to the wave rotor, the weight of the hybrid engine would increase compared to the conventional turbofan. Since the pulse detonation engine has a geometry similar to the wave rotor, it would be reasonable to assume that both devices have a similar weight. However, the wave rotor engine does not replace the continuous flow combustor whereas the pulse detonation does replace the combustor. Assuming that the combustor of a conventional turbofan engine represents 10% of the engine weight and that a geometry similar to the wave rotor increases the weight of a turbofan by 23%, it is reasonable to assume that the total weight increase of a hybrid pulse detonation engine would be 13%. If the pulse detonation engine was replacing compressor stages than it could be assumed that the weight penalty would change. It was previously calculated that the hybrid advanced wave rotor cycle has a compressor pressure ratio of 26 which would mean that 3-4 compressor stages are replaced. Applying the same assumptions to the hybrid pulse detonation engine, than the weight difference compared to the conventional turbofan would be -7.4%. However, the performance of this engine would be different. In an additional calculation, the performance of such

cycle was calculated and is given in brackets in Table 29. The overall efficiency of the hybrid pulse detonation cycle is 53% as opposed to 59%.

The cycle parameters resulting of the optimisation of the hybrid internal combustion cycle are equivalent to the constraints as can be seen in Table 29. The cycle overall efficiency is highest of all cycles and with a value of 75%. The efficiency results from high cycle temperatures in the internal combustion unit, the increased overall pressure ratio and the mode of combustion at constant volume. Depending on how the internal combustion engine is integrated with the turbofan, the weight of the hybrid internal combustion engine changes compared to the conventional turbofan. The key indicator for the size of an internal combustion engines is displacement. Engine displacement is the volume that is displaced by all pistons inside the cylinders of an internal combustion engine in a cycle from top dead centre to bottom dead centre excluding the combustion chamber. If the compression ratio is known, the volume displaced by one cylinder during one cycle is

$$V_D = V\left(1 - \frac{1}{VR}\right) \qquad \textbf{Equation 42}$$

where V is the volume of the cylinder when the piston is at the top dead centre at the beginning of the cycle. The volume V required to accommodate the mass of air m at pressure P and temperature T can be derived from the ideal gas model

$$V = \frac{mRT}{P} \qquad \textbf{Equation 43}$$

If the rotational speed, or cycle speed, of the internal combustion engine is know, then the mass of air in the cylinders during one cycle can be calculated from

$$m = \frac{\dot{m}}{n} \qquad \textbf{Equation 44}$$

where $\dot{m}$ is the average mass flow through the internal combustion engine and n the rotational speed in cycles per time unit. Since the mass flow through a turbofan is given as the sum of both the bypass and the engine core mass flow, in case of a hybrid internal combustion engine the mass flow $\dot{m}$ can be calculated from

$$\dot{m} = \frac{\dot{m}_{Total}}{1 + BPR} \qquad \textbf{Equation 45}$$

where $\dot{m}_{Total}$ is the total mass flow through the hybrid turbofan engine. Combining equations 40 to 43, the total displacement volume of the internal combustion engine is calculated from

$$V_D = \frac{\dot{m}_{Total} R T_5 \left(1 - \frac{1}{VR}\right)}{n P_5 (1 + BPR)} \qquad \textbf{Equation 46}$$

Note that Equation 44 is valid only for a one stroke internal combustion engine. The displacement volume calculated in Equation 44 would have to be multiplied with the number of strokes during one cycle.

Assuming a total mass flow through the engine of 1,000 kg/s, which is comparable to that of a modern turbofan engine for mid size, long-haul aircraft, a rotational speed of 3,000 min^{-1}, which is typical for modern automobile engines and 1940s piston propeller engines, an inlet temperature to the internal combustion engine of 1,000 K and inlet pressure of 30 bar, which are typical combustor inlet conditions, a bypass ratio of 15 indicating high bypass ratio turbofan technology, and a compression ratio of 3, the displacement volume of a hybrid internal combustion engine can be calculated to be 79.7 litres. The parameters are summarised in Table 30. In comparison, the displacement volumes of high performance piston propeller engines of the 1940s era range from 30 to 50 litres[63]. One of the most powerful piston aero engines built in the 1930/1940s was the Napier Sabre, a British 24 cylinder, liquid cooled engine. With a displacement volume of 36.7 litres, the engine dry weight was 1,070 kg[64], which included a gearbox. Linear scaling to 79.7 litres displacement volume would yield 2,327 kg as an approximation for the weight of an internal combustion engine substituting the combustor of a turbofan with a mass flow of 1,000 kg/s.

RPM [min^{-1}]	3,000
Total Mass Flow [kg/s]	1,000
R [$J(kg\ K)^{-1}$]	287
Inlet Temperature [K]	1,000
Inlet Pressure [bar]	30
Bypass Ratio [-]	15
Compression Ratio [-]	3

Table 30: Parameters for the calculation of the displacement volume of an internal combustion engine.

The dry weight of a modern mid size, long haul turbofan engine approximates to about 5,444 kg[65]. Adding the weight of the turbofan and the internal combustion engine together would yield a total weight of 7,771 kg of which the internal combustion engine would contribute 30%.The increase in weight from the conventional to the hybrid configuration would thus be 43%. This would not include weight savings associated with the replaced combustor and compression stages of the turbofan, improved design and manufacturing techniques of the internal combustion engine, new materials, or the absence of a gear. Table 31 shows the gain in weight of the resulting engine if a piston engine with a state of the art turbofan

were merged compared to the turbofan engine alone. The different columns and rows show scenarios where weight can be saved of either the turbofan or the piston engine prior to the hypothetical merge. Based on the assumption that replacing the combustor would result in a 10% weight saving and the internal combustion engine would be 10% lighter than aircraft piston engine designs of the 1940s, the resulting hybrid internal combustion engine would be 28% heavier than the comparable turbofan.

Weight savings turbofan → Weight savings piston engine ↓	0%	-10%	-20%	-30%
0%	43%	33%	23%	13%
-10%	38%	28%	18%	8%
-20%	34%	24%	14%	4%
-30%	30%	20%	10%	0%

Table 31: Wight of the resulting engine if a scaled version of a 1940s piston engine with a state of the art turbofan were merged. Hypothetical weight changes prior to the merge shown in the left hand column and top row.

Although the theoretical value of the specific fuel consumption of a particular cycle gives an indication on its fuel efficiency, more importantly is the fuel consumption of the aircraft with which the engines are used. Higher overall efficiency mean less fuel is required to generate the force that overcomes the drag and holds the aircraft airborne. However, the fuel consumption also increases with the force required to overcome the drag. The drag of an aircraft depends on its weight and how it is built. Assuming equal aerodynamic designs, the lighter jet with less efficient engines does not necessarily require less fuel to travel a certain distance than the heavier jet with more fuel efficient engines. The weight and aerodynamics of aircraft are subject to many factors and a in depth analysis would be outside the scope of this thesis. However, the installed performance of the cycles considered in this thesis would indicate their potential to be a more fuel efficient alternative to current turbofan designs. The empty weight of a modern, long range, mid size airliner is approximately 110 tons[66]. Both engines combined weigh approximately 10.9 tons[65]. The airframe without the engines would hence be 99.1 tons which means that in relative terms the engines increase the airframe weight by 11%. Since the theoretical specific fuel consumption of the cycles is known and estimates with regards to engine weight are given, the installed performance can be estimated with the Breguet equation

$$D = \frac{v}{g} L/D \frac{1}{SFC} \ln\left(\frac{m_{airframe} + m_{engines} + m_{fuel}}{m_{airframe} + m_{engines}}\right) \qquad \textbf{Equation 47}$$

where D is the distance c is the aircraft speed, g g the gravitational acceleration, L/D the lift to drag ratio and m denotes mass or weight. The Breguet equation assumes continuous climb and constant lift to drag ratio. If the engine weight is expressed in relative terms compared to the airframe weight without engines, rearranging Equation 47 yields

$$\frac{m_{fuel}}{m_{aircraft}} = \left[e^{D \frac{g}{v} \frac{SFC}{L/D}} - 1 \right] \left(1 + \frac{m_{engine}}{m_{airframe}} \right) \qquad \textbf{Equation 48}$$

Assuming that the airframe weight would not be affected by the difference in engine design or engine weight, Equation 48 will enable to calculate the block fuel consumption of the cycles investigated in this thesis. The aircraft speed was assumed to be 255 m/s and the distance travelled 15,000 km; a lift to drag ratio of 20 was chosen resembling state of the art technology.

A summary of the results is given in Table 32. Taking the turbofan engine as reference point, the less fuel efficient and heavier hybrid wave rotor cycles would result in a higher block fuel consumption of 14% and 34%, respectively. The hybrid pulse detonation cycles result in net fuel savings. Theoretically 19% could be saved with the heavier version whereas 11% could be saved with the lighter design. The hybrid internal combustion engine offers greatest block fuel savings even though the weight of the engine is assumed to increase by 28%. If the assumptions hold then 37% could be saved in terms of block fuel consumption. It should be noted that an increasing ratio of block fuel weight to airframe weight

indicates heavier structures to carry the fuel weight, which is not taken into account in this study.

	Turbofan	Hybrid Wave Rotor	Hybrid Advanced Wave Rotor	Hybrid Pulse Detonation (a)	Hybrid Pulse Detonation (b)	Hybrid Internal Combustion
SFC [10^{-5} (kg/s)/N]	1.21	1.33	1.54	1.00	1.11	0.79
Engine weight change compared to turbofan	0%	+17.9%	+2.6%	+13.0%	-7.4%	+28.0%
Engine weight in % of airframe weight	11.0%	13.0%	11.3%	12.4%	10.2%	14.1%
Ratio block fuel weight to airframe weight	0.46	0.53	0.62	0.38	0.41	0.29
Block fuel consumption change relative to turbofan	0%	+14%	+34%	-19%	-11%	-37%

Table 32: Comparison of installed performance of the engine cycles.

6.8 Technology Readiness

An internationally adapted scale to assess the stage at which a certain technology has arrived is the Technology Readiness Level (TRL) scale developed by the National Aeronautics and Space Administration (NASA) in the Unites States of America. It is a measure adapted by many of the world's major companies and agencies to assess the maturity of evolving technologies including materials, components, devices, etc prior to incorporating that technology into a system or subsystem. A new technology that is first invented or conceptualised is not necessarily suitable for immediate application. Instead, new technologies are usually subject to further development, refinement, and application under increasingly realistic circumstances. Once the technology is sufficiently proven, it can be incorporated into an existing system or subsystem. A description of the NASA TRL scale can be found in the Appendix. It ranges from one to nine whereas one denotes the least advances stage and nine the stage where the actual system is 'flight proven' through successful mission operations.

Wave rotor technology has only been tested in a laboratory environment in an aviation context where the concept has been proven successfully. Technology similar to the wave rotor is used for supercharging automotive engines. Although the basic technological elements are in place, the validation of wave rotors applied in a turbofan environment remains relatively ‘low-fidelity’. More research is required on mechanical integrity issues, sealing and diffuser designs. Since some of these aspects are becoming part of current research activities, the technology readiness level of wave rotors is valued at 4 to 5.

As for the wave rotor, the pulse detonation engine is confined to laboratory research only. The pulse detonation concept has been applied for the direct propulsion of unmanned air vehicles in the 1940s and a manned test aircraft has successfully been flown more recently in 2008[67]. Pulse detonation cycles suited for the application in turbofan engines have been investigated and analytical results and prediction were proven by experiments. Although basic pulse detonators are becoming more frequently assessed in a more integrated system environment, experiments remain somewhat simplistic compared to the eventual system. Hence the technological readiness level of pulse detonators is valued at 3 to 4.

The hybrid internal combustion engine is more advanced than the wave rotor or pulse detonation engine. Both, piston and gas turbine engines have been extensively developed and manufactured in the past and have become machines deeply integrated with the modern society. The Napier Nomad engine developed in the 1950s was an engine incorporating both axial flow turbomachinery and piston technology. It was successfully tested in flight and can be attributed to a technology readiness level of 9. Since the nearest equivalent to the hybrid internal combustion engine has been tested more than sixty years before this thesis was written, the technology readiness level of the integration of an internal combustion engine with a modern turbofan engine is downgraded. Although the hybrid internal combustion engine consists of already existing parts, it will require further intensive development and can hence be considered as TRL 6 to 7.

7 Conclusions

The dream of flight has led to the development of an advanced, ever increasing air transport industry. The jet engine was an important facilitator and a disruptive technology at the time when it was first developed. In the light of global warming, the projected shortage of primary energy resources and the associated socio economical consequences, it becomes important to enhance the sustainability of aviation by improving the fuel efficiency of aircraft. As we are approaching the limits of conventional turbofan technology and smaller, incremental improvements in engine technology require increasing investments, new technologies of more disruptive character are sought that offer a safe, reliable, practical and low risk alternative. This thesis compares the potential for hybrid aircraft engine cycles to reduce fuel consumption of passenger aircraft and contributes to developing a roadmap for more sustainable aviation.

A one dimensional engine performance model was developed to calculate the key performance parameters of thermodynamic cycles to allow a comparison of hybrid cycles with a conventional turbofan cycle. The model is based on simplifying assumptions to make relative comparisons rather than producing accurate predictions.

The baseline cycle is a turbofan cycle consisting of a fan driven by the low pressure turbine, a compressor driven by the high pressure turbine, a bypass duct, a wave rotor and a continuous flow combustor. The bypass duct separates the core mass flow and bypass mass flow after the fan stage.

The wave rotor can be understood as an additional shaft consisting of a compressor and a turbine where the pressure exchange is based on wave processes. In between the flow is a continuous flow combustor. In the absence of blades, the wave rotor allows higher peak cycle temperatures that are usually limited by the material properties and cooling techniques applied for turbine blades

The pulse detonation cycle facilitates combustion whereas the pressure is increased during the combustion process. Replacing the continuous flow combustor in a conventional turbofan engine, the hybrid pulse detonation cycle allows higher pressures and, together with the more advanced combustion process, facilitates lower fuel consumption.

The internal combustion cycle enables constant volume combustion similar to a one stroke Otto cycle. As in case of the hybrid pulse detonation cycle, the internal combustion engine is replacing the conventional combustor. Higher pressures and temperatures in combination with constant volume combustion enable significant fuel savings.

The technical feasibility of the physical engines is based on the assumption that technology currently operated under laboratory conditions or applied in different fields can be scaled suitable for the application in hybrid turbofan engines.

The cycles were optimised where the objective was to adjust the design parameters to obtain a cycle operating with maximum possible efficiency. The design parameters were bypass ratio, fan pressure ratio and compressor pressure ratio. All other engine parameters and gas properties were constant throughout all calculations. In an additional set of calculations the theoretical performance of engine cycles was calculated whereas design variables were constrained during optimisa-

tion to justify the assumption that the engine would be a derivative of current turbofan designs. The weight of the engines incorporating the cycles was discussed and estimated relative to the weight of a comparable turbofan. In addition, the installed performance was estimated and the block fuel consumption over a flight mission compared to the turbofan cycle. A summary of the hybrid cycles with respect to technology readiness level and fuel savings compared to the conventional turbofan cycle is given in Figure 46.

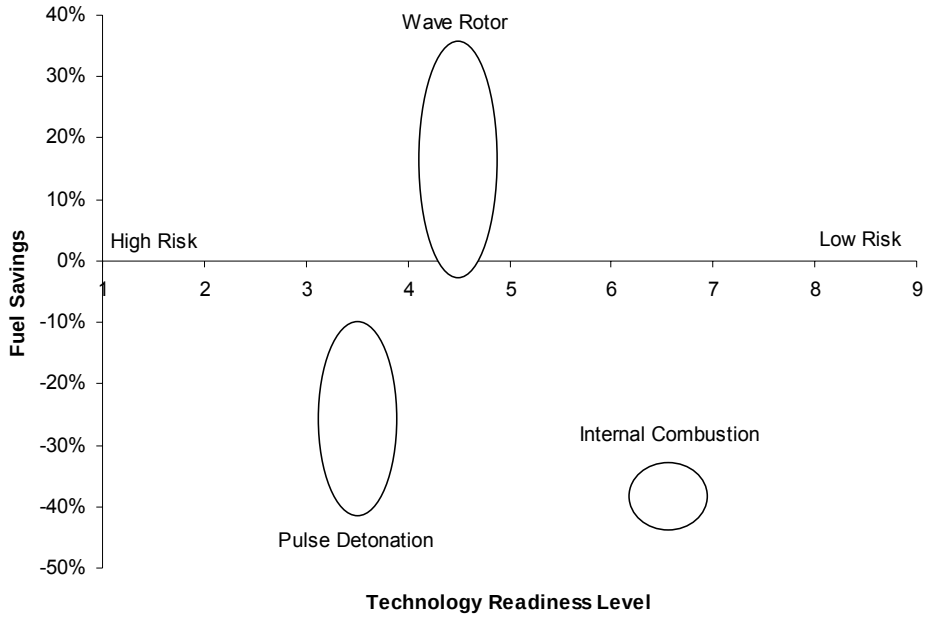

Figure 48: Summary of technologies – block fuel savings versus technology readiness level. At the current level of understanding, the hybrid internal combustion engine exhibits the highest potential for more fuel efficient engines and offers more a more balanced risk to investment.

According to the results, the most promising hybrid engine cycle with regards to fuel efficiency is the theoretical hybrid internal combustion cycle. The low specific fuel consumption of the hybrid internal combustion engine stems from the high overall pressure ratio and maximum cycle temperature in combination with constant volume combustion. Even though the weight of the hybrid engine is expected to increase compared to the conventional turbofan engine, the efficiency gains prevail and the block fuel consumption in installed configuration is expected to decrease significantly. The results of this study suggest the reduction in block fuel consumption can be as high as 37% compared to a conventional turbofan cycle. The technical challenges that need to be overcome in building an engine running on this cycle are the weight and dimensions of the internal combustion engine since the mass flow through a turbofan engine for a long range airliner would require large displacement volumes. New design approaches to combine axial flow technology with internal combustion engine technology are hence sought. Hybrid internal combustion engines operating with high bypass ratios or relatively high fan pressure ratios would offer the highest efficiency improvements, which indicated the requirement for novel propulsor technologies. A possible solution is the application of distributed propulsion where the thrust is generated by a large number of fans integrated with the fuselage. This enables very high bypass ratios but requires further development in power transmission technology such as superconductivity. Since a vast pool of experience and knowledge in designing internal combustion engines is available and a flying prototype of an aero engine based on axial flow technology consisting of a piston engine core was already tested in the mid 1950s, risks and investment associated with this technology would be more balanced compared to less developed technologies. An industry as regulated and risk averse as aircraft manufacturers[68] would welcome this feature in particular.

Future research should be directed at engine integration methods whereas distributed propulsion may offer high synergies since the hybrid internal combustion cycle offers greatest advantages with high bypass ratios. The interaction of non continuous flow devices with continuous flow technology may yield challenges that require additional work which will help to develop a better understanding of the physical design of the engine. This will enable design point and off design point performance analysis and allow a better assessment of the environmental compatibility with respect to other emissions than carbon dioxide.

The hybrid pulse detonation cycle offers better fuel efficiency than the conventional turbofan cycle due to higher peak cycle temperature and a combustion process based on wave interaction that enables a pressure gain during the combustion of fuel. Depending on the overall configuration, the overall pressure ratio of the cycle can be increased or alternatively compressor stages are replaced. A decrease in overall engine weight can be expected if the pulse detonation is replacing compressor stages; the opposite is true if the pulse detonation engine is applied to boost the overall pressure ratio. However, in both cases the specific fuel consumption can be expected to decrease compared to a conventional turbofan cycle due to higher cycle efficiencies. Under installed conditions, the better performance of the cycle with higher overall pressure ratios allows higher block fuel savings even though the engine can be expected to be heavier. It is calculated that 19% saving can be achieved if the pulse detonation engine is used to increase the overall pressure ratio whereas the reduction would be 11% if it was replacing compressor stages. This assumes that the performance of pulse detonation engines found in the laboratory can be applied on a larger scale. Compared to the hybrid internal combustion engine, relatively lower bypass ratios and fan pressure ratios

are required to obtain the fuel savings, which would indicate less advanced propulsor technology would be required. The author could not find any suggestion in the public domain that a hybrid pulse detonation engine was ever tested. A manned vehicle directly powered by a pulse detonation engine was successfully tested recently where thrust is directly generated by the pulse detonation engine. Compared to the internal combustion cycles, the technology readiness is far below that of internal combustion cycles. The technical feasibility of the hybrid pulse detonation engine depends on the ability to combine discontinuous flow with axial flow turbomachinery and if forecasted performance can be achieved in scaled up versions.

The least fuel efficient cycles studied in this thesis are the hybrid wave rotor cycles, which have higher specific fuel consumption than conventional turbo fan cycles. The reason is that combustion occurs in a continuous flow combustion chamber equivalent to that of a conventional turbofan cycles. In addition, the compression and expansion of the air in the wave rotor is less efficient compared to axial flow turbomachinery. The wave hybrid wave rotor engine would very likely also suffer from a weight increase compared to a conventional turbofan engine. Inferior performance in combination with an engine weight increase indicates higher block fuel consumption. An increase of up to 34% was calculated compared to the conventional turbofan cycle. However, if the compression and expansion efficiency of the wave rotor could be improved, substitution of compressor stages would possibly yield in a much compacter engine. This would be especially beneficial for smaller engines where less efficient compressors are used and turbine cooling techniques are limited. As for pulse detonation engines, the wave rotor engine has only been tested under laboratory conditions or for the purpose of su-

percharging piston engines but not in a hybrid turbofan context. However, research is more advanced and the wave rotor found its application in the automotive industry so that risk and investment would be more balanced. More research directed at improving the compression and expansion efficiency of the wave rotor cycle will help to understand if the hybrid wave rotor cycle has a potential for an application in smaller engines.

It should be noted that results presented in this study are best estimates to support in decision making processes for further research and are subject to uncertainties due to the nature of this study. However, even if the theoretical cycles outlined in this thesis cannot be achieved with a physical design, it can be expected that an engine running on a cycle deviating from the ideal cycle calculated in this thesis would still be a promising alternative to existing axial flow and continuous combustor technology. The uncertainties arise due to manifold reasons. Firstly, it is assumed that the actual engine can be built around the cycles and it should also be noted that the cycle of a particular engine varies over the flight envelope so the cycles here provide a snapshot of an engine operating during cruise conditions; secondly, engine weights used to calculate block fuel savings are not derived from physical designs but first estimates; and thirdly, block fuel calculations do not take into account aerodynamic aspects or airframe weight differences for the different cycles and only consider the cruise component of a mission with constant climb.

The hybrid pulse detonation cycle and the hybrid internal combustion cycle theoretically offer significant block fuel savings compared to the conventional turbofan cycles if the assumptions made in this study hold or come close to what is actually achievable. Of these two cycles, the hybrid internal combustion cycle can

potentially offer higher fuel savings and is based on technology that has been tested outside the laboratory and developed and applied extensively in aviation and other contexts.

Appendix

A1: NASA TRL Scale

The NASA technology readiness level (TRL) scale is a systematic metric and assessment system to evaluate and compare the maturity of particular technologies. The scale ranges from one to nine and a brief description of each technology readiness level is provided below. They comprise an estimate of the investment costs involved[69].

TRL 1: Basic principles observed and reported

This is the lowest "level" of technology maturation and is the level at which scientific research begins to be translated into applied R&D.

Cost to Achieve: Very low "unique" cost (the investment cost is borne by scientific research programs).

TRL 2: Technology concept and/or application formulated

Once basic physical principles are observed, then at the next level of maturation practical applications are identified. At this level, the application is still speculative and there is no experimental proof.

Cost to Achieve: Very low "unique" cost (the investment cost is borne by scientific research programs).

TRL 3: Analytical and experimental critical function and/or characteristic proof of concept

At this stage, active R&D is initiated to set the technology into an appropriate context and laboratory based studies are undertaken to physically validate whether or not the analytical predictions are correct. These studies and experiments constitute "proof of concept" validation of the applications/concepts defined at TRL 2.

Cost to Achieve: Low "unique" cost (technology specific).

TRL 4: Component and/or breadboard validation in a laboratory environment

Following successful "proof of concept" work (undertaken at TRL 3), basic technological elements must be integrated to establish that the system will work together to achieve concept-enabling levels of performance. The validation is relatively "low-fidelity" compared to the eventual system.

Cost to Achieve: Low-to-moderate "unique" cost (technology specific, but probably several factors greater than the investment required for TRL 3).

TRL 5: Component and/or breadboard validation in a relevant environment

At TRL 5, the fidelity of the component / breadboard being tested has to increase significantly. The basic technological elements must be integrated with reasonably

realistic supporting elements so that the total applications can be tested in a realistic environment.

Cost to Achieve: Moderate "unique" cost (technology specific, but probably several factors greater than the investment required for TRL 4).

TRL 6: System/subsystem model or prototype demonstration in a relevant environment (ground or space)

TRL 6 is a major step from TRL 5. At TRL 6, a representative model or prototype system, which would go well beyond discrete component level bread-boarding, would be tested in a relevant environment (ground or space). The demonstration might represent an actual system application, or it might only be similar to the planned application, but using the same technologies.

Cost to Achieve: Technology and demonstration specific (a fraction of TRL 7 if on ground but similar if space is required).

TRL 7: System prototype demonstration in a space environment

TRL 7 is a significant step from TRL 6 and requires an actual system prototype demonstration in a space environment. The driving purposes for achieving this level of maturity are to ensure system engineering and development management confidence (more than that required for R&D purposes). TRL 7 would normally only be performed in cases where technology and/or subsystem application is mission critical and relatively high risk.

Cost to Achieve: Technology and demonstration specific (a significant fraction of TRL 8 cost).

TRL 8: Actual system completed and "flight qualified" through test and demonstration (ground or space)

By definition all technologies being applied in actual systems go through TRL 8. In almost all cases, this level is the end of true "system development" for most technology elements.

Cost to Achieve: Mission specific (typically the highest cost for a new technology).

TRL 9: Actual system "flight proven" through successful mission operations

By definition all technologies being applied in actual systems go through TRL 9. In almost all cases, this level is the end of the last "bug fixing" aspects of true "system development". TRL 9 does not include planned product improvement of ongoing or reusable systems. Such technology upgrades would start over at the appropriate level in the TRL system

Cost to Achieve: Mission specific (less than TRL 8).

References

[1] Sagan, C., The Dragons of Eden – Speculations on the evolution of human intelligence, Ballentine Books, New York, 1977.

[2] Lehman, M., This high man; the life of Robert H. Goddard, New York, Farrar, Straus 1963

[3] Gibran, K., The Prophet, Pan Books. April 1991.

[4] Needham, R., volume 4, part 1.

[5] Freud, S., The Future of an Illusion, chapters 3 and 4, 1927.

[6] Becker, E., The Denial of Death, 1973.

[7] Davies, P., Other Worlds, May 1997.

[8] Dawkins, R., The Selfish Gene, 1976.

[9] Feifel, H., The Meaning of Death, chapter 6, 1959.

[10] Maslow, The Need to Know, pp. 118-119

[11] Greenacre, The Fetisch and the Transitional Object, Psychoanalytical Study of the child, 1969, 24:161-162.

[12] "Fear of Flying", A special report on air travel, The Economist, 16 June 2007.

[13] Niedzballa, H. A. and Schmitt, D., Comparison of the specific energy demand of aeroplanes and other vehicle systems, Aircraft Design 4, 2001, 163-178.

[14] Ameyugo G., and Noppel F., From three to zero and beyond: clean propulsion for civil aviation, Whittle Reactionaries 2007, Institution of Mechanical Engineers, 2007.

[15] Whittle, I., The dawn of the jet age, in Whittle 2007, Cranfield University, 2007.

[16]Lee, J. J., Lukachki, S. P., Waitz, I. and Schafer, A., Historical and Future Trends in Aircraft Performance, Cost, and Emissions. Annu. Rev. Energy Environ. 2001, 26:167-200.

[17] Howse, M., 2004, Aero gas turbines – an ever-changing engineering challenge, 3 February 2004 Whittle lecture, Royal Aeronautical Society, 2004.

[18] Penner, E. J., Aviation and the global atmosphere, Special Report, Intergovernmental Panel on Climate Change, November 2001.

[19] Zimbrick, R. A. and Colehour, J. L., Investigations of Very High Bypass Ratio Engines for Subsonic Transports, Journal of Propulsion and Power, 1990, vol. 6, no. 4, pp. 490.

[20] Hoheisel, H., Aerodynamic Aspects of Engine-Aircraft Integration of Transport Aircraft, Aerospace Science and Technology, 1997, no 7, 475-487.

[21] Torenbeek et al, Innovative configurations and advanced concepts for future civil aircraft, Greener by design ,Von Karman Institute, June 2005.

[22] Air Travel – Greener by Design Annual Report 2007 – 2008, Royal Aeronautical Society, 2008.

[23] McMasters, J. H., From Farther, Faster, Higher to Leaner, Meaner, Greener – Future Directions in Airplane Design in the New Century, AIAA 2003-553, 41st Aerospace Sciences Meeting and Exhibit, 6-9 January 2003.

[24] Solomon, S., Qin, D., Manning, M., Chen, Z., Marquis, M., and Averyt, K. B., Climate Change 2007: The Physical Science Basis. Contribution of Working Group I to the Fourth Assessment Report of the Intergovernmental Panel on Climate Change, 2007.

[25] Singh, R., Civil aerospace propulsion: the challenge of the environment, presented at the 6th International Defence and Aerospace Exhibition, Aero India, 2007.

[26] Schumann, U., Formation, Properties and Climate Effects of Contrails, Comptes Rendus Physique, Vol. 6, 2005.

[27] Noppel, F. and Singh, R., "Contrail and Cirrus Cloud Avoidance Technology," Journal of Aircraft, Vol. 44, No. 5, 2007, pp. 1721–1726.

[28] Cazenave, A. and Llovel, W., Annu. Rev. Mar. Sci. 2010. 2:145–73.

[29] Battisti1, D.S. Naylor, R. L., Science, Vol 323, January 2009.

[30] Data from http://data.giss.nasa.gov/gistemp/graphs/Fig.A2.txt following the methodology outlined by Hansen, J., et al. (2006) "Global temperature change". Proc. Natl. Acad. Sci. 103: 14288-14293.

[31]World Energy Outlook 2010, International Energy Agency, November 2010.

[32] Marland, G., T.A. Boden, and R. J. Andres, Global, Regional, and National CO2 Emissions. Carbon Dioxide Information Analysis Center, Oak Ridge National Laboratory, United States Department of Energy, 2007.

[33] Statistical Review of World Energy 2010, British Petroleum, 2010.

[34] The World Factbook 2009. Washington, DC: Central Intelligence Agency, 2009.

[35] http://inflationdata.com/Inflation/images/charts/Oil/Inflation_Adj_Oil_Prices_Chart.htm.

[36] Superfreakonomics, Levitt, S. D. and Dubner, S. J., William Morrow, 2009.

[37] Seidel, J. A., Sehra, A. K., Colantonio, R. O., NASA Aeropropulsion Research: Looking Forward, TM-2001-211087, ISABE, July 2001.

[38] J. E., Lister, D. H., Griggs, D. J., Dokken, D. J., McFarland, M.., Aviation and the atmosphere, Special Report, IPCC, 1999.

[39] International Standard Atmosphere in Thermodynamic and Transport Properties of Fluids, SI Units, 5th Edition, Gogers & Mayhew.

[40] Turbofan data, Department of Power and Propulsion, Cranfield University, 2005.

[41] Fletcher, R. and M.J.D. Powell, A Rapidly Convergent Descent Method for Minimization, Computer Journal, Vol. 6, pp. 163-168, 1963.

[42] Goldfarb, D., A Family of Variable Metric Updates Derived by Variational Means, Mathematics of Computing, Vol. 24, pp. 23-26, 1970.

[43] Han, S.P., A Globally Convergent Method for Nonlinear Programming, Vol. 22, Journal of Optimization Theory and Applications, p. 297, 1977.

[44] Powell, M.J.D., A Fast Algorithm for Nonlinearly Constrained Optimization Calculations, Numerical Analysis, ed. G.A. Watson, Lecture Notes in Mathematics, Springer Verlag, Vol. 630, 1978.

[45] Powell, M.J.D., The Convergence of Variable Metric Methods For Nonlinearly Constrained Optimization Calculations, Nonlinear Programming 3, Academic Press, 1978.

[46] Gill, P.E., W. Murray, and M.H. Wright, Practical Optimization, London, Academic Press, 1981.

[47] Ameyugo, G. and Singh, R., Advanced Cycles for Distributed Propulsion". ISABE-2007-1154, Proceedings 18th International Symposium on Airbreathing Machines, Beijing, 2007.

[48] P. Akbari, R. Nalim, N. Mueller. Performance Enhancement of Microturbine Engines Topped with Wave Rotors. Journal of Engineering for Gas Turbines and Power. 128. Jan 2006.

[49] Foa, J. V., Elements of Fight Propulsion. John Whiley & Sons, Inc, New York and London, 1960.

[50] Welch, G. E. and Jones, S. M. and Paxson, D. E. Wave Rotor-Enhanced Gas Turbine Engine. NASA Technical Memorandum 106998, AIAA-95-2799, 1995.

[51] Wilson, J. and Paxson, D. E., Jet Engine Performance Enhancement Through Use of a Wave Rotor Topping Cycle, NASA Technical Memorandum 4486, 1993.

[52] Marthur, A., A Brief Review on the GE Wave Engine Program (1958-1963). Proc. Of the 1985 ONR/NAVAIR Wave Rotor Research and Technology Workshop, Report NPS-67-85-008, Naval Postgraduate School, Monterey, CA, May, 1985.

[53] Dempsey, E., Akbari, P., Muller, N., Nalim, R., Optimum Application of Four-Port Wave Rotors for Gas Turbine Enhancement, ISABE 2005-1214, Proceedings Symposium for Air Breathing Engines, 2005.

[54] Sehra, A. K. and Whitlow, W., Propulsion and power for 21st century aviation, Progress in Aerospace Sciences 40, 199-235, 2004.

[55] Maclin, H. et al, Fifty years down, fifty years to go, AIAA 2003-2788, Proceedings International Air and Space Symposium and Exposition, 14-17 July 2003.

[56] E. Wintenberger and J.E. Shepherd, "Detonation Waves and Pulse Detonation Engines" Presentation Ae103, January 27, 2004.

[57] Akbari, P. and Nalim, R., Analysis of Flow Processes in Detonative Wave Rotors and Pulse Detonation Engines, AIAA 2006-1236, January 2006.

[58] J. Goldmeer, V. Tangirala, A. Dean., "System-Level Performance Estimation of a Pulse Detonation Based Hybrid Engine", Journal of Engineering for Gas Turbines and Power, January 2008.

[59] Paxson, D. E, "Performance Evaluation Method For Ideal Air-breathing Pulse Detonation Engines," Journal of Propulsion and Power, 20 (5), October 2004.

[60] Brown, R., Popular Science Monthly, Vol 123, No 1, July 1933

[61] J. Whurr, Otto Cycle Core Turbofan Concepts, MSc Thesis, Cranfield University, UK, 1995

[62] R. C. Taussig, "Wave Rotor Turbofan Engines for Aircraft," ed. Sladky, J. F., Jr., Machinery for Direct Fluid-Fluid Energy Exchange, The American Society of Mechanical Engineers, 1984.

[63] Jane's Fighting Aircraft of World War II. London. Studio Editions Ltd, 1998.

[64] Lumsden, A., British Piston Aero Engines and Their Aircraft, The Crowood Press Ltd, First Edition.

[65] Trent 1000, Rolls-Royce, VCOM13797, Issue 4, August 2008.

[66] Boeing 787 Airport Compatibility Brochure, Boeing, December 2009.

[67] Norris, G., Pulse Power: Pulse Detonation Engine-powered Flight Demonstration Marks Milestone in Mojave, Aviation Week & Space Technology, Vol. 168, No. 7, 2008, pp. 60.

[68] The Economist, March 12 – 18, p89:90, April 2011.

[69] John C. Mankins, "Technology Readiness Levels", A. White Paper, April 6, 1995. URL: http://www.hq.nasa.gov/office/codeq/trl/trl.pdf.